A Theoretical Framework for Evaluation of Random Cognitive Radio Network

By

Saifur Rahman Sabuj
Student ID Number: 1178006

A dissertation submitted to the
Engineering Course, Department of Engineering,
Graduate School of Engineering,
Kochi University of Technology,
Kochi, Japan

in partial fulfillment of the requirements for the degree of
Doctor of Philosophy

KOCHI UNIVERSITY OF TECHNOLOGY
SEPTEMBER 2017

Assessment Committee:
Supervisor: Masanori Hamamura
Co-Supervisor: Masahiro Fukumoto
Co-Supervisor: Xiangshi Ren
Member: Katsushi Iwashita
Member: Toru Kurihara

CANDIDATE'S DECLARATION

It is hereby declared that this thesis or any part of it has not been submitted elsewhere for the award of any degree or diploma.

_____

Saifur Rahman Sabuj

Dedicated to my Parents
Md. Aminur Rahman
Saleha Begum
and my Siblings
Sazzad Hussain Sajib
Ammatul Uzma Sathi

Table of Contents

List of Tables

List of Figures

List of Abbreviations

CR: Cognitive Radio

FCC: Federal Communication Commission

I.D.: Imperfect Detection

NICT: National Institute of Information and Communications Technology

P.D.: Perfect Detection

PER: Primary Exclusion Region

PPP: Poisson Point Process

PR: Primary Receiver

PT: Primary Transmitter

PU: Primary User

QoS: Quality of Service

SINR: Signal-to-Interference-plus-Noise Ratio

SNR: Signal-to-Noise Ratio

SR: Secondary Receiver

ST: Secondary Transmitter

SU: Secondary User

Acknowledgements

First of all, I would like to thank Almighty Allah for his mercy and charity. This dissertation is the most significant, most challenging accomplishment of my life, and would have been impossible without the will and wish of the Almighty and I am grateful to him.

Then most of all, I would like to express my deepest gratitude to my supervisor, Prof. Masanori Hamamura, Graduate School of Engineering, Kochi University of Technology, for introducing me to the arena of random cognitive radio networks and for his continuous inspiration, guidance and invaluable support during this research work. I would also thank my committee members Prof. Masahiro Fukumoto, Prof. Xiangshi Ren, Prof. Katsushi Iwashita and Prof. Toru Kurihara for their enlightening discussion, invaluable comments and suggestions about my research work.

Next, I greatly appreciate Kochi University of Technology (KUT) for giving me a chance to study abroad and offering me financial support. Without the Special Scholarship Program for international students, I could not have pursued my studies abroad. Moreover, I appreciate all the teachers and staff of KUT and especially the staff of the International Relations Division for their kindness, warmth cordial help and assistance during my study period.

My KUT life has been so memorable; I will never forget it. I have enjoyed the friendly research environment in Hamamura Lab. In particular, Yoshimasa Hashida, Shougo Kuwamura, Kento Hachikubo, Sayuri Fukui, Akihisa Hino, Ayaka Abe, Yingsong Li and Kittipong Warasup were great warm supporters. I will never forget their kind and warmhearted help in my life and their encouragement in my research.

Finally, I would like to thank my parents, brother and sister for their continuous support, encouragement and sacrifice throughout the years. I will be obliged to them forever for all they have done for me.

Saifur Rahman Sabuj
Kochi, Japan, August 2017

Abstract

With the current state of research on wireless networks, the dominant paradigm used hexagonal lattices and square lattices in early generation, but modern wireless networks follow the irregular deployment of large base stations (BSs) and small BSs. As a result, wireless network design has shifted from deterministic to random wireless networks, and stochastic geometry has attracted much attention as a tool for the design and analysis of modern wireless networks. In the meantime, cognitive radio (CR) has been proposed as a means of adapting to radio frequency spectrum scarcity and also as a way of improving spectral utilization efficiency. In that light, holistic approaches to random CR network have recently attracted widespread research attention in both academia and industry. In this dissertation, we focus an uplink and downlink model of random CR network that is not only tractable but also relevant with current deployment of BSs.

Firstly, we investigate the outage probability and energy efficiency of the primary receiver (PR) and secondary receiver (SR) in CR network, modelling the locations of primary user (PU) and secondary user (SU) as a Poisson point process (PPP). We derive closed-form expressions for outage probability and energy efficiency, with consideration of the probabilities of unoccupied (not utilized by PU) channel selection and successful transmission for imperfect detection in CR network. Furthermore, we propose a method for transmit antenna selection of secondary transmitter (ST) in such networks and accordingly develop closed-form expressions for outage probability and energy efficiency with imperfect detection. The study reported here highlights the importance of combining the capabilities of unoccupied channel selection and successful transmission in CR network to achieve optimal performance regarding outage probability and energy efficiency. In terms of energy efficiency, there is an optimal threshold that maximizes energy efficiency. For implementation in transmit antenna selection, the outage probability can significantly decrease as the number of transmit antennas increases, even though energy efficiency is maximized under the target outage probability.

Secondly, we investigate the performance of CR network using a stochastic geometry approach in Rayleigh-lognormal fading. We present a geometric model of CR network where primary transmitters (PTs), PRs, STs, and SRs are distributed as a PPP. We analytically derive the coverage probability and transmission rate of that network. Moreover, we obtain

closed-form expressions of coverage probability and transmission rate. We then numerically evaluate coverage probability and transmission rate performance. It is shown that for the coverage probability and transmission rate, the results are better for lower densities of PTs and STs.

Thirdly, we investigate the coverage probability and spectral efficiency of a CR network with a single-tier uplink model based on a stochastic geometry framework. The locations of STs, SRs, PTs, and PRs are modeled as independent PPP. We derive mathematical expressions for the coverage probability and spectral efficiency of this network, as well as closed-form expressions for a path-loss exponent equal to 4. For the uplink transmission, truncated channel inversion power control is employed for the ST with a cutoff threshold at the SR because of the limited transmission power. We consider two locations of the SR (i.e., inside and outside the primary exclusion region) for uplink transmission. We found that the location of the SR impacts on coverage probability and spectral efficiency. Numerical analysis confirms that (i) the coverage probability is higher and (ii) the spectral efficiency is higher when the SR is outside the primary exclusion region.

Fourthly and last, we report a comprehensive study of energy harvesting CR network where locations of users of primary and secondary networks follow a PPP. In our design of random CR network, we focus on the two-slope path-loss function so as to have a realistic scenario of propagation environments. A new expression of outage probability is theoretically derived for SR in active mode. Also, we obtain an explicit expression of harvested energy for SR in active and inactive modes. Finally, we investigate the harvested energy maximization problem under a particular outage probability constraint, and also obtain an optimal solution of transmission power and density of STs. Numerical results for outage probability, harvested energy and maximization of harvested energy are presented for evaluation of the performance and characteristics of this network.

Chapter 1

Introduction

1.1 Motivation

The demand for cognitive radio technology has led to the current situation in which more bandwidth and resources will be needed for next-generation wireless networks. In the future, a significant number of cellular phone users will be making wireless demands as they access the Internet, watch mobile TV, play online games, participate in video conferences and so forth. This means that cellular phone subscribers will face problems related to bandwidth and energy consumption. The number of cellular phone users is growing rapidly, by approximately 0.18 billion per year [1], as shown in Fig. 1.1. On the other hand, the number of smartphone users is currently increasing by approximately 0.22 billion per year. In Japan, the number of smartphone users is increasing more rapidly than that of cellular phone users, as shown in Fig. 1.2. Overall the large volume of available data suggests that the percentage of smartphone users using the Internet will exceed that of cellular phone users. Clearly more bandwidth will be needed to accommodate future subscribers.

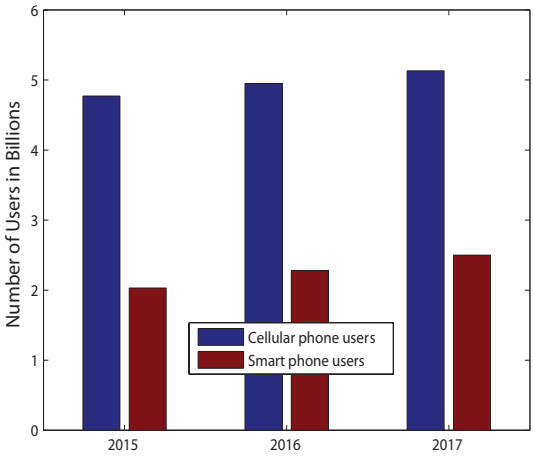

Figure 1.1: Number of users worldwide [1].

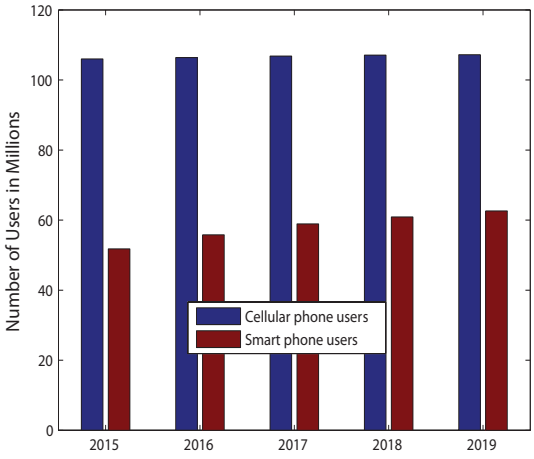

Figure 1.2: Number of users in Japan [2].

Nowadays energy consumption is considered a crucial issue in the wireless industry. As

shown in Fig. 1.3, energy consumption by fixed networks and user devices is more than 85% of total energy consumption. Also, Fig. 1.3 indicates that energy consumption is increasing; overall energy consumption is predicted to reach approximately 1080 TWh by 2020 [3]. Owing to the increasing number of mobile subscribers, energy consumption, energy cost, and carbon dioxide (CO_2) emissions by mobile networks in the Asia-Pacific region are approximately 58%, 58%, and 60% of the worldwide totals, respectively. According to the GSM Associations mobile energy efficiency benchmarking analysis, energy consumption, energy cost, and CO_2 emissions by mobile networks are approximately 29.3 kWh, $3.00, and 17.6 kg CO_2 per mobile connection in the Asia-Pacific region [4]. The mobile cellular industry produces about 0.14% of the worlds CO_2 [5] emissions. As a result, the wireless industry is not only consuming a large amount of energy, but it is also causing increased electromagnetic pollution, negatively affecting the global environment.

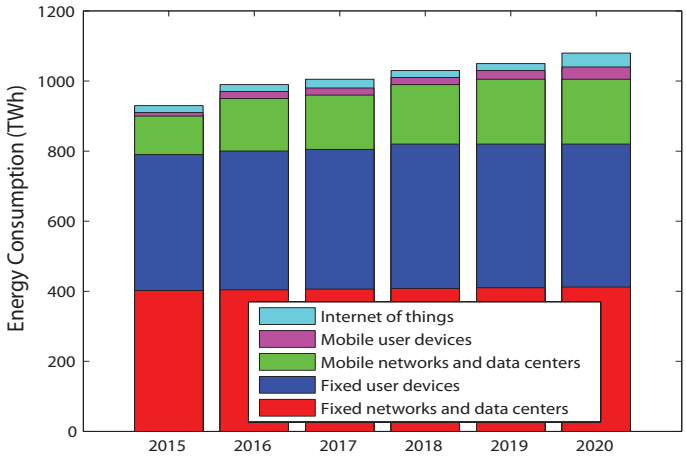

Figure 1.3: Worldwide energy consumption by network infrastructure and user devices.

For consideration of two parameters (i.e. bandwidth and energy), we aim to investigate the coverage probability, outage probability, spectral efficiency and energy efficiency of random cognitive radio networks.

1.2 Cognitive Radio

According to a technical report by the Federal Communications Commission (FCC), spectrum measurement in the USA indicates that most of spectrum is underutilized. FCC reports that 70% of allocated spectrum is not properly utilized [6]. This observation points to a need for new spectrum policy, under which unlicensed users (secondary users, also known as cognitive users) are allowed to use a share of the spectrum allocated to licensed users (primary users) as long as they do not interfere with access by licensed users, whenever the licensed users' frequency bands are not being utilized. Also, FCC suggests that a possible solution for cellular users is to use other frequency bands, for example, TV, radio, satellite and radar frequency bands.

To resolve the issue of spectrum scarcity, the use of cognitive radio (CR) is proposed in [7]. Subsequently, Spectrum Sensing CR has been proposed, defined as a technique that focuses on the radio frequency band [8]. In [9], CR adapts to the transceiver parameters of the surrounding environment, for example, transmission power, frequency, bandwidth and modulation schemes; it also detects unused frequency band and assigns it completely to transmission parameters.

1.2.1 Dynamic Spectrum Management Framework

In general, CR has four main functions: spectrum sensing, spectrum decision, spectrum mobility, and spectrum sharing, as shown in Fig. 1.4 [10–12]. Under spectrum sensing technique, a CR user (secondary user) detects a spectrum hole or idle spectrum which can be taken advantage of by utilizing idle primary user (PU) spectrum without interference. Spectrum decision refers to the ability of a secondary user (SU) to choose the best available frequency band with consideration of internal and external policies. In spectrum mobility, an SU needs seamless communication requirements to change its frequency operation. This means that an SU exits the frequency band when a licensed user is preparing for utilization. Spectrum sharing provides fair spectrum scheduling method and prevents collisions among multiple SUs.

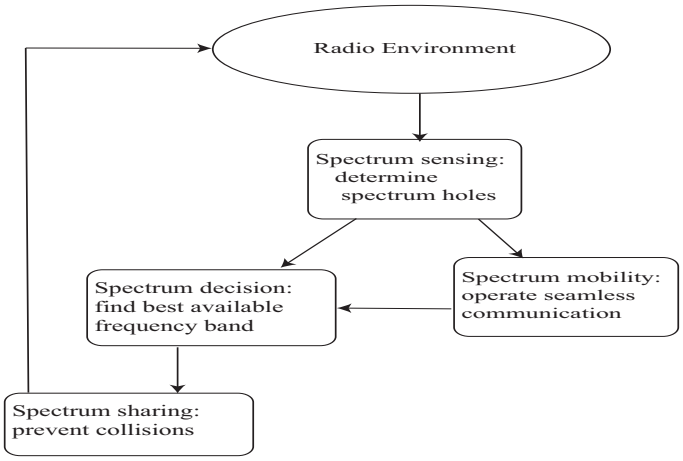

Figure 1.4: Dynamic spectrum management framework for CR [10].

1.2.2 CR Network Paradigms

Several approaches to CR network configuration have been proposed, notably underlay, overlay, and interweave scenarios [13, 14]. Among those approaches, the underlay scheme is similar to the overlay scheme because both allow PUs and SUs to operate in the same frequency band. All schemes are briefly described below:

(a) Underlay: Underlay is the most promising approach of the three, since it allows SUs to access the radio spectrum even when PUs are active, as shown in Fig. 1.5(a). The

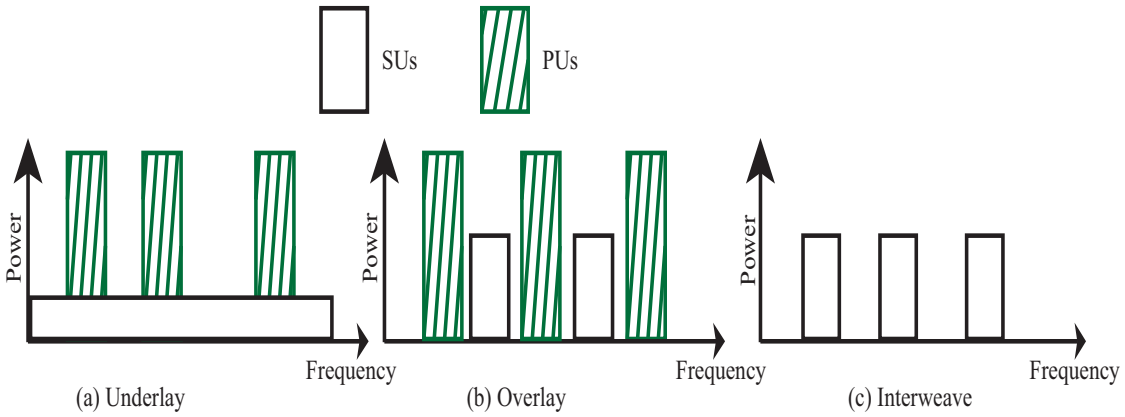

Figure 1.5: Spectrum underlay, overlay, and interweave scenarios [9].

transmission power of SUs is below the interference-temperature limit so that it does not create interference with the PUs. This technique is used in spread spectrum (e.g., CDMA) and ultra-wideband (UWB) communication systems.

(b) Overlay: Overlay allows SUs to access the radio spectrum when PUs are active, but spectrum sensing is needed before transmission, as shown in Fig. 1.5(b). If an idle spectrum hole is found, an SU may access the radio spectrum. In this scheme, there is no transmission power limit or interference-temperature limit. This technique is used in TDMA, FDMA and OFDM wireless

(c) Interweave: SUs utilize the frequency bands when the PUs are not actively transmitting, as shown in Fig. 1.5(c). In other words, interweave is different from other schemes that PUs and SUs may not transmit in a frequency band simultaneously. This is the initial idea after study of FCC technical report.

1.3 Spectrum Allocation in Japan

The initial concept of CR was introduced in the "e-Japan" policy [15, 16] announced in 2000 by the Japanese government under its "e-Japan strategy and program" policy. In 2003, Japan launched terrestrial digital broadcasting in three metropolitan areas, and expanded to terrestrial digital broadcasting in all prefectures in 2006. After transmission was successful in place, analog broadcasting was terminated in 2011. At that time, various Japanese organizations, including National Institute of Information and Communications Technology (NICT), KDDI, Hitachi, Mitsubishi Electric, and ATR started collaborative work on the use of TV spectrum by cellular phone. NICT said, "*Japan is the second country to allow commercial frequency sharing of TV white spectrum* [17]".

The evolution of spectrum allocation in Japan is shown in Fig. 1.6, in terms of of spectrum allocation in the past, the present[1] and the future.

[1]The period is 2011-2018.

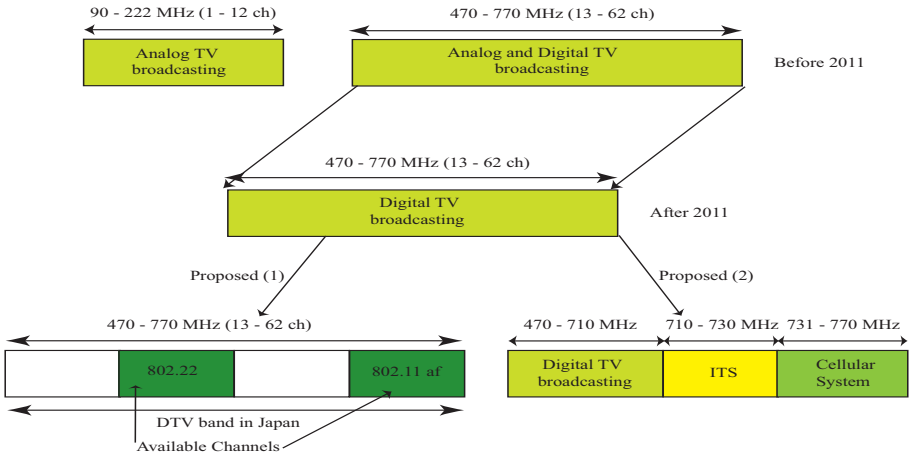

Figure 1.6: Evolution of spectrum allocation in Japan.

NICT proposed the following two spectrum allocations.

Proposal 1: Through the combined work of NICT and Hitachi Kokusai Electric Inc., IEEE 802.11af and IEEE 802.22 based wireless systems were developed. Successful transmission in long-range wireless communications was achieved using IEEE 802.22 and IEEE 802.11af based systems in Tono City, Iwate, Japan. Subsequently a multihop network was created with throughput of 15.5 Mbps in downlink and 9.0 Mbps in uplink over 6.3 km with two discontinuous TV channels operating at the same time [18, 19].

Proposal 2: NICT created extensive infrastructure for public broadband (PBB) wireless in Japan. NICT reorganized very high frequency and ultra-high frequency (UHF). UHF was divided for use by three categories, digital TV broadcasting, ITS, and cellular system. In future, those categories will operate in the assigned spectrum bands [20].

1.4 Random Networks

The most popular and widely used traditional cellular network models are the hexagonal grid model or Wyner model [21] and the square lattice model, where the base stations (BSs) are assumed to be located on a grid. However, modern cellular networks consist of BSs of various types and shapes, including macro-BSs, micro-BSs, pico-BSs, and femto-BSs, as shown in Fig. 1.7 [22, 23], so these cellular networks do not follow the Wyner model or the square lattice model. Now, arbitrary locations of BSs can be accounted for in modern cellular networks, called random wireless cellular networks. For this reason, stochastic geometry has received much attention as a tool for the design and analysis of modern cellular networks. Most related studies have focused on use of the Poisson point process (PPP) for the design of modern cellular networks owing to PPP's useful analytical approach. If stochastic geometry is implemented, wireless cellular networks can be characterized as random networks.

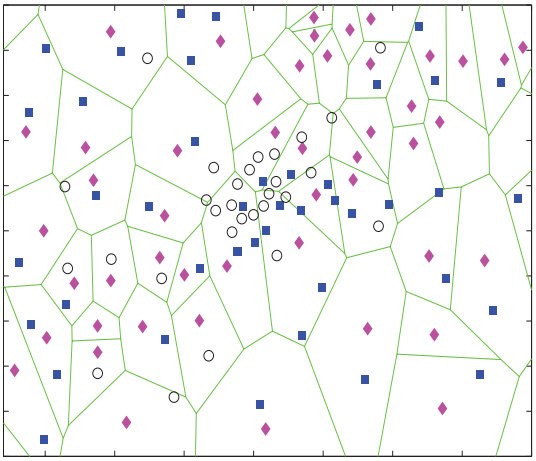

Figure 1.7: HCNs model where macro-BSs are represented by magenta diamonds, Voronoi cell boundaries by green lines, Micro-BSs by blue squares and pico-BSs by black circles.

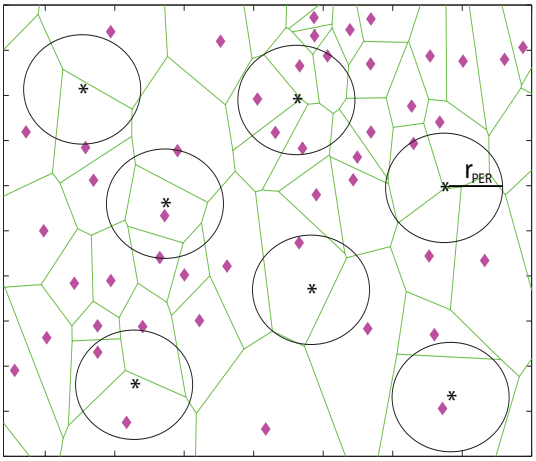

Figure 1.8: CR network model where cognitive macro-BSs are represented by magenta diamonds, Voronoi cell boundaries by green lines, PTs by black asterisks and the PER by a black circle.

The actual BSs locations shown in Fig. 1.7 [24, 25], were obtained from Ofcom[2]. Ofcom determines the exact location of BSs in the UK. From the collected data in [24], we plotted a network model of macro-BSs, micro-BSs and pico-BSs in the HCNs by means of the MATLAB command voronoi, as shown in Fig. 1.7. Then we plotted random CR networks with a large number of cognitive macro BSs[3], shown Fig. 1.8. In the networks, there are two types of users: PUs in the primary network (PN), using licensed frequency, and SUs, in cognitive network (CN), using unlicensed frequency. In this networks, SUs share licensed spectrum with PUs. For that reason, we introduce some primary transmitters (PTs), as shown in Fig. 8, where the PTs are denoted by black asterisks and the primary exclusion region (PER) is denoted by a black circle. Under CR network policy, SUs are not permitted to transmit inside the PER because of interference [26]. The main problem with this approach is that there are a large number of cognitive BSs inside the PER, so deployment of the CR network model is an open problem.

From the above discussion, it is evident that random CR network is a more complex form of cellular network. Therefore, it is necessary to develop an analytical model of random CR network and evaluate its performance. For this reason, holistic approaches to random CR network have recently attracted widespread research attention in both academia and industry.

[2]Ofcom is an independent regulator and competition authority for the UK communications industry.

[3]We avoided using other BSs because we intended to design a single-tier CR network. The macro BS was replaced by a cognitive BS capable in cognitive radio technology, which as a result has knowledge of spectrum sensing, spectrum decision, spectrum sharing, and spectrum mobility [10].

1.5 Contribution of this Thesis

The objective of this thesis is to provide an efficient analytical model of random CR networks. In this thesis, we focus on two main demanding tasks: (i) to develop an analytical model of random CR network where the deployment of BSs and PTs locations is irregular; and (ii) to analyze performance metrics such as coverage probability, outage probability, spectral efficiency and energy efficiency based on the analytical model.

The following is an outline of the main contributions of the thesis, described chapter-by-chapter.

Chapter 2

In chapter 2, we present our design, based on random locations of PUs and SUs as PPP in CR networks. The contributions of this work are summarized below.

1. First, we derive the outage probability of primary receiver (PR) and secondary receiver (SR) in CR networks where the PU and CU locations are modeled by a PPP. In our earlier work [27], we provided the same expressions for the perfect detection of probabilities of unoccupied channel selection and transmission schedule, but this did not explain the relation between density (i.e., λ_p and λ_s) and outage probability. Here we consider imperfect detection. In that sense our work differs from other current studies, e.g., [31], which do not consider the probabilities of unoccupied channel selection and successful transmission.

2. Second, we derive some theoretical expressions for energy efficiency to evaluate transmission performance in terms of energy efficiency under imperfect detection. Also, we consider the sensing and data transmission time in our analysis of energy efficiency, different from the previous study [27]. A relevant work [31] was not evaluated energy efficiency in CR network.

3. Finally, based on our derived theoretical expression, we propose transmit antenna selection at secondary transmitter (ST) in this network so as to minimize the probability of secondary receiver (SR) outage. Simulation results show that outage probability performance can be improved significantly, though with some different characteristics of energy efficiency.

Chapter 3

In chapter 3, since random CR network in Rayleigh-lognormal fading environment has not been explored using PPP, though clearly this is an important issue impacting on the development of future networks, we offer the following two main contributions.

1. We analytically derive the coverage probability and transmission rate of CR network composite with Rayleigh-lognormal fading, in which PUs and SUs are modeled as PPP. We obtain closed-form expressions for coverage probability and transmission rate of this type of network, and formulate the coverage probability and transmission rate for an interference-limited regime.

2. We examine the effect of parameters including transmission power, transmitter densities (PTs and STs), and Shannon capacity gap using the theoretical expressions of coverage probability and transmission rate developed here.

Chapter 4

In this chapter, we report the modelling of uplink transmission with truncated channel inversion power control in a CR network, where the ST communicates with its serving SR. Our contributions in this chapter are threefold.

1. Firstly, we develop an analytical model of a CR network with a ST-SR pair and a PT-PR pair. We discuss the position of the ST, where the ST is allowed to transmit in two cases: (a) when the SR is inside the PER and (b) when the SR is outside the PER.

2. Secondly, we derive mathematical expressions for the coverage probability and spectral efficiency, considering four assumptions of spectrum sensing for the uplink transmission of the CR network. Also, we develop closed-form expressions of coverage probability.

3. Thirdly, we compare the four assumptions of spectrum sensing and evaluate the performance of the CR network for cases (a) and (b). Also, we investigate the transmission power of a ST in the uplink by considering the impact of the path-loss exponent, density, and cutoff threshold.

Chapter 5

In this chapter, we apply a PPP to develop a secondary network model considering the two-slope path-loss model, and develop some new analytical formulas. The contributions of this chapter are summarized as follows:

1. We use stochastic geometry to provide a tractable analytical framework for the analysis of energy harvesting from primary transmitters and secondary transmitters in secondary networks. For the two-slope path-loss model, we derive an analytical expression for outage probability in inactive mode. We also obtain a closed-form expression of outage probability for inactive mode. Furthermore, we evaluate the performance of outage probability.

2. We analyze harvested DC power for active and inactive modes in the secondary network. In addition, we present the harvested DC power in closed-form. Furthermore, we also compare the performance of active and inactive modes numerically.

3. Finally, we formulate the optimization problem for the closed-form expressions and present the optimal design with some numerical solutions for energy harvesting via this network. To develop closed-form expressions of outage probability and harvested DC power, we derive the solution to harvested DC power maximization for active mode.

1.6 Organization of this Thesis

This dissertation is organized in five chapters as follows:

Chapter 1, the introduction, describes the motivation for the series of studies reported in this dissertation, the basic notions of CR and random network, spectrum allocation in Japan and the contributions of this dissertation.

Chapter 2 begins with of a review of the literature on network modelling and a description of the network model developed here, specifically: the timeslot structure for probabilities of unoccupied channel selection and successful transmission for both perfect and imperfect detection; and the channel model. This is followed by a description of the derivation of the interference, outage probability, and energy efficiency of this network, and of the outage probability and energy efficiency for transmit antenna selection at ST. The numerical results for this network are provided.

Chapter 3 begins with of a review of the literature on network topology, channel models and timeslot structure. The analysis of secondary networks in terms of coverage probability and transmission rate for Rayleigh-lognormal fading environment is presented, along with the numerical results for this network.

Chapter 4 begins with of a review of the literature on CR, followed by a description of the CR network model developed here. This is followed by a description of the derivation of the coverage probability and spectral efficiency for this network and of an investigation of the impact of the main parameters on the network's coverage probability and spectral efficiency.

Chapter 5 presents literature review, an overview of the CR network model, channel model, timeslot structure, and receiver design. Then the analysis of the performance metrics, e.g., outage probability and harvested power of this network are presented. Also, the numerical results of CR networks discuss about the findings of this study.

Chapter 2

Analysis of Downlink CR Network

2.1 Literature Review

Earlier research work[1] on the environment of CR networks using stochastic geometry has focused on interference, coverage probability and outage probability. An earlier in research towards energy- and spectral efficiency trade-off of cognitive cellular networks is discussed in short [29] here, followed by an account of recent advancements and the presentation of three design guidelines for future cognitive cellular networks. A comprehensive study of stochastic geometry models for multi-tier and cognitive cellular wireless networks can be found in [30]. Note that authors [30] classified five techniques using four processes, Poisson point process (PPP), binomial point process, hard core point process and Poisson cluster process, for the evaluation of performance. As for CR networks, outage probability was investigated in [31]. However, this work found PPP impractical for assessing interference and outage probability. The authors in [32] investigated outage probability considering probability of channel selection and that of medium access for CR network under a self-coexistence constraint. In [33], the impact on medium access probability, coverage probability and throughput was investigated for communication between primary and secondary users and theoretical expressions were given for those impacts. In [34], the authors proposed a novel approach for spectrum sharing networks, and derived a closed-form expression of outage probability for primary service (PS). As well, investigation determined that truncated channel inversion power control correlated strongly with PS outage probability. [35] presented a statistical scheme for aggregated interference in spectrum sensing of CR networks, with consideration for sensitivity, transmission power, density and underlying propagation environment. The results prompted further discussion of cooperative spectrum sensing using this interference.

Some studies have been explored cognitive cellular networks using stochastic geometry. In [36], closed-form expressions of the outage probability and average spectral efficiency on the tagged receiver in two-tier cellular networks with macrocells and femtocells were derived, with consideration for lognormal shadowing and Nakagami fading channel model. In

[1]This chapter was published at IEEE CSCN, 2015 [27] and Pervasive and Mobile Computing, Elsevier, 2017 [28]. Please follow the copyright rule of IEEE and Elsevier.

theoretical work, the authors of [37] investigate outage probability with regard to the effects of the probability of picking the same resource blocks and the probability of current time slot in the two-tier cognitive heterogeneous cellular networks, while primary (macro BSs) and secondary (femto BSs) nodes were randomly located using the theory of homogeneous PPP. [38] considers a two-tier heterogeneous network using cognitive femto APs with lower transmission power and macro BSs with higher transmission power. However, the results of this study indicate that outage probability can be decreased by approximately 60% for the proper choice of the spectrum sensing threshold in femto users. The authors [39] analyzed the performance of cognitive and energy harvesting-based device-to-device communication in a multi-channel downlink-uplink cellular network. The performance results show that downlink channels perform better for low density BSs in these networks, although uplink channels are preferred.

Several significant energy-efficient techniques have been proposed for heterogeneous cellular networks, including active/sleep BS operation, cooperative relaying and coordinated multi-point (CoMP) transmission with BS sleeping. Energy efficiency in homogeneous single-tier and K-tier wireless networks has been developed for two sleeping configurations, random sleeping and strategic sleeping [40]. The numerical results show that the sleeping strategy is viable. A cooperative relaying system was proposed in [41], in order to maximize energy efficiency. A sleep control technique was proposed for on-off switching of pico BSs based on traffic variation; however spectral efficiency may be damaged [42]. Considering combined CoMP transmission and BS sleeping system under heterogeneous networks, coverage probability and energy efficiency are derived to evaluate performance. Both approaches were found to enhance performance [43].

2.2 Problem Description

A problem occurs in CR networks with a large number of cognitive BSs. In the networks, there are two types of users: primary users (licensed users) included in primary network (PN), who use licensed frequency, and secondary users (unlicensed users) included in secondary network (SN), who use unlicensed frequency. In this network, secondary users (SUs) share the licensed spectrum with primary users (PUs). For that reason, we introduce some primary transmitters (PTs), as shown in Fig. 2.2, where the PTs are denoted by black asterisks and the primary exclusion region (PER) is denoted by a blue circle. As regulation CR network policy, SUs are not permitted to transmit inside the PER because of interference [26]. From Fig. 2.2, the problem is that there are a large number of cognitive BSs inside the PER, so it is an open problem to deploy an underlay[2] scheme, mainly for cognitive BSs inside the PER of PT. We can solve this problem two ways. Firstly, cognitive BSs inside the PER can be used as in an interweave[3] scheme. Other cognitive BSs (i.e., the ones outside the PER) can be used as in an underlay for CR networks. Secondly, all

[2]In the CR network environment, there are two main CR network paradigms, interweave and underlay. In underlay, SUs can access the spectrum while PUs are active in CR network transmission [44].

[3]In interweave, SUs can utilize the spectrum when the PUs are not actively transmitting [44].

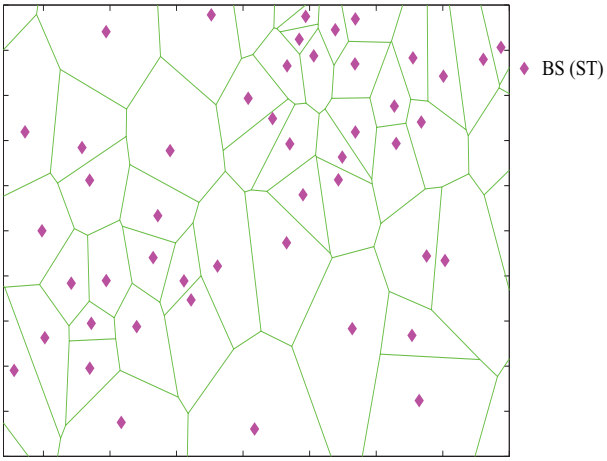

Figure 2.1: Cognitive BSs are located in the Voronoi cell and are distributed as a homogeneous PPP.

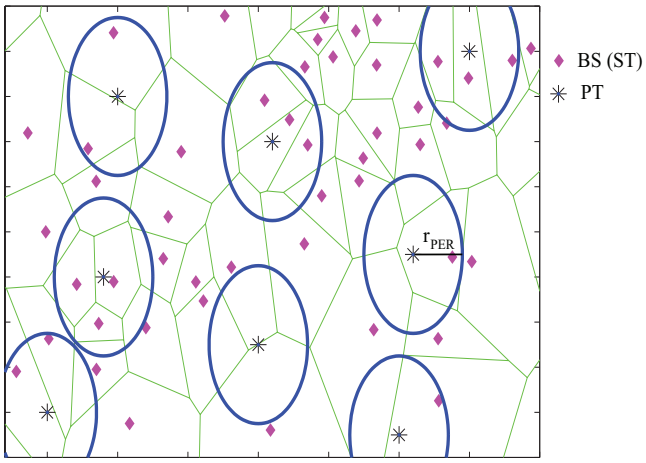

Figure 2.2: The CR network model with the STs and PTs.

cognitive BSs can use underlay CR networks, but they must be capable of strong spectrum sensing [45] capacity. All the cognitive BSs possess full information regarding the location of the primary transmitter-receiver pairs and their utilized spectrum, and of unoccupied spectrum as well. In this chapter, we consider an underlay CR network scheme (for such applications as development of a design framework for the IEEE 802.22-based wireless regional area networks [46]). Thus, strong spectrum sensing is required in each cognitive BSs. For simplicity of discussion, throughout this chapter cognitive BSs are denoted as secondary transmitters (STs) and their corresponding mobile users are denoted as secondary receivers (SRs). Also, the PTs and their corresponding receivers are denoted as PRs.

2.3 Network Deployment Model

2.3.1 Network Model

Here we consider the downlink scenario of a CR network model consisting of SUs (STs and SRs) and PUs (PTs and PRs), as shown in Fig. 2.3. All active STs and PTs are assumed to be spatially distributed according to the two-dimensional homogeneous PPPs Φ_{st} and Φ_{pt} with densities λ_s and λ_p, where λ_s and λ_p are the average number of STs and PTs per unit area. Consequently, the associated SRs and PRs are located in accordance with independent PPP Φ_{sr} and Φ_{pr} with densities λ_{sr}[4] and λ_{pr}[5]. The locations of STs, SRs, PTs and PRs are denoted by the coordinates $\Phi_{st} = \{c_i : c_i \in \mathbb{R}^2, \forall i\}$, $\Phi_{sr} = \{b_i : b_i \in \mathbb{R}^2, \forall i\}$,

[4]We consider the same density of STs and SRs for simple analysis. However, in practice the density of STs and SRs are not equal.

[5]In most recent studies, the same density is considered for both transmitters and receivers. Here, we consider different density.

$\Phi_{pt} = \{p_i : p_i \in \mathbb{R}^2, \forall i\}$ and $\Phi_{pr} = \{q_i : q_i \in \mathbb{R}^2, \forall i\}$. We assume here that all SUs transmit with the same power P_s and all PUs transmit with the same power P_p.

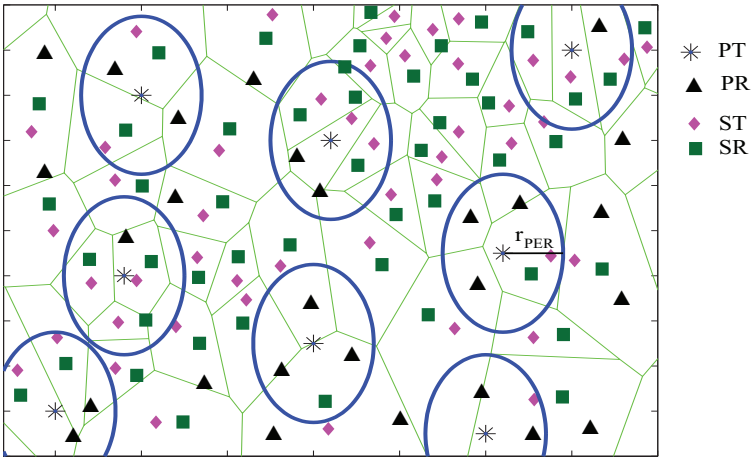

Figure 2.3: CR network model with SUs (i.e., STs and SRs) and PUs (i.e., PTs and PRs).

2.3.2 Timeslot Structure

PUs are the legitimate owners of the licensed channels (spectra), so PTs send data to the PRs utilizing whole channels or partial channels. When PUs are not using the licensed channels, the channels are unoccupied (vacant or idle). At that moment, SUs are allowed to use the unoccupied channels, but they must avoid collision with PUs. Since the PUs shown in Fig. 2.4 use their own licensed channels, spectrum sensing is not required. The PUs transmit their data in channels (e.g., channel 1, channel $n+1$, and other channels) referred to as occupied channels. The remaining channels are vacant, and are referred to as unoccupied channels. SUs utilize these unoccupied channels.

The SU frame (T_t) shown in Fig. 2.5 is divided into two parts: (1) SUs execute spectrum sensing at the beginning of each frame (known as sensing period) and detect unoccupied PUs channels during the time interval $[0, T_s]$. The SUs use spectrum sensing results to build a list of available (unoccupied) channels and decide on the best channel to be accessed; (2) based on the results of spectrum sensing, SUs transmit the data in the unoccupied channels during the time interval $[T_s, T_s + T_p]$. This period is called transmission period.

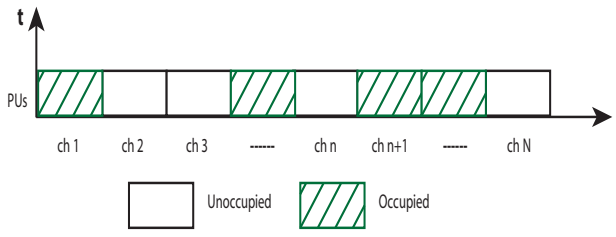

Figure 2.4: PU timeslot structure [49].

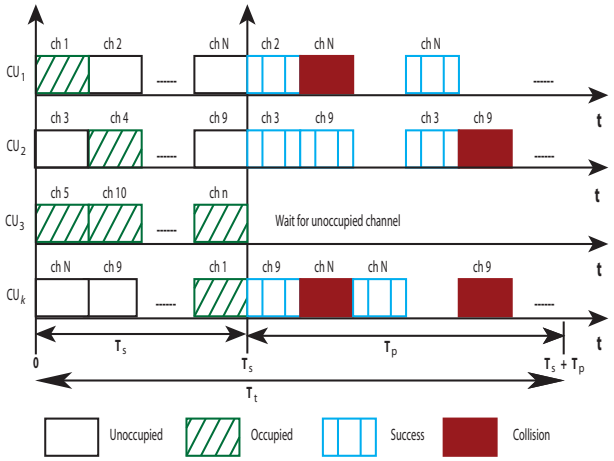

Figure 2.5: SU timeslot structure [49]. T_s and T_p represent the sensing period and the transmission period.

Spectrum sensing [45] is a significant issue in networks. During spectrum sensing, the SUs have knowledge of PTs-to-PRs and STs-to-SRs links and know their occupied and unoccupied channels. Two important parameters are needed to define the performance of spectrum sensing: probability of detection[6] and probability of false alarm[7]. When the probability of detection (P_d) is higher, the PUs are protected. On the other hand, when probability of false alarm (P_f) is low, SUs are more likely to use unoccupied channels. IEEE 802.22 committee decided that P_d is equal or above 0.9 for signal-to-noise ratio of -20 dB [47, 48].

Below we discuss the *probability of unoccupied channel selection* and the *probability of successful transmission*. For the purpose of spectrum sensing, SUs access the channels of PUs at the sensing period and determine which ones are unoccupied. So, the probability of selection of an unoccupied channel from an array of available channels is p_{ic}. For successful transmission, the slotted ALOHA protocol is used by STs, so the probability of successful transmission by STs is p_{st} in the present timeslot and the probability of deferred transmission is $1 - p_{st}$.

2.3.2.1 Probability of Unoccupied Channel Selection

Based on the above consideration, the *probability of unoccupied channel selection* can be classified in terms of the following assumptions:

(a) Perfect detection: Under perfect detection, $P_d = 1$ and $P_f = 0$. Assume that the total number of PUs channels (licensed channels) is N and the number of unoccupied channels is M. If each SU seeks out one of the M unoccupied PUs channels from among the

[6]Probability of detection is defined as $P_d := Pr\{\text{decision} = H_1 \mid H_1\}$ or, $1 - Pr\{\text{decision} = H_0 \mid H_0\}$; where H_0 and H_1 are the hypotheses of inexistent (not present) and existent (present) of a signal from a PU, respectively.

[7]Probability of false alarm is defined as $P_f := Pr\{\text{decision} = H_1 \mid H_0\}$.

N_s sensed channels ($N_s \leq N$) during the spectrum sensing period $[0, T_s]$, shown in Fig. 2.5, the *probability of unoccupied channel selection* (p_{ic}), i.e. selection of the vacant channel, can be expressed as follows [49]

$$p_{ic} = \begin{cases} \frac{1}{M}\left(1 - \frac{C(N-M,N_s)}{C(N,N_s)}\right), & \text{if } N_s \leq N - M \\ \frac{1}{M}, & \text{if } N_s \geq N - M + 1 \end{cases} \tag{2.3.1}$$

where $C(x, y)$ represents for y combinations of channels among a set of x channels.

(b) Imperfect detection: We now assume imperfect detection of unoccupied channels. This assumption holds if $P_d \neq 1$ and $P_f \neq 0$. Following this assumption, at initial the M_s unoccupied channels are found from the N_s sensed channels and then M_d unoccupied channels are identified correctly within the N_s channels.

The probability that a channel is scrutinized and included in the M_s unoccupied channels from N_s sensed channels can be expressed as [49]

$$Pr(\text{searched}) = \frac{C(M-1, M_s-1) \cdot C(N-M, N_s-M_s)}{C(N, N_s)}. \tag{2.3.2}$$

Next, the probability that an unoccupied channel is identified correctly as unoccupied can be expressed as [49]

$$\begin{aligned} Pr(\text{identified}) = &\sum_{m_{id}=\max(1,L_1)}^{\min(M_d,M_s)} C(M_s-1, m_{id}-1)(1-P_f)^{m_{id}} \cdot P_f^{M_s-m_{id}} \\ &\cdot C(N_s-M_s, M_d-m_{id}) \cdot (1-P_d)^{M_d-m_{id}} \cdot P_d^{N_s-M_s-M_d+m_{id}}, \end{aligned} \tag{2.3.3}$$

where $L_1 = M_d + M_s - N_s$. m_{id} is the number of unoccupied channels identified accurately can be expressed as $m_{id} \in [\max\{1, L_1\}, \min\{M_s, M_d\}]$.

Using eqs. (2.3.2) and (2.3.3), the *probability of unoccupied channel selection* ($p_{ic,im}$) can be expressed as [49]

$$p_{ic,im} = \sum_{M_s=\max(1,L_2)}^{\min(M,N_s)} \sum_{M_d=1}^{N_s} \frac{1}{M_d} \cdot Pr(\text{searched}) \cdot Pr(\text{identified}), \tag{2.3.4}$$

where $L_2 = M + N_s - N$.

2.3.2.2 Probability of Successful Transmission

Success of transmission depends on the success of the transmission of data in the unoccupied channel during the transmission period. In this situation, there are two types of outcome:

(a) Perfect detection: Under the assumption of perfect detection, $P_d = 1$ and $P_f = 0$ are considered. During the transmission period $[T_s, T_s + T_p]$ shown in Fig. 2.5, each SU applies the slotted ALOHA for the packet transmission. For successful transmission, two conditions must be fulfilled:

(a) each SU must utilize a unique unoccupied channel, for example, SU_1, SU_2 and SU_K use different channels 2, 3 and 9 in the first timeslot of transmission period in Fig. 2.5. This is the scenario of successful transmission. On the other hand, SU_1 and SU_K use the same channel N in the second timeslot of transmission period in Fig. 2.5. This is called collision.

(b) Neither SU could find an unoccupied channel during N_s channel sensing, so SU waits for the next spectrum sensing period.

Hence, STs send a single packet through the M unoccupied channels. Applying Bernoulli trail, the probability of successful transmission p_{st} in the transmission timeslot is expressed as

$$p_{st} = Mp_{ic}(1 - p_{ic})^{M-1}. \tag{2.3.5}$$

(b) Imperfect detection: Under imperfect detection, $P_d \neq 1$ and $P_f \neq 0$ are taken into account. Following the same procedure as that used for perfect detection, the probability of successful transmission $p_{st,im}$ in the transmission timeslot can be written as

$$p_{st,im} = Mp_{ic,im}(1 - p_{ic,im})^{M-1}. \tag{2.3.6}$$

Throughout this chapter, we assume the probability of perfect detection to be $p_p = p_{ic}p_{st}$ and that of imperfect detection to be $p_{im} = p_{ic,im}p_{st,im}$.

2.3.3 Channel Model

To an imitative spontaneous power-law path-loss model, transmission power decays at rate $\|r\|^{-\alpha}$ with propagation distance $\|r\|$ and path-loss exponent α, which is varied from 2 to 5. $\|\cdot\|$ is the Euclidean distance. Throughout this chapter, we use distance r for simple notation. The channel gain from PT to its corresponding PR is denoted by h_p and the channel gain from ST to its corresponding SR is denoted by h_s. Channel gains follow $h_p \sim \exp(\mu_p)$ and $h_c \sim \exp(\mu_s)$ with mean $1/\mu_p$ and $1/\mu_s$.

According to the system model, each PR receives a signal with distance (r_p) from the nearest PT. There is no PT which is nearer than r_p. In other words, all the interfering PT are at a distance greater than r_p. The cumulative distribution function (cdf) of r_p, derived for this network over a circular area (πR^2), can be written as

$$\begin{aligned} F_{r_p}(R) &= \mathbb{P}\left[r_p < R\right] \\ &= 1 - \mathbb{P}\left[r_p > R\right] \\ &= 1 - \mathbb{P}\left[\text{No PT in the circle of area } \pi R^2\right] \\ &= 1 - \exp(-\lambda\pi R^2). \end{aligned} \tag{2.3.7}$$

By differentiating cdf with respect to distance we obtain the probability density function (pdf) over the same area

$$f_{r_p}(r_p) = \frac{dF_{r_p}(r_p)}{dr_p} = 2\pi\lambda_p r_p \exp(-\lambda_p \pi r_p^2). \tag{2.3.8}$$

Following the same procedure, the pdf of r_s between the ST and SR was derived for this network over a circular area and expressed as

$$f_{r_s}(r_s) = 2\pi\lambda_s r_s \exp(-\lambda_s \pi r_s^2). \tag{2.3.9}$$

2.4 Analysis of Outage Probability and Energy Efficiency

Interference is one of the main problems in networks because both SUs and PUs use the same channels. The interference with SRs and PRs is considered individually here. For each case, interference by the STs and PTs occurs at the SRs and PRs. As mentioned in [31], four types of interference occur: (a) I_{pp} is the interference at the position of the PR transmitted from the PTs; (b) I_{ps} is the interference at the position of the PR transmitted from the STs; (c) I_{ss} is the interference at the position of the SR transmitted from the STs and (d) I_{sp} is the interference at the position of the SR transmitted from the PTs. In the case of PUs, the interferences I_{pp} and I_{ps} are explained in detail in **lemma** 1 and 2 and their proofs are provided in Appendix A. As for SUs, the interferences I_{ss} and I_{sp} are explained in detail in **lemma** 3 and 4 and their proofs are provided in Appendix A.

2.4.1 Outage Probability of PR

In CR network scenario downlink, outage probability depends on the signal-to-interference-plus-noise-ratio (SINR) of the PR. The PR is located at the origin. The SINR of the PR at a distance r_p from the PT can be expressed as

$$\text{SINR} = \frac{P_p h_p r_p^{-\alpha}}{I_{pp} + I_{ps} + \sigma^2}, \tag{2.4.1}$$

where P_p is the transmission power of PT, h_p is the channel gain between PT and corresponding PR, and σ^2 is the noise power.

A PR successfully receives a packet when its SINR is larger than the target threshold θ_p and drops from the CR network when its SINR is below than the target threshold. Thus

coverage probability can be expressed by the relation

$$\begin{aligned}
\mathbb{P}\left[\text{SINR} > \theta_p\right] &= \mathbb{P}\left[\frac{P_p h_p r_p^{-\alpha}}{I_{pp} + I_{ps} + \sigma^2} > \theta_p\right] \\
&= \mathbb{P}\left[h_p > \frac{(I_{pp} + I_{ps} + \sigma^2)\theta_p r_p^{\alpha}}{P_p}\right] \\
&= \mathbb{E}_{I_{pp,ps}}\left[\mathbb{P}\left[h_p > \frac{(I_{pp} + I_{ps} + \sigma^2)\theta_p r_p^{\alpha}}{P_p}\right]\right] \\
&\overset{(i)}{=} \mathbb{E}_{I_{pp,ps}}\left[\exp\left[-\mu_p \frac{(I_{pp} + I_{ps} + \sigma^2)\theta_p r_p^{\alpha}}{P_p}\right]\right] \\
&= \exp\left[-\sigma^2 s_p\right] \mathbb{E}_{I_{pp}}\left[\exp\left[-I_{pp} s_p\right]\right] \mathbb{E}_{I_{ps}}\left[\exp\left[-I_{ps} s_p\right]\right] \\
&\overset{(ii)}{=} \exp\left[-\sigma^2 s_p\right] \mathcal{L}_{I_{pp}}\left[s_p\right] \mathcal{L}_{I_{ps}}\left[s_p\right] \\
&\overset{(iii)}{=} \mathcal{L}_{I_{pp}}\left[s_p\right] \mathcal{L}_{I_{ps}}\left[s_p\right], \qquad (2.4.2)
\end{aligned}$$

where $s_p = \mu_p \theta_p r_p^{\alpha} P_p^{-1}$. The equality (i) follows the exponential function discussed in the section on channel model (**2.3.3**). (ii) follows the Laplace transform[8]. (iii) follows the interference-limited[9] since noise power is neglected ($I_{pp} + I_{ps} >> \sigma^2$).

For the distance r_p between the PT and its corresponding PR, outage probability can be expressed as

$$\begin{aligned}
\epsilon_p &= 1 - \mathbb{P}\left[\text{SINR} > \theta_p\right] \\
&= 1 - \int_0^{\infty} \mathbb{P}\left[\text{SINR} > \theta_p\right] f_{r_p}(r_p) dr_p \\
&= 1 - \int_0^{\infty} 2\pi\lambda_p r_p \exp(-\lambda_p \pi r_p^2) \mathcal{L}_{I_{pp}}\left[s_p\right] \mathcal{L}_{I_{ps}}\left[s_p\right] dr_p. \qquad (2.4.3)
\end{aligned}$$

Lemma 1. *The Laplace transform $\mathcal{L}_{I_{pp}}$ of the pdf of total interference I_{pp} experienced at the PR when signal is transmitted from the PT is given by*

$$\mathcal{L}_{I_{pp}}(s_p) = \exp\left\{\lambda_p^{'} b_d r_p^d - (\frac{d}{\alpha})\lambda_p^{'} b_d (\mu_p \theta_p r_p^{\alpha})^{\frac{d}{\alpha}} \left[(g_p)^{\frac{d}{\alpha}} V(\theta_p, \alpha)\right]\right\},$$

where $V(\theta_p, \alpha) = \Gamma(-d/\alpha, \mu_p \theta_p g_p) - \Gamma(-d/\alpha)$, $\lambda_p^{'}$ is the density of all PTs located in the area $\mathbb{R}^d \setminus b(0, r_p)$, $b(a, b)$ is a sphere of radius b centered at point a, b_d is the d-dimensional volume of a unit sphere, and g_p is the interference channel gain between tagged PR and interfering PT.

[8]The Laplace transform $\mathcal{L}$ for the pdf of interference z between the receiver and interfering transmitters can be written as $\mathcal{L}_z(s) = \mathbb{E}[\exp(-sz)]$.

[9]If overall system performance is dominated by interference, the scenario is referred to as interference-limited.

Proof: The proof is detailed in Appendix A (**A.1**).

Lemma 2. *The Laplace transform $\mathcal{L}_{I_{ps}}$ of the pdf of total interference I_{ps} experienced at the PR when signal is transmitted from the ST is given by*

$$\mathcal{L}_{I_{ps}}(s_p) = \exp\left\{\lambda_s b_d p_{im} r_{PER}^d - (\frac{d}{\alpha})\lambda_s b_d p_{im}(\mu_p\theta_p r_p^\alpha P_p^{-1}P_s)^{\frac{d}{\alpha}}\left[(g_s)^{\frac{d}{\alpha}}W(\theta_p,\alpha)\right]\right\},$$

where $W(\theta_p,\alpha) = \Gamma(-d/\alpha, \mu_p\theta_p g_s P_s P_p^{-1} r_p^\alpha r_{PER}^{-\alpha}) - \Gamma(-d/\alpha)$, $p_{im} = p_{ic,im}p_{st,im}$, r_{PER} is the radius of PER, and g_s is the interference channel gain between tagged PR and interfering ST.

Proof: The proof is detailed in Appendix A (**A.2**).

If lemma 1 and lemma 2 are substituted in eq. (2.4.3) and then the integration is performed, the result can be expressed as

$$\epsilon_p = 1 - \int_0^\infty 2\pi\lambda_p r_p \exp(-\lambda_p\pi r_p^2)\exp\left\{\lambda_p^{'} b_d r_p^d - (\frac{d}{\alpha})\lambda_p^{'} b_d(\mu_p\theta_p r_p^\alpha)^{\frac{d}{\alpha}}(g_p)^{\frac{d}{\alpha}}V(\theta_p,\alpha)\right\}$$
$$\exp\left\{\lambda_s b_d p_{im} r_{PER}^d - (\frac{d}{\alpha})\lambda_s b_d p_{im}(\mu_p\theta_p r_p^\alpha P_p^{-1}P_s)^{\frac{d}{\alpha}}(g_s)^{\frac{d}{\alpha}}W(\theta_p,\alpha)\right\} dr_p. \tag{2.4.4}$$

We assume that $r_{PER} = \beta r_p$, where β is a constant parameter and depends on the cell radius. Then plugging in the value $d = 2$, $b_2 = \pi$, and replacing r_p^2 with z yields that eq. (2.4.4). We obtain the outage probability of the tagged PR as follows

$$\epsilon_p = 1 - \int_0^\infty \pi\lambda_p \exp(-\lambda_p\pi z)\exp\left\{\lambda_p^{'}\pi z - (\frac{2}{\alpha})\lambda_p^{'}\pi(\mu_p\theta_p g_p)^{\frac{2}{\alpha}}V(\theta_p,\alpha)z\right\}$$
$$\exp\left\{\lambda_s\pi p_{im}\beta^2 z - (\frac{2}{\alpha})\lambda_s\pi p_{im}(\mu_p\theta_p P_p^{-1}P_s g_s)^{\frac{2}{\alpha}}W_b(\theta_p,\alpha,\beta)z\right\} dz$$
$$= 1 - \frac{\lambda_p}{\lambda_p - \lambda_p^{'} - \lambda_s p_{im}\beta^2 + (\frac{2}{\alpha})\left[\lambda_p^{'}\nu_p + \lambda_s p_{im}\nu_s\right]}, \tag{2.4.5}$$

where $W_b(\theta_p,\alpha,\beta) = \Gamma(-2/\alpha, \mu_p\theta_p g_s P_s P_p^{-1}\beta^{-\alpha}) - \Gamma(-2/\alpha)$, $\nu_p = (\mu_p\theta_p g_p)^{\frac{2}{\alpha}}V(\theta_p,\alpha)$, $\nu_s = (\mu_p\theta_p P_p^{-1}P_s g_s)^{\frac{2}{\alpha}}W_b(\theta_p,\alpha,\beta)$ and $p_{im} = p_{ic,im}p_{st,im}$.

2.4.2 Outage Probability of SR

The SUs are unlicensed users in this network, so they need spectrum sensing to determine whether each channel is occupied or not. To obtain the knowledge of occupancy, SUs are allowed to transmit signals in the licensed spectrum. The SR is located at the origin. In this network, the SINR of SR is defined as

$$\text{SINR} = \frac{P_s h_s r_s^{-\alpha}}{I_{ss} + I_{sp} + \sigma^2}, \tag{2.4.6}$$

where P_s is the transmission power at distance r_s between the ST and SR, σ^2 is the noise power, and h_s is the channel gain between ST and SR.

The coverage probability for a SR is defined as the probability that the SINR of the tagged SR is greater than the threshold θ_s. Therefore coverage probability can be expressed as

$$\begin{aligned}\mathbb{P}\left[\text{SINR} > \theta_s\right] &= \mathbb{P}\left[\frac{P_s h_s r_s^{-\alpha}}{I_{ss} + I_{sp} + \sigma^2} > \theta_s\right] \\ &\overset{(i)}{=} \mathbb{E}_{I_{ss,sp}}\left[\exp\left[-\mu_s \frac{(I_{ss} + I_{sp} + \sigma^2)\theta_s r_s^{\alpha}}{P_s}\right]\right] \\ &\overset{(ii)}{=} \exp\left[-\sigma^2 s_s\right] \mathcal{L}_{I_{ss}}\left[s_s\right] \mathcal{L}_{I_{sp}}\left[s_s\right] \\ &\overset{(iii)}{=} \mathcal{L}_{I_{ss}}\left[s_s\right] \mathcal{L}_{I_{sp}}\left[s_s\right], \end{aligned} \tag{2.4.7}$$

where $s_s = \mu_s \theta_s r_s^{\alpha} P_s^{-1}$. The equalities (i), (ii) and (iii) follow the same rule as in eq. (2.4.7). Following the SINR expression, the outage probability of SR is given by

$$\begin{aligned}\epsilon_s &= 1 - \mathbb{P}\left[\text{SINR} > \theta_s\right] \\ &= 1 - \int_0^{\infty} 2\pi\lambda_s r_s \exp(-\lambda_s \pi r_s^2) \mathcal{L}_{I_{ss}}\left[s_s\right] \mathcal{L}_{I_{sp}}\left[s_s\right] dr_s, \end{aligned} \tag{2.4.8}$$

where $\mathcal{L}_{I_{ss}}$ and $\mathcal{L}_{I_{sp}}$ are the Laplace transforms of the pdf of the interference at the SR signal transmitting from the STs and PTs, respectively.

According to the spectrum sensing[10] and control channel[11], the following assumptions in this model are interpreted in detail as follows.

(a) Perfect detection of existence of PTs and STs: In a CR setup with spectrum sensing and control channel, tagged ST can accurately determine whether or not PTs and STs are using the licensed channels. Thus, $P_d = 1$ and $P_f = 0$ are assumed for both users (i.e., PTs and STs). This assumption is represented as P.D.(PTs-STs).

(b) Perfect detection of existence of PTs and imperfect detection of existence of STs: With spectrum sensing, tagged ST can accurately determine when PTs are using licensed channels, so it is sufficient to consider $P_d = 1$ and $P_f = 0$. However, tagged ST can't identify when other STs are using licensed channels, so it is sufficient to consider $P_d \neq 1$ and $P_f \neq 0$. This assumption can be represented as P.D.(PTs)-I.D.(STs).

(c) Imperfect detection of existence of PTs and perfect detection of existence of STs: With the spectrum sensing, tagged ST can't accurately determine when PTs are using licensed channels, so it is considered $P_d \neq 1$ and $P_f \neq 0$. However, tagged ST accurately identifies when other STs are using the licensed channels, so it is considered $P_d = 1$ and $P_f = 0$. This assumption represents as I.D.(PTs)-P.D.(STs).

[10] During the sensing period, PTs are detected and also identified their unoccupied channels.

[11] STs and SRs communicate through control channel and the existence of STs identify when they are using licensed channels with the help of control channel.

(d) Imperfect detection of existence of PTs and STs: With spectrum sensing and control channel, tagged ST can't determine whether or not PTs and STs are using the licensed channels. Thus, the $P_d \neq 1$ and $P_f \neq 0$ are assumed for both users (i.e., PTs or STs). This assumption is represented as I.D.(PTs-STs).

(a) P.D.(PTs-STs): Each ST has full knowledge of both links (i.e., PTs-to-PRs and STs-to-SRs). For this reason, tagged SR does not receive interference from PTs and STs during the data transmission in each timeslot. The Laplace transform $\mathcal{L}_{I_{sp}}[s_s]$ of interference from PTs to tagged SR and that of $\mathcal{L}_{I_{ss}}[s_s]$ from STs to tagged SR has a value of 1.

With the following assumption in eq. (2.4.8), the outage probability of SR can be reduced as

$$\begin{aligned}\epsilon_s^{(a)} &= 1 - \int_0^\infty 2\pi\lambda_s r_s \exp(-\lambda_s \pi r_s^2) dr_s \\ &= 0. \end{aligned} \tag{2.4.9}$$

(b) P.D.(PTs)-I.D.(STs): Each ST has full knowledge of occupied channel in PTs-to-PRs links. So the tagged SR does not experience interference by the PTs during the data transmission in each timeslot. The Laplace transform $\mathcal{L}_{I_{sp}}[s_s]$ of interference from PTs to tagged SR has a value of 1. On the other hand, tagged SR is experienced the interference by the STs because of incomplete knowledge of occupied STs-to-SRs channel. Therefore, the Laplace transform $\mathcal{L}_{I_{ss}}[s_s]$ of interference from STs to tagged SR is not equal to 1.

Lemma 3. *The Laplace transform $\mathcal{L}_{I_{ss}}$ of the pdf of total interference I_{ss} experienced at the SR when signal is transmitted from the ST is given by*

$$\mathcal{L}_{I_{ss}}(s_s) = \exp\left\{ \lambda_s^{'} b_d p_{im} r_s^d - (\frac{d}{\alpha}) \lambda_s^{'} b_d p_{im} (\mu_s \theta_s r_s^\alpha)^{\frac{d}{\alpha}} \left[(G_s)^{\frac{d}{\alpha}} X(\theta_s, \alpha) \right] \right\},$$

where $X(\theta_s, \alpha) = \Gamma(-d/\alpha, \mu_s \theta_s G_s) - \Gamma(-d/\alpha)$ and $p_{im} = p_{ic,im} p_{st,im}$. G_s is the interference channel gain between tagged SR and interfering ST.

Proof: The proof is detailed in Appendix A (**A.3**).

The outage probability of a tagged SR from its transmitting ST is given by

$$\epsilon_s^{(b)} = 1 - \int_0^\infty 2\pi\lambda_s r_s \exp(-\lambda_s \pi r_s^2) \mathcal{L}_{I_{ss}}[s_s]\, dr_s. \tag{2.4.10}$$

If the values $d = 2$ and $b_2 = \pi$ are applied in eq. (2.4.10), the outage probability of SR transmitted by a ST is obtained in eq. (2.4.11)

(c) I.D.(PTs)-P.D.(STs): Each ST has no full knowledge of the PTs-to-PRs channel, so the Laplace transform $\mathcal{L}_{I_{sp}}[s_s]$ of interference from PTs to tagged SR is not 1. On the other hand, tagged SR does not experience interference from the STs because of perfect knowledge of the STs-to-SRs channel. Therefore, the value of the Laplace transform $\mathcal{L}_{I_{ss}}[s_s]$ of interference from STs to tagged SR is 1.

$$\epsilon_s^{(b)} = 1 - \int_0^\infty 2\pi\lambda_s r_s \exp\left\{-\lambda_s\pi r_s^2 + \lambda_s^{'}\pi p_{im} r_s^2 - (\frac{2}{\alpha})\lambda_s^{'}\pi p_{im}(\mu_s\theta_s G_s)^{\frac{2}{\alpha}} X(\theta_s,\alpha) r_s^2\right\} dr_s$$
$$= 1 - \frac{\lambda_s}{\lambda_s - \lambda_s^{'} p_{im} + (\frac{2}{\alpha})\lambda_s^{'} p_{im}(\mu_s\theta_s)^{\frac{2}{\alpha}}(G_s)^{\frac{2}{\alpha}} X(\theta_s,\alpha)}. \quad (2.4.11)$$

Lemma 4. *The Laplace transform $\mathcal{L}_{I_{sp}}$ of the pdf of total interference I_{sp} experienced at the SR when signal is transmitted from the PT is given by*

$$\mathcal{L}_{I_{sp}}(s_s) = \exp\left\{-\lambda_p b_d p_{ic,pt}(\mu_s\theta_s r_s^\alpha P_s^{-1} P_p G_p)^{\frac{d}{\alpha}}\Gamma(1-d/\alpha)\right\},$$

where G_p is the interference channel gain between tagged SR and interfering PT. $p_{ic,pt}$ is the probability of selection of an unoccupied channel from total no. of PUs channels.

Proof: The proof is detailed in Appendix A (**A.4**).

In line with assumption (c), we put the values $d = 2$ and $b_2 = \pi$ in eq. (2.4.8). The outage probability of SR transmitted by ST is expressed as

$$\epsilon_s^{(c)} = 1 - \int_0^\infty 2\pi\lambda_s r_s \exp\left\{-\lambda_s\pi r_s^2 - \lambda_p\pi p_{ic,pt}(\mu_s\theta_s P_s^{-1} P_p G_p)^{\frac{2}{\alpha}}\Gamma(1-2/\alpha) r_s^2\right\} dr_s$$
$$= 1 - \frac{\lambda_s}{\lambda_s + \lambda_p p_{ic,pt}(\mu_s\theta_s P_s^{-1} P_p)^{\frac{2}{\alpha}}(G_p)^{\frac{2}{\alpha}}\Gamma(1-2/\alpha)}. \quad (2.4.12)$$

(d) I.D.(PTs-STs): Each ST has no full knowledge of PTs-to-PRs and STs-to-SRs links. Thus the expected interference I_{sp} and I_{ss} is experienced at tagged SR from all PTs and STs. For this reasons, $\mathcal{L}_{I_{sp}}[s_s] \neq 1$ and $\mathcal{L}_{I_{ss}}[s_s] \neq 1$. Using lemma 3 and lemma 4, we can obtain the outage probability of SR using eq. (2.4.8)

$$\epsilon_s^{(d)} = 1 - \int_0^\infty 2\pi\lambda_s r_s \exp(-\lambda_s\pi r_s^2)\exp\left\{\lambda_s^{'} b_d p_{im} r_s^d - (\frac{d}{\alpha})\lambda_s^{'} b_d p_{im}(\mu_s\theta_s r_s^\alpha)^{\frac{d}{\alpha}}(G_s)^{\frac{d}{\alpha}} X(\theta_s,\alpha)\right\}$$
$$\exp\left\{-\lambda_p b_d p_{ic,pt}(\mu_s\theta_s r_s^\alpha P_s^{-1} P_p G_p)^{\frac{d}{\alpha}}\Gamma(1-d/\alpha)\right\} dr_s. \quad (2.4.13)$$

We consider that $d = 2$, and $b_2 = \pi$. Using eq. (2.4.13), the outage probability can be written as

$$\epsilon_s^{(d)} = 1 - \frac{\lambda_s}{a + \lambda_p p_{ic,pt}(\mu_s\theta_s P_s^{-1} P_p)^{\frac{2}{\alpha}}(G_p)^{\frac{2}{\alpha}}\Gamma(1-2/\alpha)}, \quad (2.4.14)$$

where $a = \lambda_s - \lambda_s^{'} p_{im} + (\frac{2}{\alpha})\lambda_s^{'} p_{im}(\mu_s\theta_s)^{\frac{2}{\alpha}}(G_s)^{\frac{2}{\alpha}} X(\theta_s,\alpha)$.

2.4.3 Energy- and Area Spectral Efficiency

In this subsection, we introduce the theoretical relationship between energy efficiency and area spectral efficiency (network throughput) in CR networks. As well, a similar definition of energy efficiency in terms of area spectral efficiency is analyzed in [40,50] for the cellular

networks. The energy efficiency ratio (known as energy efficiency (η_{EE})) is used as a performance metric for cellular networks. It is proportional to area spectral efficiency and inverse to network power consumption. Thus, energy efficiency can be defined as

$$\begin{aligned}\eta_{EE} &= \frac{\text{Area spectral efficiency}}{\text{Average network power consumption}} \\ &= \frac{\eta_{ASE}}{\lambda P^s_{PC}}, \qquad \text{(b/s/Hz/W) or (b/J/Hz)}\end{aligned} \tag{2.4.15}$$

where λ is the density of users (i.e., STs and PTs). η_{ASE} is the area spectral efficiency over all the links in the cellular network, defined as $\lambda(1-\epsilon)\log_2(1+\theta)$. ϵ and θ are the outage probability and target threshold, respectively. P^s_{PC} denotes ST (cognitive BS) power consumption.

This model of the power consumption of ST [51, 52] has an approximately linear relationship between radio frequency (RF) output power (P_{RFop}) and overall ST power consumption (P^s_{PC}). This power consumption model is rearranged according to the sensing and transmission time (period) [53] and is given by

$$P^s_{PC} = N_{TRX}P_oT_t + p_{ic,im}p_{st,im}\Delta_c P_{RFop}T_p + P_{sp}T_s + P_rT_p, \tag{2.4.16}$$

where $T_t = T_s + T_p$. T_s is the sensing period. T_p is the transmission period. P_{sp} is the power consumption during the sensing period. P_r is the retransmit power for the collision shown in Fig. 2.5. N_{TRX} is the number of transceivers[12]. P_o is the non-load-dependent power consumption at non-zero output power, which depends on the circuit power consumption of four types of BS (e.g., macro, micro, pico and femto). Δ_s is the slope of load-dependent power consumption, based on the transmission power consumed in the RF transmission circuits for four types of BS. P_{RFop} is the total RF output power at the antenna. In the above discussion, we observed that P_o and Δ_s are fixed for any given BSs. We can verify two aspects (i.e., N_{TRX} and P_{RFop}) for use in the design of an energy efficiency network. We assume that $P_{RFop} = P_s$ and $P_r = P_s$ for the ST. By substituting eq. (2.4.16) into eq. (2.4.15), the energy efficiency is given by

$$\eta_{EE} = \frac{(1-\epsilon)\log_2(1+\theta)}{N_{TRX}P_oT_t + p_{ic,im}p_{st,im}\Delta_s P_sT_p + P_{sp}T_s + P_rT_p}. \tag{2.4.17}$$

Since there are two categories of network (i.e. PN and SN), we can calculate the energy efficiency for the individual network or combined network. Hereafter, we use the method most likely to succeed to evaluate the relationship between energy efficiency and area spectral efficiency. We selected the following scenario of energy efficiency in CR networks.

2.4.3.1 Energy Efficiency for PN

The PN is comprised of PTs, PRs and STs where the PT data is delivered to all PRs within a range and STs are subjected to interference in this network. Each PR receives the signal

[12]A ST is assumed as a cognitive BS. Each cognitive BS has comprised of multiple transceivers. A transceiver consists of a transmitter and a receiver for downlink and uplink communication.

from the nearest PT. So the energy efficiency for the downlink channel is expressed as

$$\eta_{EE}^{PU} = \frac{(1-\epsilon_p)\log_2(1+\theta_p)}{p_{ic,pt}P_p + P_{PC}^p} = \frac{\lambda_p \log_2(1+\theta_p)}{\left\{\lambda_p - \lambda_p' - \lambda_c p_{im}\beta^2 + (\frac{2}{\alpha})\left[\lambda_p'\nu_p + \lambda_s p_{im}\nu_s\right]\right\}\mathbb{P}_{PC}^p}. \tag{2.4.18}$$

where $\mathbb{P}_{PC}^p = p_{ic,pt}P_p + P_{PC}^p$, $\nu_p = (\mu_p\theta_p g_p)^{\frac{2}{\alpha}}V(\theta_p,\alpha)$, $\nu_s = (\mu_p\theta_p P_p^{-1}P_s g_s)^{\frac{2}{\alpha}}W_b(\theta_p,\alpha,\beta)$ and P_{PC}^p is the constant circuit power consumption in PT.

In the context of CR networks, PTs are licensed users of the channels. Depending on the utilization of SUs in this network, the number of PTs are variable. The SUs share the channel with PUs based on unoccupied channel through spectrum sensing. For instance, if the SUs share the FM radio spectrum, the FM station under consideration in this case is PT. From a different standpoint, SUs share the TV spectrum, so the TV station under consideration is PT. Hence, PTs are variable in terms of SU transmission policy. For simulation purposes, we consider $P_{PC}^p = 50$ kW [54].

2.4.3.2 Energy Efficiency for SN

The SN is comprised of STs, SRs and PTs. In the investigation of the energy efficiency of SN, we take the four cases already examined regarding spectrum sensing in section **2.4.2**. Then spectrum sensing must impact on energy efficiency and area spectral efficiency in this network. Here, we will derive a theoretical expression for the relationship between energy efficiency and area spectral efficiency. The power consumption (P_{PC}^s) of ST is applied in the eq. (2.4.17) for the four assumptions in this section. Then, the energy efficiency in the four assumptions is as follows:

(a) P.D.(PTs-STs): In the network, ST is able to find an unoccupied channel with the help of spectrum sensing. At the initial, STs require the power for spectrum sensing. After the fruitful detection of unoccupied channel, STs do not require the spectrum sensing. Due to the perfect detection of PTs, spectrum sensing power is negligible compared with imperfect detection of PTs. So, it is necessary to consider $P_{sp} = 0$. For the accurate detection of STs, there is no collision for transmission. So, we consider $P_r = 0$. It is clear from eq. (2.4.9) that the outage probability is zero for perfect detection. We can then write the energy efficiency expression based on eq. (2.4.17) as follows:

$$\eta_{EE}^{(a)} = \frac{(1-\epsilon_s^{(a)})\log_2(1+\theta_s)}{N_{TRX}P_oT_t + p_{ic,im}p_{st,im}\Delta_s P_s T_p} = \frac{\log_2(1+\theta_s)}{N_{TRX}P_oT_t + p_{ic,im}p_{st,im}\Delta_s P_s T_p}. \quad \text{(b/J/Hz)} \tag{2.4.19}$$

(b) P.D.(PTs)-I.D.(STs): In this case, we assume $P_{sp} = 0$ because STs have knowledge of the PTs-to-PRs link, but $P_r \neq 0$ because STs have no awareness of the STs-to-SRs link. Sometimes collision is occurred due to chosen same timeslot. For this condition, the

outage probability is given by eq. (2.4.11). By combining eqs. (2.4.11) and (2.4.17), the energy efficiency can be described as

$$\eta_{EE}^{(b)} = \frac{(1-\epsilon_s^{(b)})\log_2(1+\theta_s)}{N_{TRX}P_oT_t + p_{ic,im}p_{st,im}\Delta_s P_sT_p + P_sT_p}$$
$$= \frac{\lambda_s \log_2(1+\theta_s)}{\left\{\lambda_s - \lambda_s' p_{im} + (\frac{2}{\alpha})\lambda_s' p_{im}(\mu_s\theta_s)^{\frac{2}{\alpha}}(G_s)^{\frac{2}{\alpha}}X(\theta_s,\alpha)\right\}\mathbb{P}^{(b)}}. \quad \text{(b/J/Hz)} \quad (2.4.20)$$

where $\mathbb{P}^{(b)} = N_{TRX}P_oT_t + p_{ic,im}p_{st,im}\Delta_c P_sT_p + P_sT_p$.

(c) I.D.(PTs)-P.D.(STs): In this situation, STs have a knowledge of the STs-to-SRs link, they are not aware of the PTs-to-PRs link. So we assume $P_{sp} \neq 0$ and $P_r = 0$. The outage probability expression is given by eq. (2.4.12). By substituting eq. (2.4.12) into eq. (2.4.17), we get the energy efficiency expression as

$$\eta_{EE}^{(c)} = \frac{(1-\epsilon_s^{(c)})\log_2(1+\theta_s)}{N_{TRX}P_oT_t + p_{ic,im}p_{st,im}\Delta_s P_sT_p + P_{sp}T_s}$$
$$= \frac{\lambda_s \log_2(1+\theta_s)}{\left\{\lambda_s + \lambda_p p_{ic,pt}(\mu_s\theta_s P_s^{-1}P_p)^{\frac{2}{\alpha}}(G_p)^{\frac{2}{\alpha}}\Gamma(1-2/\alpha)\right\}\mathbb{P}^{(c)}}. \quad \text{(b/J/Hz)} \quad (2.4.21)$$

where $\mathbb{P}^{(c)} = N_{TRX}P_oT_t + p_{ic,im}p_{st,im}\Delta_s P_sT_p + P_{sp}T_s$.

(d) I.D.(PTs-STs): In this case, STs have no awareness of either links, so the STs have imperfect sensing of the unoccupied channel whether or not SUs are using the licensed channel. In this situation more interference arises due to wrong spectrum sensing. By combining eqs. (2.4.14) and (2.4.17), the energy efficiency can be calculated as

$$\eta_{EE}^{(d)} = \frac{(1-\epsilon_s^{(d)})\log_2(1+\theta_s)}{N_{TRX}P_oT_t + p_{ic,im}p_{st,im}\Delta_s P_sT_p + P_{sp}T_s + P_sT_p}$$
$$= \frac{\lambda_s \log_2(1+\theta_s)}{\left\{a + \lambda_p p_{ic,pt}(\mu_s\theta_s P_s^{-1}P_p)^{\frac{2}{\alpha}}(G_p)^{\frac{2}{\alpha}}\Gamma(1-2/\alpha)\right\}\mathbb{P}_{PC}^{s}}, \text{ (b/J/Hz)} \quad (2.4.22)$$

where $a = \lambda_s - \lambda_s' p_{im} + (\frac{2}{\alpha})\lambda_s' p_{im}(\mu_s\theta_s)^{\frac{2}{\alpha}}(G_s)^{\frac{2}{\alpha}}X(\theta_s,\alpha)$ and $\mathbb{P}^{(d)} = N_{TRX}P_oT_t$ $+ p_{ic,im}p_{st,im}\Delta_s P_sT_p + P_{sp}T_s + P_sT_p$.

2.4.3.3 Energy Efficiency for PN and SN

Herein we consider both PN and SN for analyzing energy efficiency and area spectral efficiency. Given the energy efficiency of SN, we make four assumptions for spectrum sensing conditions. As a result, spectrum sensing must have an influence on the maximizing or the minimizing of energy efficiency in this network. Our assumptions regarding the network are

as follows.

$$\eta_{EE}^{A} = \eta_{EE}^{PU} + \eta_{EE}^{(a)}. \qquad \text{(b/J/Hz)} \tag{2.4.23}$$

$$\eta_{EE}^{B} = \eta_{EE}^{PU} + \eta_{EE}^{(b)}. \qquad \text{(b/J/Hz)} \tag{2.4.24}$$

$$\eta_{EE}^{C} = \eta_{EE}^{PU} + \eta_{EE}^{(c)}. \qquad \text{(b/J/Hz)} \tag{2.4.25}$$

$$\eta_{EE}^{D} = \eta_{EE}^{PU} + \eta_{EE}^{(d)}. \qquad \text{(b/J/Hz)} \tag{2.4.26}$$

2.4.4 Transmit Antenna Selection of ST

In this subsection, we investigate transmit antenna selection (TAS) by STs in SR network. TAS technique can minimize hardware cost and complexity, but the ST requires channel-state information from the SR via the feedback channel [55]. In this network, we consider that the transmitting antenna is N_t at the ST (cognitive BS) and receiving antenna is single at the SR. In the TAS scheme, the permitted (selected) antenna is active for transmission at the ST. For the active antennas N_t, the outage probability for the I.D.(PTs-STs) using eq. (2.4.14) can be expressed as

$$\epsilon_s^{(d)} = \left[1 - \frac{\lambda_s}{a + \lambda_p p_{ic,pt} (\mu_s \theta_s P_s^{-1} P_p)^{\frac{2}{\alpha}} (G_p)^{\frac{2}{\alpha}} b}\right]^{N_t}, \tag{2.4.27}$$

where $a = \lambda_s - \lambda_s^{'} p_{im} + (\frac{2}{\alpha}) \lambda_s^{'} p_{im} (\mu_s \theta_s)^{\frac{2}{\alpha}} (G_s)^{\frac{2}{\alpha}} X(\theta_s, \alpha)$ and $b = \Gamma(1 - 2/\alpha)$.

We can obtain the minimum transmit power P_s^* for a particular outage probability using eq. (2.4.27), and P_s^* can be expressed as

$$P_s^*(N_t) = \mu_s \theta_s P_p \left[\frac{1}{\lambda_p p_{ic,pt} (G_p)^{\frac{2}{\alpha}} b} \left(\frac{\lambda_s}{1 - (\epsilon_s^{(d)})^{\frac{1}{N_t}}} - a\right)\right]^{-\frac{\alpha}{2}}. \tag{2.4.28}$$

Proof: The proof is detailed in Appendix A (**A.5**).

Due to the procedure of TAS, P_s^* cannot be determined for the P.D.(PTs-STs) and P.D.(PTs)-I.D.(STs) because there is no relation between outage probability and transmit power. In this way, P_s^* can be obtained for I.D.(PTs)-P.D.(STs) and I.D.(PTs-STs).

Considering the TAS scheme, the analytical expression of energy efficiency for the N_t transmit antenna can be written as

$$\eta_{EE}^{N_t} = \frac{(1 - \left[\epsilon_s^{(d)}\right]^{\frac{1}{N_t}}) \log_2(1 + \theta_s)}{N_{TRX} P_o T_t + p_{ic,im} p_{st,im} \Delta_s P_s^* T_p + P_{sp} T_s + P_s^* T_p}. \tag{2.4.29}$$

Proof: The proof is detailed in Appendix A (**A.6**).

2.5 Numerical Results and Discussion

In this section we apply the theoretical model developed in the previous sections to analyze outage probability and energy efficiency. The relevant parameters are mentioned in Table 2.1. Some parameters are taken from [49, 52]. In the simulation, this network is modeled as a square area [1km x 1km] over the 2-D plan. The simulation results are obtained by averaging 10000 iterations.

Parameter	Value	Parameter	Value	Parameter	Value
N	25	α	4	λ_p	$15/km^2$
M	10	μ_p	0.6	$\lambda_p^{'}$	$13/km^2$
N_s	15	μ_s	0.3	λ_s	$50/km^2$
T_s	1ms	P_p	$50W$	$\lambda_s^{'}$	$45/km^2$
T_p	4ms	P_s	$15W$	N_{trx}	1
Δ_s	2.8	P_o	$84W$	P_{sp}	$0.2W$

Table 2.1: Numerical Parameters.

2.5.1 Outage Probability of PR

It is known that the outage probability must be minimized to obtain an acceptable CR network performance; thus, an improved CR network design is needed to minimize the outage probability. First, we verify the analytical result derived in eq. (2.4.5). The analytical and simulation results are compared in Fig. 2.6. The simulation result is fairly close to the analytical result, which validates eq. (2.4.5). Thus, we evaluate the outage probability shown in Figs. 2.7, 2.8, and 2.9 using eq. (2.4.5).

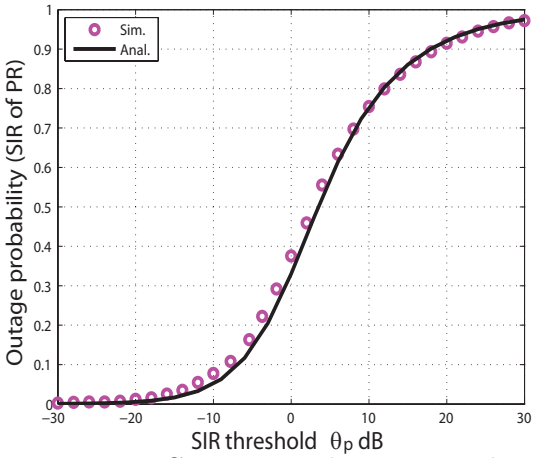

Figure 2.6: Comparison between analytical and simulation results of SIR for PR.

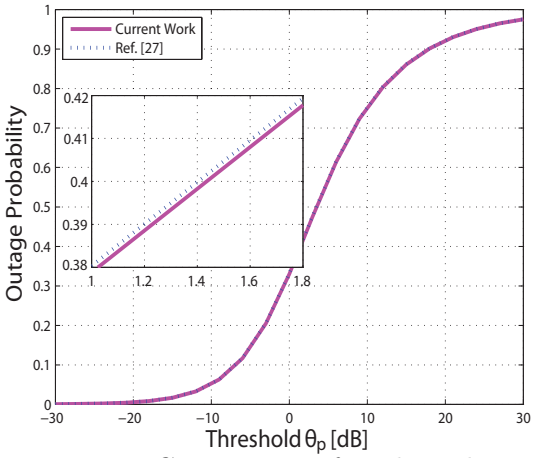

Figure 2.7: Comparison of analytical results of present and previous work for PR.

In Fig. 2.7, we compare our present analysis to that in our previous work in [27]. As can be seen in the inset in the figure, outage probability here is lower than in our previous work. Both sets of results are compared with the same parameter, given in Table 2.1. Compared with conventional results, the outage probability decreased from 0.4062 to 0.4046 at $\theta_p = 1.5$ dB, approximately 0.4% reduction. Fig. 2.8 shows the outage probability performance for various values of β. It is observed that the proposed scheme performs better for large values of β. It should be noted that β correlates strongly with r_{PER} and r_p. If β increases, r_{PER} also increases. Thus, we achieve a low outage probability here.

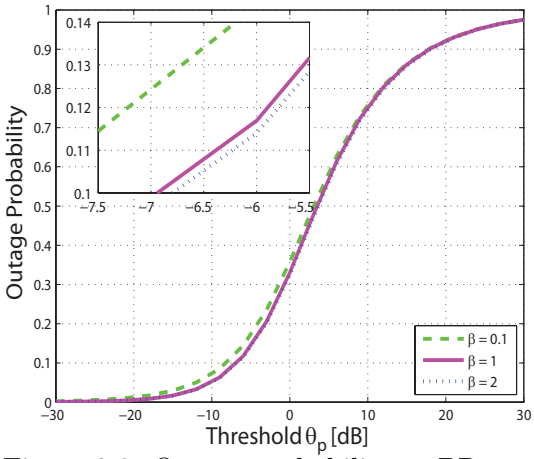

Figure 2.8: Outage probability at PR versus θ_p for various values of β.

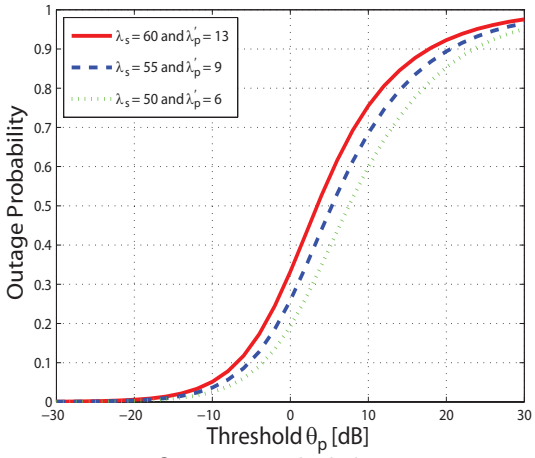

Figure 2.9: Outage probability at PR versus θ_p for different values of densities λ_s and $\lambda_p^{'}$.

Fig. 2.9 shows the outage probability performance of a PR for various values of the densities λ_s and $\lambda_p^{'}$. We note improved outage probability for lower densities of λ_s and $\lambda_p^{'}$ compared to the higher densities of λ_s and $\lambda_p^{'}$. For instance, the densities $\lambda_s = 50$ and $\lambda_p^{'} = 6$ resulted in an outage probability of approximately 0.06 lower than that for $\lambda_s = 55$ and $\lambda_p^{'} = 9$ at $\theta_p = 0$ dB.

2.5.2 Outage Probability of SR

In this subsection, we address the outage probability of a SR. Fig. 2.10 shows the outage probability performance for the four scenarios of perfect and imperfect detection. We demonstrate the simulation results for the four scenarios in comparison with the analytical results derived as eqs. (2.4.9), (2.4.11), (2.4.12) and (2.4.14). The simulation and analytical results are in good fitting. It is observed that P.D.(PTs-STs) outperforms the other scenarios (i.e., P.D.(PTs)-I.D.(STs), I.D.(PTs)-P.D.(STs), and I.D.(PTs-STs)), and that the outage probability is almost zero over the range of θ_s. Moreover, with an increase of θ_s, the performance of P.D.(PTs)-I.D.(STs) becomes increasingly superior to that of I.D.(PTs)-P.D.(STs). As expected, I.D.(PTs-STs) has the highest outage probability. The remaining figures (Figs. 2.11-2.21) were obtained using the derived expressions.

Fig. 2.11 presents the outage probability for the present study and previous work [27]. We observe that outage probability is better for the same parameter in the results of the

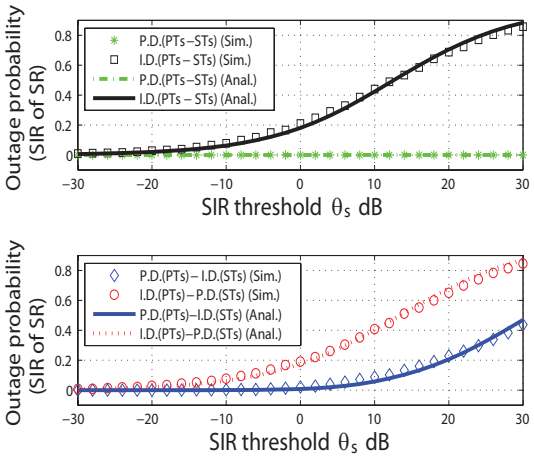

Figure 2.10: Comparison between analytical and simulation results of SIR for SR.

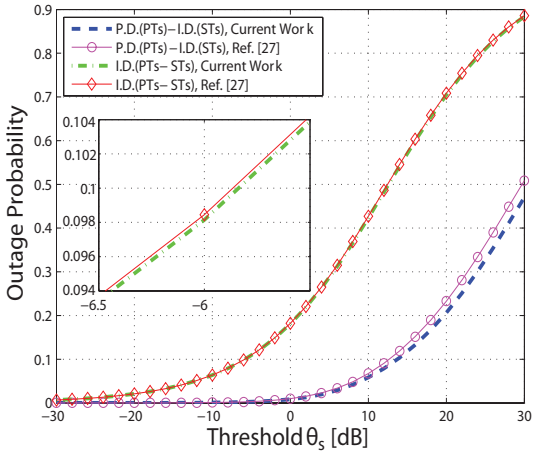

Figure 2.11: Comparison between analytical results of present and previous work for SR.

present study. For instance, calculation shows that the outage probability for I.D.(PTs-STs) in the present study and in the conventional model were 0.09844 to 0.09814 respectively at $\theta_s = -6$ dB, a reduction of 0.3%. The outage probability for P.D.(PTs-STs) and I.D.(PTs)-P.D(STs) is not provided given the similarity of the results. As depicted in Fig. 2.12, lower values of the densities $\lambda_s^{'}$ and λ_p outperformed higher values for I.D.(PTs-STs). That was because higher values of $\lambda_s^{'}$ and λ_p enhanced interference and reduced the coverage probability, which increased the outage probability.

2.5.3 Energy Efficiency and Area Spectral Efficiency

The following is an investigation of the CR network energy efficiency based on the preceding theoretical analysis.

2.5.3.1 Energy Efficiency of PN

As demonstrated in Fig. 2.13, for a particular β, the energy efficiency increases with increasing θ_p up to a certain value of θ_p and then decreases. The value of θ_p with the maximum energy efficiency is denoted as $\theta_p^{\star}$ and referred to as the optimal threshold. Fig. 2.13 implies that each β has an optimal threshold at 7 dB. The maximum values of energy efficiency are 1.83×10^{-5}, 1.79×10^{-5}, and 1.73×10^{-5} due to the consideration of $\beta = 2$, $\beta = 1$, and $\beta = 0.1$, respectively. For larger β, the energy efficiency is higher. However, there was a little variation in the energy efficiency with θ_p at different β. It is important to note that $\log_2(1 + \theta_p)$ is an increasing function of θ_p but the coverage probability is a decreasing function. Thus, both functions (i.e., $\log_2(1 + \theta_p)$ and the coverage probability) are intersect at the optimal point. Therefore, the maximum energy efficiency is obtained at the optimal threshold.

The results, shown in Fig. 2.14, show the effect of the densities λ_s and $\lambda_p^{'}$ on the energy

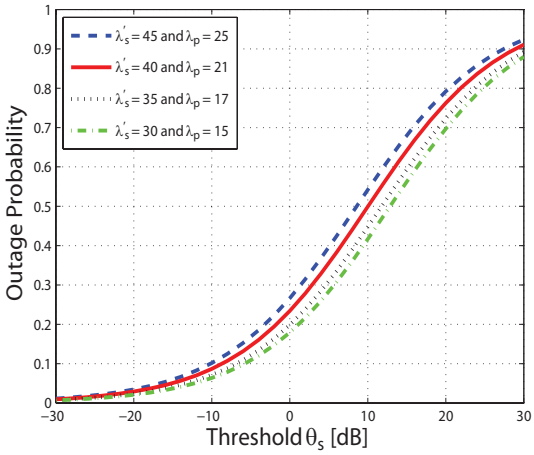

Figure 2.12: Outage probability at SR versus θ_s for different values of densities $\lambda_s^{'}$ and λ_p plotted using eq. (2.4.14).

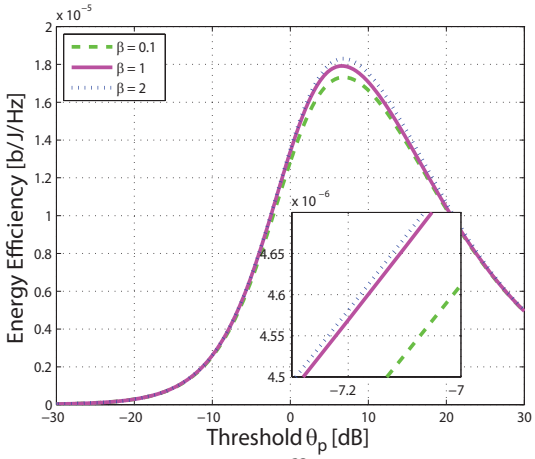

Figure 2.13: Energy efficiency at PN versus θ_p for various values of β.

efficiency. In this figure, the energy efficiency is lower for high λ_s and $\lambda_p^{'}$ than for low λ_s and $\lambda_p^{'}$. As mentioned earlier, the interference is increased for a high λ_s and $\lambda_p^{'}$. Also, this figure illustrates the existence of an optimal threshold $\theta_p^{\star}$ which maximizes energy efficiency.

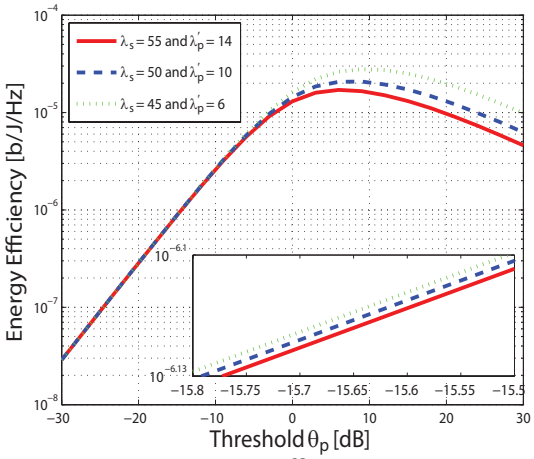

Figure 2.14: Energy efficiency at PN versus θ_p for different values of densities λ_s and $\lambda_p^{'}$.

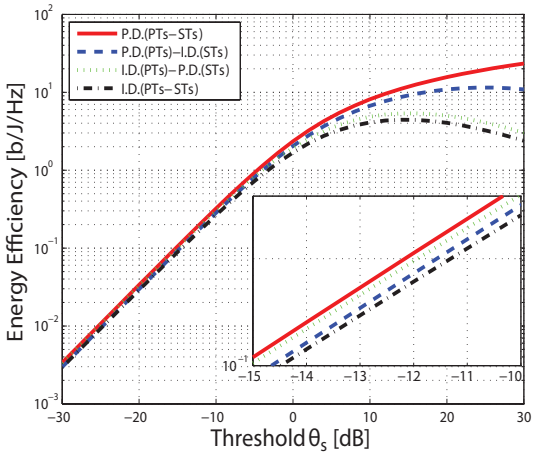

Figure 2.15: Energy efficiency at SN versus θ_s for the four scenarios.

2.5.3.2 Energy Efficiency of SN

The energy efficiency of a SN was evaluated using eqs. (2.4.19), (2.4.20), (2.4.21), and (2.4.22). As shown in Fig. 2.15, energy efficiency increases with the threshold θ_s; however, it decreases above a given θ_s for the P.D.(PTs)-I.D.(STs), I.D.(PTs)-P.D.(STs), and I.D.(PTs-STs) scenarios. Thus, the optimal threshold $\theta_s^{\star}$ which maximizes the energy efficiency for the P.D.(PTs)-I.D.(STs), I.D.(PTs)-P.D.(STs), and I.D.(PTs-STs) scenarios was determined.

At the initial value of θ_s, we see that the energy efficiency is only slightly influenced by the four scenarios. Overall, P.D.(PTs-STs) has the best energy efficiency and therefore has lower power consumption than the other scenarios.

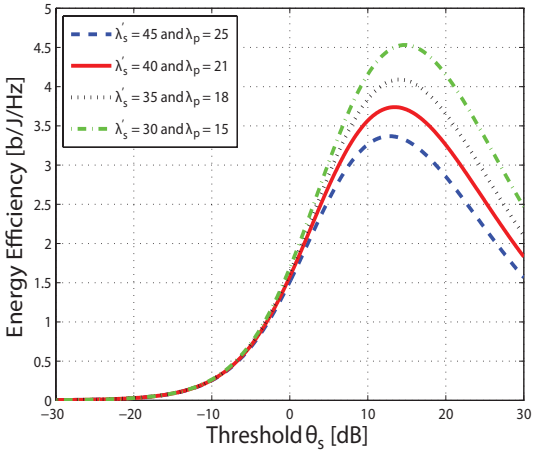

Figure 2.16: Energy efficiency versus θ_s for different values of densities $\lambda_s^{'}$ and λ_p plotted using eq. (2.4.22).

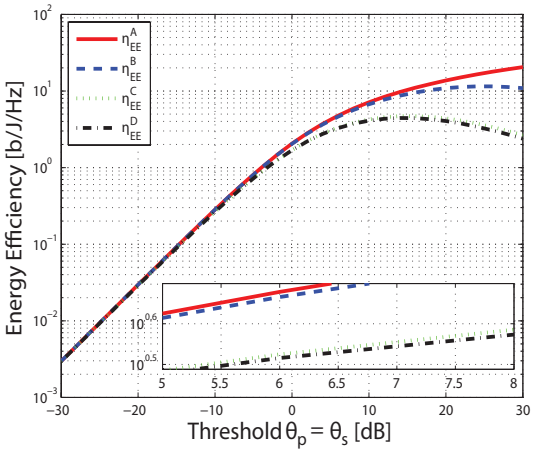

Figure 2.17: Energy efficiency versus θ_s plotted using eqs. (2.4.23), (2.4.24), (2.4.25), and (2.4.26).

In Fig. 2.16, we illustrate the effect of the densities $\lambda_s^{'}$ and λ_p on the energy efficiency. It was observed that the energy efficiency increases as θ_s increases up to a certain θ_s and then decreases. This observation suggests that there is a point of maximum energy efficiency for an optimal threshold $\theta_s^{\star}$, for various $\lambda_s^{'}$ and λ_p. Similar behavior was observed in Figs. 2.13 and 2.16 for the same reason. The maximum values of the energy efficiency are 4.53, 4.09, 3.73, and 3.36 for the four different densities. The energy efficiency is low for high values of $\lambda_s^{'}$ and λ_p. This behavior indicates that high values of $\lambda_s^{'}$ and λ_p will have a significant impact on the deployment of CR networks.

2.5.3.3 Energy Efficiency of PN and SN

In this subsection, we provide graphical representations of the energy efficiency for both a PN and SN. Fig. 2.17 depicts the energy efficiency performance versus the threshold θ_s. The optimal threshold can be found numerically for η_{EE}^{B}, η_{EE}^{C}, and η_{EE}^{D}. This is typical behavior as observed in Fig. 2.15.

2.5.4 Transmit Antenna Selection of ST

In this subsection, we evaluate the expressions derived for the TAS of a ST. As in the results of TAS, here we consider only the cases of a single receiver and up to four transmit antennas. As shown in Fig. 2.18, the number of ST antennas plays a significant role in the outage probability of a SR. Above 0 dB, the outage probability increases for $N_t = 3$ and $N_t = 4$. It can be deduced that in this network, where the threshold θ_s is low, the case of $N_t = 4$ has significantly better outage probability. Similar results are also found due to the

high threshold. For example, $N_t = 4$ has an outage probability of approximately 0.09 at θ_s = 30 dB, better than that for $N_t = 3$.

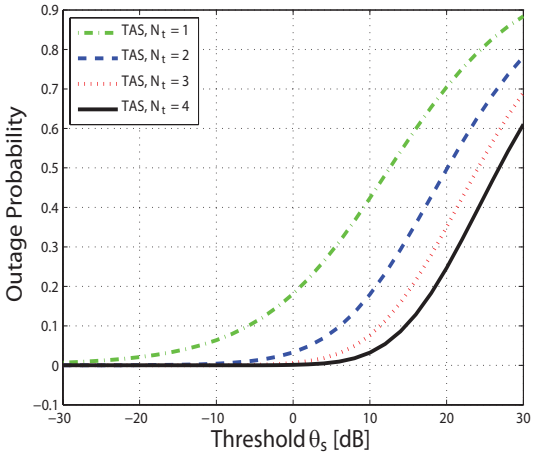

Figure 2.18: Outage probability performance versus θ_s for TAS of STs.

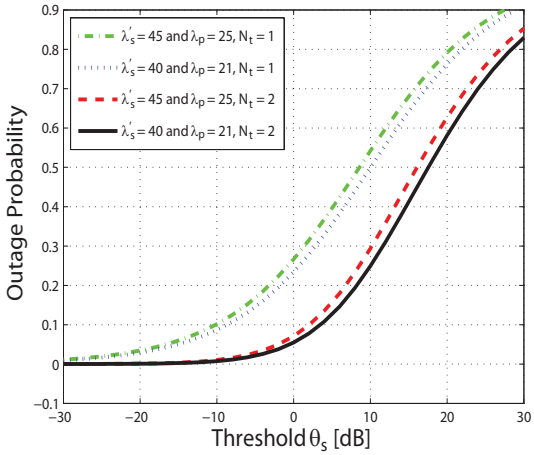

Figure 2.19: Outage probability performance versus θ_s for TAS of STs.

As shown in Fig. 2.19, the case of $N_t = 2$ achieves lower outage probability than that of $N_t = 1$ in TAS. It was also observed that the outage probability decreases with decreasing $\lambda_s^{'}$ and λ_p. This result confirms that there is a low outage probability if low densities are applied. The effect of N_t on the energy efficiency is illustrated in Fig. 2.20. It can be seen that there are minimum and maximum values of energy efficiency for each number of transmit antennas (i.e., $N_t = 1$, 2, 3, and 4.). The maximum energy efficiency is 0.26, 1.35, and 2.51 for $N_t = 2$, 3, and 4, respectively. For $N_t = 4$, the energy efficiency is high for a particular value of θ_s. Two observations can be made from Fig. 2.20: (i) when N_t increases, we obtain high energy efficiency at a large threshold θ_s for a particular value of ϵ_s. (ii) when ϵ_s increases, we achieve high energy efficiency at a high θ_s for a large number of antennas. This also indicates that a large number of antennas has lower power consumption for low θ_s and higher power consumption for high θ_s, although they have better outage probability. Another important issue is that the energy efficiency decreases above the value of θ_s giving the maximum energy efficiency and eventually reaches a minimum energy efficiency. After that, the energy efficiency again increases as θ_s increases. On the basis of Fig. 2.20, there are two important threshold points: an optimal point where the energy efficiency is maximum and a worst-case point where the energy efficiency is minimum. Between the optimal and worst-case points, the energy efficiency is decreased by the limitation of the minimum power of $P_s^*(N_t)$. After the worst-case point, the energy efficiency increases since it is dominated by the increasing function $\log_2(1 + \theta_s)$.

In Fig. 2.21, we examine the impact of the outage probability (ϵ_s) on the energy efficiency. As expected, the energy efficiency increases with ϵ_s. For a lower ϵ_s, a large number of transmit antennas ($N_t = 4$) is better. Each antenna has the same maximum efficiency but at different values of ϵ_s. This is because θ_s was assumed to have the same value in the analysis of the energy efficiency for each number of antennas. This figure reveals the

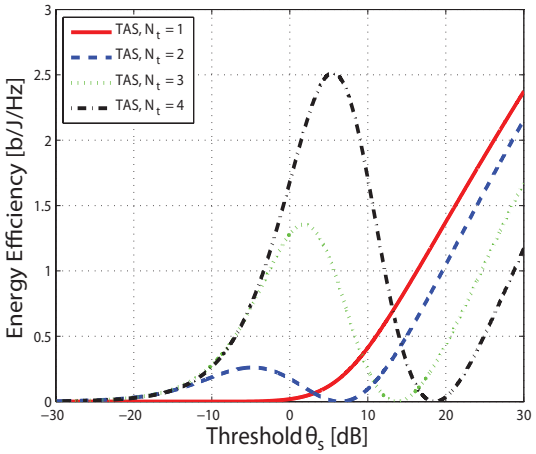

Figure 2.20: Energy efficiency performance versus θ_s for TAS of STs plotted for $\epsilon_s = 10^{-3}$.

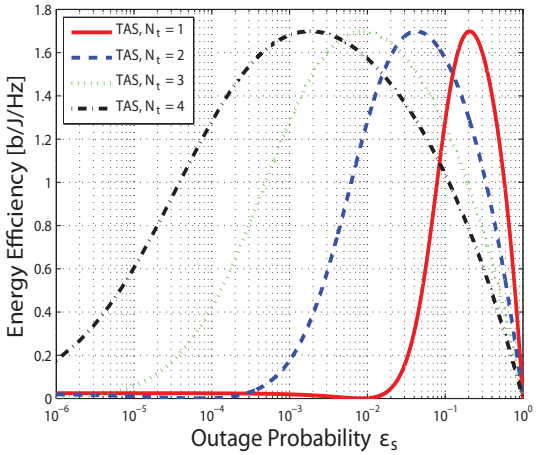

Figure 2.21: Energy efficiency performance versus ϵ_s for TAS of STs plotted for $\theta_s = 0$ dB.

existence of an optimal $\epsilon_s^\star$ where the energy efficiency is maximized. For instance, the maximum energy efficiency is 1.7 when ϵ_s is 1.8×10^{-3} for $N_t = 4$. This behavior was observed for every number of antennas, but with higher values of ϵ_s. Through our theoretical analysis, we observed that TAS has a potential impact on the outage probability and energy efficiency.

Chapter 3

Analysis of Downlink CR Network: Rayleigh-lognormal

3.1 Literature Review

Considerable previous work[1] related to applications of stochastic geometry have been discussed in this study. The outage probability of wireless ad hoc networks considering path-loss and shadowing was investigated in [57]. A mathematical model for enumeration of the average rate of downlink heterogeneous cellular networks using correlated lognormal shadowing has been presented [58]. The theoretical expression of Poisson cellular networks with lognormal shadowed Rayleigh fading has been derived and evaluated [59]. The coverage probability for a small cell network assuming Rayleigh fading and lognormal shadowing was investigated [60]. Zhang *et al.* [61] derived finite-integral expressions for the downlink coverage probability of inter-cell interference coordination and intra-cell diversity with lognormal shadowing. Mahmud *et al.* [62] proposed fractional frequency reuse and soft frequency reuse systems based on the cellular interference management technique. They presented the area spectral efficiency for both uplink and downlink, with consideration of Nakagami fading and lognormal shadowing. Recently, coverage probability analysis of cellular networks considering Rayleigh-lognormal fading was investigated in [63]. Uplink transmission developed where cellular network operating over path-loss and combined Rayleigh-lognormal fading was investigated using a power control technique [64]. In 2009, Win *et al.* [65] explored interference in CR networks, interference in wireless packet networks, radio-frequency emission of wireless networks, and coexistence between ultrawideband and narrowband systems, taking into account path-loss, shadowing, and multipath fading. Wen [66] *et al.* developed a model of CR network to explore the asymptotic and non-asymptotic outage probability based on heavy tail and saddle-point approximation theories, and went on to present interference cancellation and fading such as Rayleigh and lognormal. In [67], Dung *et al.* investigated the connectivity of CR ad hoc networks under lognormal shadow fading from

[1]This chapter was published at IEEE CCNC, 2017 [56]. Please follow the copyright rule of IEEE.

three perspectives, communication probability, link probability, and multi-hop path connectivity.

3.2 System Model

3.2.1 Network Topology

A downlink CR network a composite of two types of network, primary- and secondary network, as shown in Fig. 3.1. In the primary network, primary transmitter (e.g., TV station) and primary receiver (e.g., TV user equipment) are assumed. In the secondary network, secondary transmitter (e.g., macro BS) and secondary receiver (e.g., BS user equipment) are considered. The locations of primary transmitters (PTs) are distributed according to a homogeneous PPP Φ_{Pt} with density λ_{Pt} and their associated receivers (PRs) follow as an independent PPP Φ_{Pr} with density λ_{Pr}. The locations of secondary transmitters (STs) are modeled as a homogeneous PPP Φ_{St} with density λ_{St} and their associated receivers (SRs) are also modeled as an independent PPP Φ_{Sr} with density λ_{Sr}.

Assuming a power law path-loss model, the received power at the PR and SR from the PT and ST is defined as

$$P_{pr} = P_p g_p \left\| r_p \right\|^{-\alpha} \tag{3.2.1}$$

$$P_{sr} = P_s g_s \left\| r_s \right\|^{-\alpha} \tag{3.2.2}$$

where P_p and P_s are the transmission power of PT and ST, respectively, and g_p and g_s are the respective fading channel gains that have Rayleigh-lognormal distribution, detailed in channel model. r_p is the distance between PT and its corresponding PR, r_s is the distance between ST and its corresponding SR, $\|\cdot\|$ is the Euclidean norm, and α is the path-loss exponent.

3.2.2 Channel Model

In CR network, the performance of the system depends on the state of the wireless environment, as the characteristics of wireless channel are progressive and unforeseeable. Depending on the wireless environment, it can be quite difficult to analyze the wireless system accurately. Also, the strength of the received signal is variable at the receiver [68]. Transmitted signals are affected by a number of effects (e.g., free-space path-loss, fast- and slow fading). Thus, random CR network is required for evaluation of the Rayleigh and lognormal fading channel.

Assuming Rayleigh and lognormal fading, the probability density function (PDF) of power gain g of the signal is computed as the PDF of the product of the two composite channels. The two composite channels are defined as Rayleigh-lognormal fading, expressed as

$$f_{RL}(g) = \int_0^\infty \frac{1}{x} \exp\left(-\frac{g}{x}\right) \frac{1}{x\sigma_x\sqrt{2\pi}} \exp\left(-X\right) dx \tag{3.2.3}$$

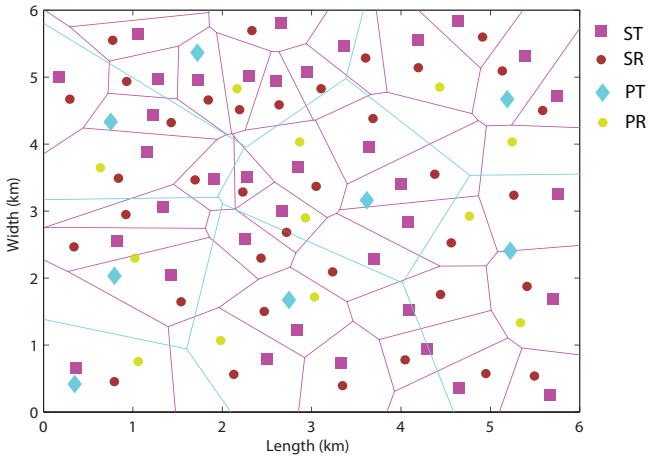

Figure 3.1: CR network model composed of ST, SR, PT, and PR in $[0,6]^2\,\mathrm{km}^2$. STs are denoted by magenta squares, SRs by red circles, and Voronoi cell boundaries by magenta lines. PTs are denoted by cyan diamonds, PRs by dark-yellow circles, and Voronoi cell boundaries by cyan lines. In this figure, we omit the primary exclusion region (PER) of PT [27]. For simple analysis, we consider that the target STs are outside the PER because transmission is not allowed inside the PER.

where $X = \frac{(\ln(x)-\mu_x)^2}{2\sigma_x^2}$. μ_x and σ_x are the mean and standard deviation of lognormal shadowing, respectively. Applying the Gauss-Hermite quadrature [69], the PDF is denoted as

$$f_{RL}(g) = \sum_{n=1}^{N_p} \frac{w_n}{\sqrt{\pi}} \cdot \frac{1}{\gamma(a_n)} \exp\left(-\frac{g}{\gamma(a_n)}\right) \tag{3.2.4}$$

where $\gamma(a_n) = \exp(\sqrt{2}\sigma_x a_n + \mu_x)$. w_n and a_n denote the weights and the abscissas of the Gauss-Hermite polynomial, respectively. The result is more accurate for an increase of order N_p, as illustrated in Fig. 3.2.

Proof: Please see [63] for details.

3.2.3 Timeslot and Sensing

The timeslot structure of CR network is explained in detail in [49]. One timeslot is divided into two parts. The first part, the frequency band of the primary network, is scanned and the idle- and occupied frequency bands are identified. This is known as the sensing period, an important element of CR network, since if STs accurately detect the idle- and occupied frequency band, interference does not occur among the STs and PTs. This is called perfect spectrum sensing. On the other hand, in the case of incorrect detection of idle- and occupied frequency band, interference occurs among the STs and PTs. this is called imperfect spectrum sensing. In the second part, called the transmission period, transmission takes place in the idle frequency band.

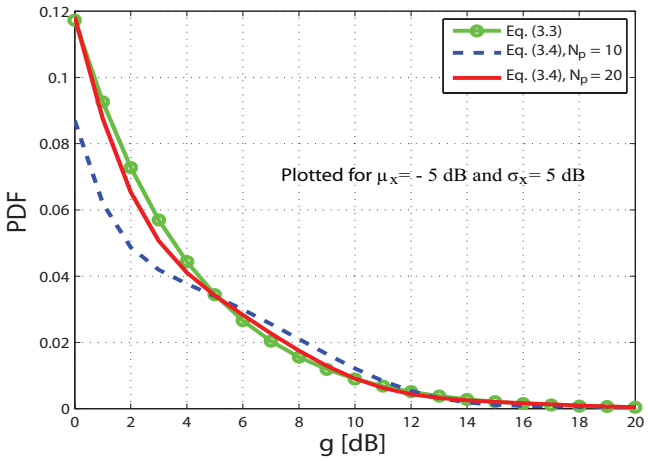

Figure 3.2: This plot shows the effect of PDF on the order of weights and abscissas of the Gauss-Hermite polynomial. Since the parameters are the same, it can be seen that the PDF is a smoothly decreasing function for higher order weights and abscissas, but is unevenly decreasing for lower order. For that reason we consider higher order weights and abscissas in this chapter.

3.2.4 Signal-to-Interference-plus-Noise Ratio

In this study, we assume imperfect spectrum sensing in the CR network, so PR experiences interference due to PTs and STs, just as SR experiences interference due to PTs and STs. For received signal power (3.2.1) and (3.2.2), signal-to-interference-plus-noise ratio (SINR) from PT to its serving PR and from ST to its serving SR are defined as

$$\mathrm{SINR}_{pr} = \frac{P_p g_p \left\| r_p \right\|^{-\alpha}}{I_{pp} + I_{ps} + \sigma_p^2} \tag{3.2.5}$$

$$\mathrm{SINR}_{sr} = \frac{P_s g_s \left\| r_s \right\|^{-\alpha}}{I_{ss} + I_{sp} + \sigma_s^2} \tag{3.2.6}$$

where I_{pp} and I_{ps} are interference at PR from PTs and STs, respectively, I_{ss} and I_{sp} are interference at SR from STs and PTs, respectively, σ_p^2 and σ_s^2 are the additive white Gaussian noise at PR and SR, respectively. I_{pp}, I_{ps}, I_{ss} and I_{sp} can be expressed as

$$I_{pp} = \sum_{i \in \Phi_{Pt} \setminus \{x\}} P_{pi} G_{ppi} \left\| R_{ppi} \right\|^{-\alpha} \tag{3.2.7}$$

$$I_{ps} = \sum_{i \in \Phi_{St}} P_{si} G_{psi} \left\| R_{psi} \right\|^{-\alpha} \tag{3.2.8}$$

$$I_{ss} = \sum_{i \in \Phi_{St} \setminus \{y\}} P_{si} G_{ssi} \left\| R_{ssi} \right\|^{-\alpha} \tag{3.2.9}$$

$$I_{sp} = \sum_{i \in \Phi_{Pt}} P_{pi} G_{spi} \left\| R_{spi} \right\|^{-\alpha} \tag{3.2.10}$$

where x and y are the target PT and ST, which are in communication with their associated PR and SR. G_{pp} is the fading channel gain at the target PR from interfering PT and R_{pp} is the distance between target PR and the interfering PT. G_{ps} is the fading channel gain at the target PR from interfering ST and R_{ps} is the distance between target PR and the interfering ST. G_{ss} and G_{sp} are the fading channel gains at the target SR from interfering ST and PT, respectively. R_{ss} and R_{sp} are the distances from the target SR to interfering ST and from the target SR to interfering PT.

3.3 Performance Analysis

In this section, we analyze secondary networks in terms of coverage probability and transmission rate for Rayleigh-lognormal fading environment.

3.3.1 Coverage Probability

In the context of secondary network, we define the coverage probability as the probability that the instantaneous SINR of a typical SR is greater than the threshold value [70]. For that analysis, a typical SR is located at the origin. Then by the definition of coverage probability, it can be expressed as

$$\begin{aligned}
\mathbb{C}_s &= \mathbb{P}\left[\mathrm{SINR}_{sr} > T_s\right] \\
&= \mathbb{P}\left[\frac{P_s g_s \left\|r_s\right\|^{-\alpha}}{I_{ss} + I_{sp} + \sigma_s^2} > T_s\right] = \mathbb{P}\left[g_s > \frac{T_s(I_{ss} + I_{sp} + \sigma_s^2)}{P_s \left\|r_s\right\|^{-\alpha}}\right] \\
&= \mathbb{E}_{I_{ss},I_{sp}}\left[\sum_{n=1}^{N_p} \frac{w_n}{\sqrt{\pi}} \exp\left(-\frac{T_s(I_{ss} + I_{sp} + \sigma_s^2)\left\|r_s\right\|^{\alpha}}{P_s \gamma(a_n)}\right)\right] \\
&\overset{(i)}{=} \sum_{n=1}^{N_p} \frac{w_n}{\sqrt{\pi}} \exp\left(-f(n)\sigma_s^2\right) \mathbb{E}_{I_{ss},I_{sp}}\left[\exp\left(-(I_{ss} + I_{sp})f(n)\right)\right] \\
&\overset{(ii)}{=} \sum_{n=1}^{N_p} \frac{w_n}{\sqrt{\pi}} \exp\left(-f(n)\sigma_s^2\right) \mathcal{L}_{I_{ss}}(f(n))\mathcal{L}_{I_{sp}}(f(n))
\end{aligned} \tag{3.3.1}$$

where T_s is the detection threshold of SR. In equality (i), $f(n) = \frac{T_s\|r_s\|^{\alpha}}{P_s\gamma(a_n)}$. Equality (ii) follows the definition of Laplace transform. $\mathcal{L}_{I_{ss}}(\cdot)$ and $\mathcal{L}_{I_{sp}}(\cdot)$ denote the Laplace transforms of the PDFs of interference I_{ss} from the active ST and that of interference I_{sp} from the active PT, respectively.

Plugging the value of $\mathcal{L}_{I_{ss}}(f(n))$ and $\mathcal{L}_{I_{sp}}(f(n))$ into (3.3.1), we can obtain the coverage probability as

$$\mathbb{C}_s = \sum_{n=1}^{N_p} \frac{w_n}{\sqrt{\pi}} \exp\left(-\frac{T_s \left\|r_s\right\|^{\alpha} \sigma_s^2}{P_s \gamma(a_n)} - \pi \left\|r_s\right\|^2 \left[\lambda_{St} \left(\sum_{n_1=1}^{N_{p_1}} \frac{w_{n_1}}{\sqrt{\pi}} \left[\frac{2\pi C_{ss}^{\frac{2}{\alpha}}}{\alpha \sin\left(\frac{2\pi}{\alpha}\right)} \right.\right.\right.\right.$$
$$\left.\left.\left.\left. -{}_2F_1\left([1, 2/\alpha]; 1 + 2/\alpha; -1/C_{ss}\right)\right] \right) + \lambda_{Pt} \sum_{n_2=1}^{N_{p_2}} \frac{w_{n_2}}{\sqrt{\pi}} \cdot \frac{2\pi C_{sp}^{\frac{2}{\alpha}}}{\alpha \sin\left(\frac{2\pi}{\alpha}\right)} \right] \right) \quad (3.3.2)$$

where ${}_2F_1\left([a, b]; c; t\right)$ is a hypergeometric function, $C_{ss} = \frac{T_s \gamma(a_{n_1})}{\gamma(a_n)}$ and $C_{sp} = \frac{T_s P_p \gamma(a_{n_2})}{P_s \gamma(a_n)}$.

Proof: The detailed proof of $\mathcal{L}_{I_{ss}}(f(n))$ and $\mathcal{L}_{I_{sp}}(f(n))$ is provided in Appendix B (**B.1 & B.2**).

Special Case 1: If we assume $\alpha = 4$, (3.3.2) reduces to the closed-form expression, given by

$$\mathbb{C}_s^1 = \sum_{n=1}^{N_p} \frac{w_n}{\sqrt{\pi}} \exp\left(-\frac{T_s \left\|r_s\right\|^4 \sigma_s^2}{P_s \gamma(a_n)} - \pi \left\|r_s\right\|^2 \left[\lambda_{St} \left(\sum_{n_1=1}^{N_{p_1}} \frac{w_{n_1}}{\sqrt{\pi}} \left[\frac{\pi\sqrt{C_{ss}}}{2} \right.\right.\right.\right.$$
$$\left.\left.\left.\left. -\sqrt{C_{ss}} \tan^{-1}\left(\frac{1}{\sqrt{C_{ss}}}\right)\right]\right) + \lambda_{Pt} \sum_{n_2=1}^{N_{p_2}} \frac{w_{n_2}}{\sqrt{\pi}} \cdot \frac{\pi\sqrt{C_{sp}}}{2} \right] \right) \quad (3.3.3)$$

Special Case 2: If we assume $\alpha = 4$ and $\sigma_s^2 = 0$, (3.3.2) can be defined as interference-limited in which noise is negligible. So the coverage probability reduces to

$$\mathbb{C}_s^2 = \sum_{n=1}^{N_p} \frac{w_n}{\sqrt{\pi}} \exp\left(-\pi \left\|r_s\right\|^2 \left[\lambda_{St} \left(\sum_{n_1=1}^{N_{p_1}} \frac{w_{n_1}}{\sqrt{\pi}} \left[\frac{\pi\sqrt{C_{ss}}}{2} - \sqrt{C_{ss}} \tan^{-1}\left(\frac{1}{\sqrt{C_{ss}}}\right)\right]\right) \right.\right.$$
$$\left.\left. + \lambda_{Pt} \sum_{n_2=1}^{N_{p_2}} \frac{w_{n_2}}{\sqrt{\pi}} \cdot \frac{\pi\sqrt{C_{sp}}}{2} \right] \right) \quad (3.3.4)$$

3.3.2 Transmission Rate

Transmission rate is another important metric for the evaluation of CR network performance. Transmission rate is given by Shannon's formula and is expressed in terms of

nat/sec/Hz [70]. For CR network, the transmission rate can be expressed as

$$\begin{aligned}\mathbb{T}_r &= \int_0^\infty \mathbb{P}\left[\ln(1+\mathrm{SINR}_{sr}/G) > z\right] dz \\ &= \int_0^\infty \mathbb{P}\left[\mathrm{SINR}_{sr} > G(e^z-1)\right] dz \\ &\overset{(i)}{=} \int_0^\infty \sum_{n=1}^{N_p} \frac{w_n}{\sqrt{\pi}} \exp\left(-f_z(n)\sigma_s^2\right) \mathcal{L}_{I_{ss}}(f_z(n)) \mathcal{L}_{I_{sp}}(f_z(n)) dz \\ &\overset{(ii)}{=} \int_0^\infty \frac{1}{1+y} \sum_{n=1}^{N_p} \frac{w_n}{\sqrt{\pi}} \exp\left(-f_y(n)\sigma_s^2\right) \mathcal{L}_{I_{ss}}(f_y(n)) \mathcal{L}_{I_{sp}}(f_y(n)) dy \end{aligned} \tag{3.3.5}$$

where G is the Shannon capacity gap ($G \geq 1$), $f_z(n) = \frac{G(e^z-1)\|r_s\|^\alpha}{P_s\gamma(a_n)}$ and $f_y(n) = \frac{yG\|r_s\|^\alpha}{P_s\gamma(a_n)}$. (i) is followed by (3.3.1). (ii) is achieved by substituting the variables $y = e^z - 1$. Then, the transmission rate is obtained by substituting the variable $f_y(n)$ instead of $f(n)$ in (3.3.5) such that

$$\begin{aligned}\mathbb{T}_r = \int_0^\infty \frac{1}{1+y} \sum_{n=1}^{N_p} \frac{w_n}{\sqrt{\pi}} \exp\Bigg(-\frac{yG\left\|r_s\right\|^\alpha \sigma_s^2}{P_s\gamma(a_n)} - \pi\left\|r_s\right\|^2 \Bigg[\lambda_{St} \Bigg(\sum_{n_1=1}^{N_{p_1}} \frac{w_{n_1}}{\sqrt{\pi}} \Bigg[\frac{2\pi C_{st}^{\frac{2}{\alpha}}}{\alpha \sin\left(\frac{2\pi}{\alpha}\right)} \\ -{}_2F_1\left([1, 2/\alpha]; 1+2/\alpha; -1/C_{st}\right)\Bigg] + \lambda_{Pt} \sum_{n_2=1}^{N_{p_2}} \frac{w_{n_2}}{\sqrt{\pi}} \cdot \frac{2\pi C_{pt}^{\frac{2}{\alpha}}}{\alpha \sin\left(\frac{2\pi}{\alpha}\right)} \Bigg] \Bigg) dy \end{aligned} \tag{3.3.6}$$

where $C_{st} = \frac{yG\gamma(a_{n_1})}{\gamma(a_n)}$ and $C_{pt} = \frac{yGP_p\gamma(a_{n_2})}{P_s\gamma(a_n)}$.

Proof: A similar proof of $\mathcal{L}_{I_{ss}}(f_y(n))$ and $\mathcal{L}_{I_{sp}}(f_y(n))$ is provided in Appendix B (**B.1 & B.2**).

Special Case 3: Conditioned on $\alpha = 4$, transmission rate can be obtained from (3.3.6) as follows:

$$\begin{aligned}\mathbb{T}_r^3 = \int_0^\infty \frac{1}{1+y} \sum_{n=1}^{N_p} \frac{w_n}{\sqrt{\pi}} \exp\Bigg(-\frac{yG\left\|r_s\right\|^4 \sigma_s^2}{P_s\gamma(a_n)} - \pi\left\|r_s\right\|^2 \Bigg[\lambda_{St} \Bigg(\sum_{n_1=1}^{N_{p_1}} \frac{w_{n_1}}{\sqrt{\pi}} \Bigg[\frac{\pi\sqrt{C_{st}}}{2} \\ -\sqrt{C_{st}} \tan^{-1}\left(\frac{1}{\sqrt{C_{st}}}\right)\Bigg] \Bigg) + \lambda_{Pt} \sum_{n_2=1}^{N_{p_2}} \frac{w_{n_2}}{\sqrt{\pi}} \cdot \frac{\pi\sqrt{C_{pt}}}{2} \Bigg] \Bigg) dy \end{aligned} \tag{3.3.7}$$

Special Case 4: With the assumption of $\alpha = 4$ and $\sigma_s^2 = 0$, (3.3.6) can be simplified as follows:

$$\begin{aligned}\mathbb{T}_r^4 = \int_0^\infty \frac{1}{1+y} \sum_{n=1}^{N_p} \frac{w_n}{\sqrt{\pi}} \exp\Bigg(-\pi\left\|r_s\right\|^2 \Bigg[\lambda_{St} \Bigg(\sum_{n_1=1}^{N_{p_1}} \frac{w_{n_1}}{\sqrt{\pi}} \Bigg[\frac{\pi\sqrt{C_{st}}}{2} \\ -\sqrt{C_{st}} \tan^{-1}\left(\frac{1}{\sqrt{C_{st}}}\right)\Bigg] \Bigg) + \lambda_{Pt} \sum_{n_2=1}^{N_{p_2}} \frac{w_{n_2}}{\sqrt{\pi}} \cdot \frac{\pi\sqrt{C_{pt}}}{2} \Bigg] \Bigg) dy \end{aligned} \tag{3.3.8}$$

3.4 Results and Discussion

In this section, we evaluate the performance of CR network in the Rayleigh-lognormal environment in terms of coverage probability and transmission rate. For the numerical results in this chapter, we use the following parameters: P_s = 1W, P_p = 100W, λ_{St} = 5/km^2, λ_{Pt} = 1/km^2, α = 4, μ_x = -10 dB, σ_x = 5 dB, σ_s = 3 dB, G = 0 dB, ${r_s}^2$ = 2 and $N_p = N_{p1} = N_{p2} = 20$. Variations of some parameters are indicated in the figure.

Fig. 3.3 shows the variation of coverage probability for different threshold T_s. We observe that coverage probability decreases with increasing T_s. We also observe that coverage probability increases with increasing transmission power P_s. For instance, the coverage probability increases from approximately 0.126 to 0.2 when P_s varies from 1W to 3W at T_s = 0 dB. Also, T_s increases by approximately 5 dB for an increase of P_s from 1W to 3W at coverage probability 0.2.

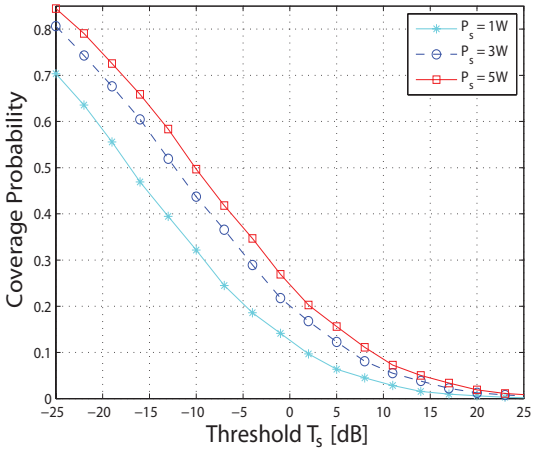

Figure 3.3: Coverage probability vs. threshold for different P_s.

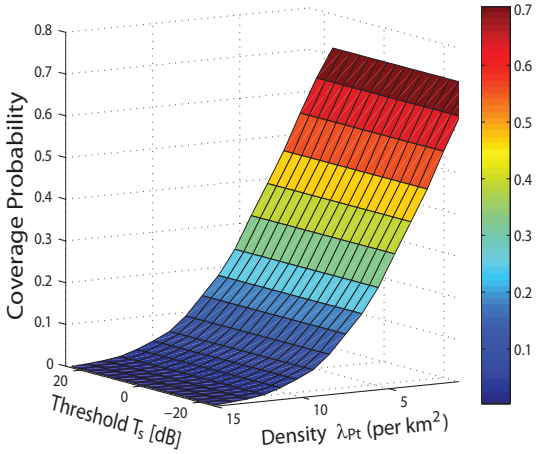

Figure 3.4: Coverage probability with varying threshold and λ_{Pt}.

We now present the impact of λ_{Pt} on coverage probability with different T_s, as shown in Fig. 3.4. It is observed that coverage probability is a decreasing function of λ_{Pt}. For low λ_{Pt}, the coverage probability function decreases with T_s. However, coverage probability is almost constant with different T_s for high λ_{Pt}. Similar results may be seen in Fig. 3.5, which shows the coverage probability for different T_s and λ_{St}.

It is shown in Fig. 3.6 that the transmission rate is a decreasing function with r_s for different P_s. Specifically, transmission rate rapidly decreases at short distance r_s ($r_s \leq 1$). On the other hand, transmission rate is gradually reduced when $r_s \geq 1$. The numerical result shows an increase in transmission rate of approximately 0.5 *nat/sec/Hz* between P_s = 1W and P_s = 3W at r_s = 1. In Fig. 3.7, we present transmission rate vs. r_s for various Shannon capacity gap G. A higher Shannon capacity gap G leads to a lower

[2]This distance is the Euclidean norm. The Euclidean norm [71] is calculated as $\|\mathbf{a}\| = d(\mathbf{a}, 0) = \sqrt{\sum_{i=1}^{n} \mathbf{a}_i^2}$, where $\mathbf{a}$ is a Euclidean vector. For example, we consider that a typical ST is located at (1.45, -1.45). The Euclidean norm is 2.0506.

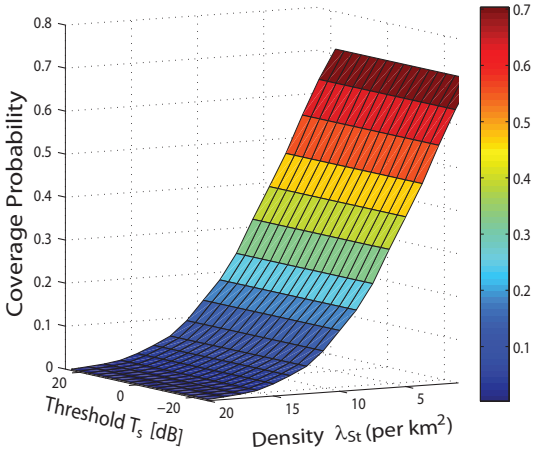

Figure 3.5: Coverage probability with varying threshold and λ_{St}.

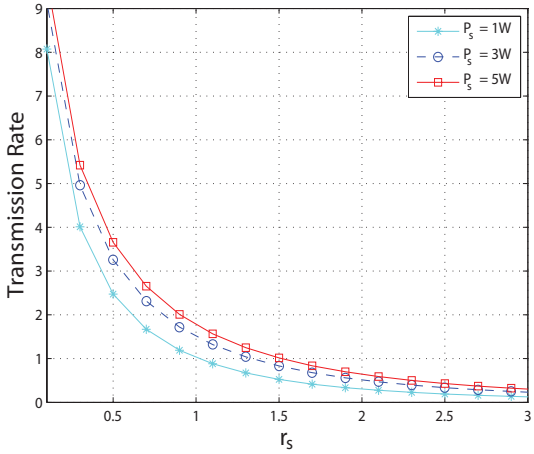

Figure 3.6: Transmission rate vs. r_s for different P_s.

transmission rate in this network. So, G is more sensitive issue in the design of network for high transmission rate requirements. From $G = 3$ dB to $G = 6$ dB, the transmission rate decreases by approximately 0.2 *nat/sec/Hz* when $r_s = 1$. For transmission rate of 2 *nat/sec/Hz*, r_s decreases by approximately 0.1 compared to that for the values of $G = 3$ dB and 6 dB.

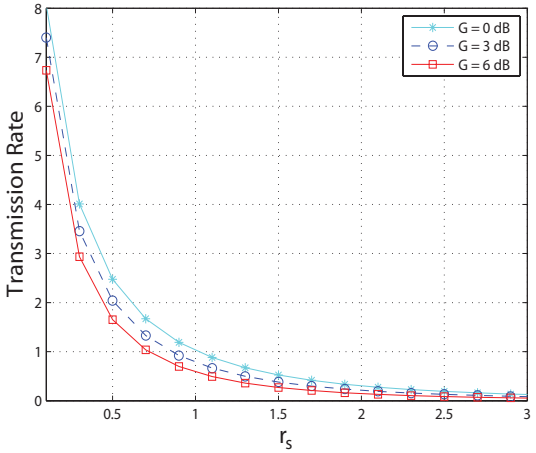

Figure 3.7: Transmission rate vs. r_s for different G.

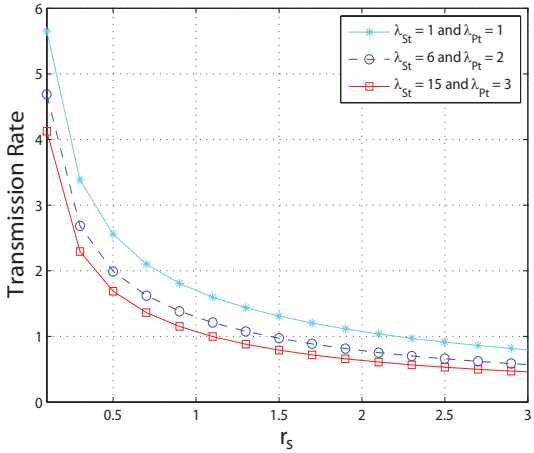

Figure 3.8: Transmission rate vs. r_s for different λ_{Pt} and λ_{St}.

Fig. 3.8 presents the impact of λ_{Pt} and λ_{St} on transmission rate. In this figure, we assume $\sigma_x = 10$ dB instead of $\sigma_x = 5$ dB so as to clearly distinguish among the curves. All the densities are represented per km^2. It is clear that transmission rate decreases with increasing λ_{Pt} and λ_{St}. This is because interference at target SR increases with increasing densities (λ_{St} and λ_{Pt}). We note that transmission rate is 1.695 *nat/sec/Hz* and 1.292 *nat/sec/Hz* for $\lambda_{Pt} = 1/\text{km}^2$ & $\lambda_{St} = 1/\text{km}^2$ and $\lambda_{Pt} = 2/\text{km}^2$ & $\lambda_{St} = 6/\text{km}^2$, respectively,

at $r_s = 1$. In addition, the same transmission rate can be achieved for lower densities λ_{Pt} & λ_{St} and longer r_s as for higher densities λ_{Pt} & λ_{St} and shorter r_s.

Chapter 4

Analysis of Uplink CR Network

4.1 Literature Review

A few studies have addressed the issue of uplink transmission using a homogenous PPP. The concept of uplink transmission in a signal-tier cellular network using a PPP was proposed in [73], where it was assumed that cellular phones and BSs are randomly located in cellular networks and that the uplink transmission is designed using fractional channel inversion power control. In a subsequent work, multiuser uplink cellular networks with fractional power control assuming a PPP were proposed, and the coverage probability [74] was analyzed. For the uplink transmission of CR cellular networks, mathematical expressions for the link rate and cell throughput in primary and secondary networks were derived in [75]. In another work on CR networks, the uplink capacity of a secondary network using a PPP, where a secondary BS was located at the center, was investigated [76]. Thereafter, an accurate theoretical expression was developed in [77] to obtain the outage probability and spectral efficiency for both single- and multi-tier cellular networks with truncated channel inversion power control[1]. In [78], two approximation models for uplink cellular networks were proposed, where BSs were deployed in accordance with the Ginibre point process. In [79], RF energy harvesting in K-tier uplink cellular networks with channel inversion power control was comprehensively modeled. In [80], the authors investigated uplink transmission in cellular networks with power control schemes in a Rayleigh lognormal shadowing environment. The authors investigated successive interference cancellation for uplink communications and evaluated its performance in [81].

4.2 Statement of Problem

The following is a consideration of the case of independent PPP nodes in a CR network where secondary users (SUs) and primary users (PUs) are randomly distributed. A SU consists of a secondary transmitter (ST) (e.g., cellular phone) and a secondary receiver

[1]Truncated channel inversion power control is interpreted in detail in [77, 82].

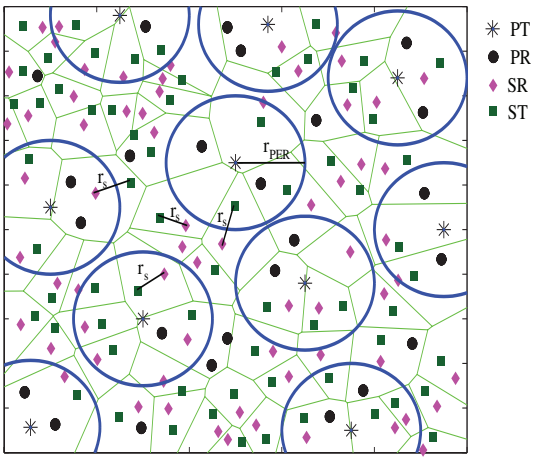

Figure 4.1: Locations of the SRs in part of the UK provided by Ofcom [24]. From the provided data, we plotted the CR locations via the MATLAB command *voronoi*. SRs are denoted by magenta diamonds, STs by green squares, PTs by black asterisks, and PRs by black circles.

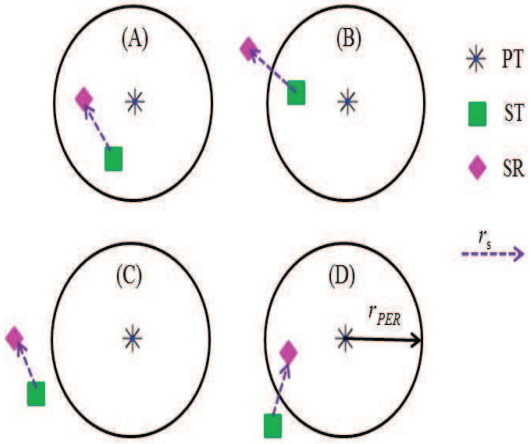

Figure 4.2: Four possible scenarios for ST-SR pair locations: (A) ST-SR pair inside the PER, (B) ST inside the PER but SR outside the PER, (C) ST-SR pair outside the PER, and (D) ST outside the PER but SR inside the PER.

(SR) (e.g., cognitive BS[2]), and a PU consists of a primary transmitter (PT) and a primary receiver (PR), as shown in Fig. 4.1. In our model, the PR does not affect the tagged SU because our design is for uplink modeling[3] in a CR network.

Fig. 4.1 depicts the CR network where PTs are encircled by the PER. To avoid interference [26] with the PU, the transmission of a ST is not permitted inside the PER. However, a ST may transmit outside the PER. Fig. 4.1 contains four possible scenarios for ST-SR pair location, which are depicted in Fig. 4.2. With regard to the CR network, scenarios A and B shown in Fig. 4.2 are not permitted because the ST is inside the PER. However, in scenarios C and D shown in Fig. 4.2, a ST may transmit a signal because it is outside the PER. In terms of the position of the ST, we assume that uplink transmission is possible for two cases: (a) the SR is inside the PER, as shown in Fig. 4.2(D), and (b) the SR is outside the PER, as shown in Fig. 4.2(C). In our model, we design the CR network for cases (a) and (b).

4.3 System Model

We consider an uplink transmission in a CR network with truncated channel inversion power control in which STs, SRs PTs, and PRs are randomly located in the $\mathbb{R}^2$ plane. The

[2]A cognitive BS is built using cognitive radio technology and has four main functions: spectrum sensing, spectrum decision, spectrum sharing, and spectrum mobility [10].

[3]In uplink transmission, a ST communicates with its nearest cognitive BS. Thus, interference occurs at the cognitive BS for STs other than the tagged ST and the PT.

STs are modeled by an independent homogeneous[4] PPP $\Phi_{ST} = \{c_i : \forall i\}$ with density $\lambda_s^{'}$. The locations of SRs are distributed in accordance with an independent homogeneous PPP $\Phi_{SR} = \{b_i : \forall i\}$ with density λ_s. The PTs are arranged following an independent homogeneous PPP $\Phi_{PT} = \{p_i : \forall i\}$ with density λ_p. The PRs are modeled as an independent PPP $\Phi_{PR} = \{q_i : \forall i\}$ with density $\lambda_p^{'}$. Fig. 4.3 schematically shows the CR network, where we consider two SRs at positions (a) and (b). In this figure, four interference signals I_{sp1}, I_{sp2}, I_{sp3}, and I_{sp4} are transmitted from the PTs to the SR at position (a). Thus, the total interference is $I_{sp} = I_{sp1} + I_{sp2} + I_{sp3} + I_{sp4}$. However, I_{sp2}, I_{sp3}, and I_{sp4} are negligible compared with I_{sp1} because of the long distance. Thus, $I_{sp} \approx I_{sp1}$. Hence, a strong signal is transmitted from the nearest PT.

A general path-loss model is adopted, where the signal power transmitted by the STs decays at a rate of $r_s^{-\alpha}$, where α is the path-loss exponent and r_s is the propagation distance between a ST-SR pair. In Fig. 4.3, there are two SRs at different locations. The distances of the SRs from the ST are r_{s1} and r_{s2}. Following the same path-loss model, the signal power transmitted by the PT decays at a rate of $r_p^{-\alpha}$, where r_p is the propagation distance between a PT-SR pair. Rayleigh fading is considered in the design of this model, and the channel power gains h_s for a ST-SR pair and h_p for a PT-SR pair are exponentially distributed random variables with unit mean.

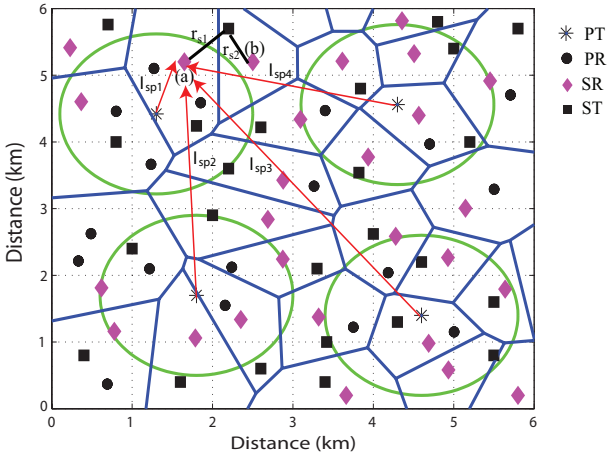

Figure 4.3: System model of CR network showing a practical example of uplink interferences from the PTs to a tagged SR. A ST-SR pair uses the power control policy, but a PT-PR pair does not use the power control policy.

For uplink communications, all STs have maximum transmission power P_{max}, and their transmissions are managed by truncated channel inversion power control, which is a suboptimal transmission strategy. In the truncated channel inversion policy, all STs compensate

[4]In practical scenarios, the densities of STs and SRs are different. Thus, STs are located following as an independent PPP. In this chapter, we assume the same density of STs and SRs because we consider one active ST per SR.

for fading to maintain the received signal power equal to a certain threshold[5] ρ_{so} at the SR [82], where ρ_{so} is a cutoff threshold (i.e., the minimum received power required at the receiver) defined for the network. This is a variable parameter that depends on the SR and it also impacts the overall performance of the system. The transmission power of the PT associated with this network is P_p.

According to [77], the uplink transmission for STs depends on the path-loss exponent α, the maximum transmission power P_{max}, the threshold ρ_{so}, and the density λ_s. The ratio P_{max}/ρ_{so} impacts on CR network performance. The density λ_s of STs is inversely proportional to the βth moment of the transmission power P_s of the ST. It was shown in [77] that the βth moment of P_s in the uplink can be expressed as

$$\mathbb{E}\left[P_s^{\beta}\right] = \frac{\rho_{so}^{\beta}\gamma\left(\frac{\alpha\beta}{2}+1, \pi\lambda_s\left(\frac{P_{max}}{\rho_{so}}\right)^{\frac{2}{\alpha}}\right)}{(\pi\lambda_s)^{\frac{\alpha\beta}{2}}\left[1-\exp\left\{-\pi\lambda_c\left(\frac{P_{max}}{\rho_{so}}\right)^{\frac{2}{\alpha}}\right\}\right]}, \tag{4.3.1}$$

where $\beta \in \mathbf{R}^+$ and $\gamma(u,v) = \int_0^v t^{u-1}e^{-t}dt$ is the lower incomplete gamma function. A detailed proof of (4.3.1) is provided in [77].

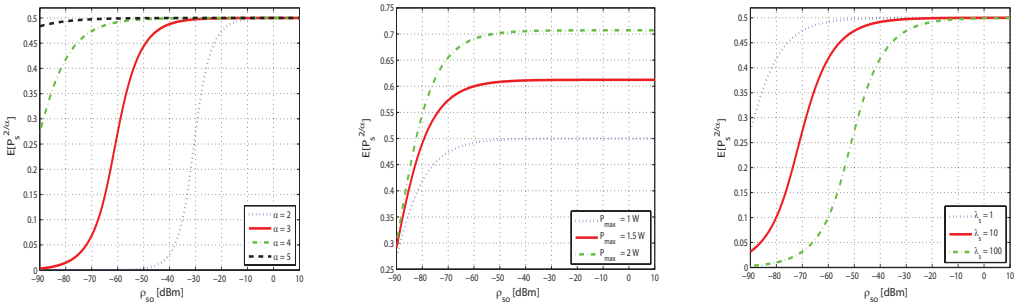

(a) $\mathbb{E}\left[P_s^{2/\alpha}\right]$ for $\lambda_s = 1/\text{km}^2$ & $P_{max} = 1$ W. (b) $\mathbb{E}\left[P_s^{2/\alpha}\right]$ for $\lambda_s = 1/\text{km}^2$ & $\alpha = 4$. (c) $\mathbb{E}\left[P_s^{2/\alpha}\right]$ for $P_{max} = 1$ W & $\alpha = 4$.

Figure 4.4: Impact of path-loss exponent α, maximum transmission power P_{max}, and density λ_s on $\mathbb{E}\left[P_s^{\beta}\right]$ with different values of the threshold ρ_{so}. To obtain this graph, $\beta = 2/\alpha$ is assumed in (4.3.1).

Now, we investigate the impact of α, P_{max}, and λ_s on the βth moment of the transmission power P_s of a ST, which is illustrated in Fig. 4.4. We assume $\beta = 2/\alpha$ and consider ρ_{co} from -90 dBm to 10 dBm. We find the value of β in the calculation of interference, which is conferred in Appendix C. The trade-off between $\mathbb{E}\left[P_s^{\beta}\right]$ and ρ_{so} is shown in Fig. 4.4(a) for various values of α. It can be seen that $\mathbb{E}\left[P_s^{\beta}\right]$ increases with increasing ρ_{so} for lower

[5]For a certain threshold, both the ST and SR know the channel-state information (CSI) and the ST can adapt a power adaptation scheme. According to the scheme, the ST controls its transmission power so that the received signal power at the tagged SR is equal to the threshold ρ_{so} [82].

values of ρ_{so} and saturates when ρ_{so} exceeds a particular value, which depends on α. This is explained by the maximum transmission power P_{max} being fixed for a ST. As expected, for higher values of α, the expected transmission power is high. Fig. 4.4(b) illustrates the impact of P_{max} on $\mathbb{E}\left[P_s^{\beta}\right]$. In the low-$\rho_{so}$ region, $\mathbb{E}\left[P_s^{\beta}\right]$ is variable, whereas $\mathbb{E}\left[P_s^{\beta}\right]$ is constant in the high-ρ_{co} region. For the highest value of P_{max}, we find a high saturation point of approximately 0.71. Furthermore, the effect on $\mathbb{E}\left[P_s^{\beta}\right]$ is investigated for various densities as shown in Fig. 4.4(c). $\mathbb{E}\left[P_s^{\beta}\right]$ increases with ρ_{so} for lower values of ρ_{so} but remains constant at high values of ρ_{so}. For a high density, the value of $\mathbb{E}\left[P_s^{\beta}\right]$ is low. This is because $\mathbb{E}\left[P_s^{\beta}\right]$ is inversely proportional to λ_s. From Fig. 4.4, we observe that the expected transmission power of a ST is required to be high for a high-threshold ρ_{so} at its tagged SR since STs are maintained to overturn the path-loss. Hence, the expected transmission power saturates at $\lim_{\rho_{so}\to\infty} \mathbb{E}\left[P_s^{2/\alpha}\right] = P_{max}/2$ when $P_{max} = 1$ W.

4.4 Analysis of Performance Metric

On the basis of the CR network model described above, we derive mathematical expressions of coverage probability and spectral efficiency in the uplink of the CR network.

4.4.1 Coverage Probability

In this network, a transmitted signal is considered to be decoded successfully if the received signal-to-interference-plus-noise ratio (SINR) is greater than a predefined threshold T. If the SINR is below T, the communication link between the ST and SR suffers from outage. If a SR receives a desired signal from its ST, interference signals are also received from the neighboring STs and PT. Without loss of generality, we consider that both SRs[6] are located at the origin. Hence the SINRs experienced at the SRs can be expressed as

$$\mathrm{SINR}_{(\mathrm{a})} = \frac{\rho_{so} h_s^{(\mathrm{a})}}{\sigma^2 + I_{ss}^{(\mathrm{a})} + I_{sp}^{(\mathrm{a})}}, \tag{4.4.1}$$

$$\mathrm{SINR}_{(\mathrm{b})} = \frac{\rho_{so} h_c^{(\mathrm{b})}}{\sigma^2 + I_{ss}^{(\mathrm{b})} + I_{sp}^{(\mathrm{b})}}, \tag{4.4.2}$$

where $\rho_{so} h_s^{(\mathrm{a})}$ and $\rho_{so} h_s^{(\mathrm{b})}$ are the desired signal powers compensated by truncated channel inversion power control. For the accurate evaluation of interferences in both cases, the noise power is set to $\sigma^2_{(\mathrm{a})} = \sigma^2_{(\mathrm{b})} = \sigma^2$ at the SR. $I_{ss}^{(\mathrm{a})}$ and $I_{sp}^{(\mathrm{a})}$ are the interferences from the neighboring STs except for the tagged ST to the SR at position (a) and from the PT to the

[6]We consider two SRs corresponding to cases (a) and (b). The SR for case (a) is located at the origin when the interference from STs and PT is calculated. The same situation is considered for the SR in case (b) (i.e., it is located at the origin), the interference is calculated.

SR at position (a), respectively. $I_{ss}^{(\mathrm{b})}$ and $I_{sp}^{(\mathrm{b})}$ are the interferences from the neighboring STs except for the tagged ST to the SR at position (b) and from the PT to the SR at position (b), respectively. In terms of the SINR, the coverage probabilities can be obtained as

$$\begin{aligned} C_p^{(\mathrm{a})} &= \mathbb{P}\left[\frac{\rho_{so} h_s^{(\mathrm{a})}}{\sigma^2 + I_{ss}^{(\mathrm{a})} + I_{sp}^{(\mathrm{a})}} > T\right] \\ &\overset{(i)}{=} \mathbb{E}\left[\exp\left(-T\frac{\sigma^2 + I_{ss}^{(\mathrm{a})} + I_{sp}^{(\mathrm{a})}}{\rho_{so}}\right)\right] \\ &= \exp\left(-T\frac{\sigma^2}{\rho_{so}}\right)\mathcal{L}_{I_{ss}^{(\mathrm{a})}}(s_s)\,\mathcal{L}_{I_{sp}^{(\mathrm{a})}}(s_s), \end{aligned} \tag{4.4.3}$$

$$C_p^{(\mathrm{b})} = \exp\left(-T\frac{\sigma^2}{\rho_{so}}\right)\mathcal{L}_{I_{ss}^{(\mathrm{b})}}(s_s)\,\mathcal{L}_{I_{sp}^{(\mathrm{b})}}(s_s), \tag{4.4.4}$$

where $s_s = \frac{T}{\rho_{so}}$. The equality (i) is obtained from the exponential function. $\mathcal{L}_{I_{ss}^{(\mathrm{a})}}(s_c)$, $\mathcal{L}_{I_{sp}^{(\mathrm{a})}}(s_s)$, $\mathcal{L}_{I_{ss}^{(\mathrm{b})}}(s_s)$, and $\mathcal{L}_{I_{sp}^{(\mathrm{b})}}(s_s)$ are the Laplace transforms[7] of the probability density functions (pdfs) of the interferences $I_{ss}^{(\mathrm{a})}$, $I_{sp}^{(\mathrm{a})}$, $I_{ss}^{(\mathrm{b})}$, and $I_{sp}^{(\mathrm{b})}$, respectively. Here, we assume the same threshold T for cases (a) and (b) because we evaluate the effect of the interferences of STs and PT.

The transmission scenario for a CR network is discussed in detail in [49]. The packet delivery time of the ST is divided into two slots: spectrum-sensing slots and transmission slots. To enable the use of the frequency band of the SU in the CR network, spectrum sensing is the key factor and also the most challenging task. During a spectrum-sensing slot, STs[8] are required to sense the PT-to-SR[9] and STs-to-SR links and know their occupied and unoccupied frequency bands. The working group of IEEE 802.22 selected a probability of detection (P_D) of above 90% for a signal-to-noise ratio of -20 dB [47] because spectrum sensing is accurate when $P_D \geq 0.9$. Otherwise, spectrum sensing is imperfect. To simplify the analysis, we consider perfect detection for accurate spectrum sensing and imperfect detection for defective spectrum sensing. Thus, STs have perfect knowledge of both links (i.e., PT-to-SR and STs-to-SR) and interference does not occur because each ST is allocated an idle channel (i.e., the ST assigns one channel for the SR) for the associated SR in the CR network. With regard to spectrum sensing, there are four assumptions for the perfect and imperfect detection of PT-to-SR and STs-to-SR links:

(i) Perfect detection of PT-to-SR and STs-to-SR links: in this case, the Laplace transforms of interferences are equal to one, i.e., $\mathcal{L}_{I_{sp}^{(\mathrm{a})}}(s_s) = 1$, $\mathcal{L}_{I_{ss}^{(\mathrm{a})}}(s_s) = 1$, $\mathcal{L}_{I_{sp}^{(\mathrm{b})}}(s_s) = 1$, and $\mathcal{L}_{I_{ss}^{(\mathrm{b})}}(s_s) = 1$.

[7] The Laplace transform $\mathcal{L}$ of z is denoted as $\mathcal{L}_z(s) = \mathbb{E}[\exp(-sz)]$.

[8] STs are cellular phone users, so their operation mode change between a transmitter and a receiver.

[9] The PT-to-SR link is replaced by a PT-to-PR link, because, if STs perfectly sense the PT-to-PR link, they know the frequency band of the PU. So, STs avoid the use of the PU frequency band or the same frequency band. For this reason, the PT does not create interference in the SR.

(ii) Perfect detection of PT-to-SR link and imperfect detection of STs-to-SR links: the Laplace transforms of the interferences are $\mathcal{L}_{I_{sp}^{(\mathrm{a})}}(s_s) = 1$, $\mathcal{L}_{I_{ss}^{(\mathrm{a})}}(s_s) \neq 1$, $\mathcal{L}_{I_{sp}^{(\mathrm{b})}}(s_s) = 1$, and $\mathcal{L}_{I_{ss}^{(\mathrm{b})}}(s_s) \neq 1$.

(iii) Imperfect detection of PT-to-SR link and perfect detection of STs-to-SR links: the Laplace transforms of the interferences are $\mathcal{L}_{I_{sp}^{(\mathrm{a})}}(s_s) \neq 1$, $\mathcal{L}_{I_{ss}^{(\mathrm{a})}}(s_s) = 1$, $\mathcal{L}_{I_{sp}^{(\mathrm{b})}}(s_s) \neq 1$, and $\mathcal{L}_{I_{ss}^{(\mathrm{b})}}(s_s) = 1$.

(iv) Imperfect detection of PT-to-SR and STs-to-SR links: the Laplace transforms of the interferences are not equal to one, i.e., $\mathcal{L}_{I_{sp}^{(\mathrm{a})}}(s_c) \neq 1$, $\mathcal{L}_{I_{ss}^{(\mathrm{a})}}(s_s) \neq 1$, $\mathcal{L}_{I_{sp}^{(\mathrm{b})}}(s_s) \neq 1$, and $\mathcal{L}_{I_{ss}^{(\mathrm{b})}}(s_s) \neq 1$.

Following the four assumptions, a noise-limited environment is considered in assumption (i). According to this assumption, the coverage probability and spectral efficiency are noise-limited in which interference is insignificant. In other words, interfering STs and PT do not affect the tagged SR. However, the other assumptions (i.e., (ii), (iii), and (iv)) correspond to noise-plus-interference-limited. Interfering STs and PT cause interference on the tagged SR. Thus, the coverage probability and spectral efficiency are noise-plus-interference-limited for these assumptions [83].

In this portion, we analyze the theoretical expressions of coverage probability for all assumptions in the CR network. The four assumptions of the coverage probability are given by the following lemmas. In the lemmas, we assume two cases: (a) the SR is inside the PER and (b) the SR is outside the PER (as already explained in Fig. 4.2 in section 4.2).

Lemma 1. *In the single-tier uplink modeling of a Poisson CR network considering assumption* (i)*, the coverage probability for the tagged ST can be expressed as*

$$C_p^{(\mathrm{ia})} = \exp\left(-T\frac{\sigma^2}{\rho_{so}}\right), \tag{4.4.5}$$

$$C_p^{(\mathrm{ib})} = \exp\left(-T\frac{\sigma^2}{\rho_{so}}\right). \tag{4.4.6}$$

Proof: We set assumption (i) in (4.4.3) and (4.4.4).

Lemma 2. *In the single-tier uplink modeling of a Poisson CR network considering interfering STs, the coverage probability for the tagged ST can be expressed as*

$$C_p^{(\mathrm{iia})} = \exp\left[-T\frac{\sigma^2}{\rho_{so}} - 2T^{\frac{2}{\alpha}}P_{STR}\int_{T^{\frac{-1}{\alpha}}}^{\infty}\frac{x}{1+x^{\alpha}}dx\right], \tag{4.4.7}$$

$$C_p^{(\mathrm{iib})} = \exp\left[-T\frac{\sigma^2}{\rho_{so}} - 2T^{\frac{2}{\alpha}}P_{STR}\int_{T^{\frac{-1}{\alpha}}}^{\infty}\frac{x}{1+x^{\alpha}}dx\right], \tag{4.4.8}$$

where $P_{STR} = \dfrac{\gamma\left(2,\pi\lambda_s\left(\frac{P_{max}}{\rho_{so}}\right)^{\frac{2}{\alpha}}\right)}{1-\exp\left\{-\pi\lambda_s\left(\frac{P_{max}}{\rho_{so}}\right)^{\frac{2}{\alpha}}\right\}}$.

Proof: We assume assumption (ii) in lemma 2. For cases (a) and (b), a SR located at the origin is considered in the calculation of the interferences of the STs except tagged ST. Thus, the interference is approximately the same for each ST because of truncated channel inversion power control. For this reason, we assume $\mathcal{L}_{I_{ss}^{(\mathrm{a})}}(s_s) = \mathcal{L}_{I_{ss}^{(\mathrm{b})}}(s_s)$. The detailed derivation of $\mathcal{L}_{I_{ss}}(s_s)$ is given in Appendix C (**C.1**).

Lemma 3. *In the single-tier uplink modeling of a Poisson CR network considering an interfering PT, the coverage probability for the tagged ST can be expressed as*

$$C_p^{(\mathrm{iiia})} = \exp\left[-T\frac{\sigma^2}{\rho_{so}} - 2\pi\lambda_p\left(\frac{T}{\rho_{so}}\right)^{\frac{2}{\alpha}} P_p^{\frac{2}{\alpha}} \int_0^{U_l} \frac{y}{1+y^\alpha}dy\right], \tag{4.4.9}$$

$$C_p^{(\mathrm{iiib})} = \exp\left[-T\frac{\sigma^2}{\rho_{so}} - 2\pi\lambda_p\left(\frac{T}{\rho_{so}}\right)^{\frac{2}{\alpha}} P_p^{\frac{2}{\alpha}} \int_{L_l}^{\infty} \frac{y}{1+y^\alpha}dy\right], \tag{4.4.10}$$

where $U_l = L_l = \left(\frac{r_{PER}^\alpha \rho_{so}}{TP_p}\right)^{\frac{1}{\alpha}}$ and r_{PER} is the radius of the PER.

Proof: We consider assumption (iii) in lemma 3. The detailed derivation of $\mathcal{L}_{I_{sp}^{(\mathrm{a})}}(s_s)$ and $\mathcal{L}_{I_{sp}^{(\mathrm{b})}}(s_s)$ is provided in Appendix C (**C.2**).

Lemma 4. *In the single-tier uplink modeling of a Poisson CR network considering interfering STs and an interfering PT, the coverage probability for the tagged ST can be expressed as*

$$C_p^{(\mathrm{iva})} = \exp\left[-T\frac{\sigma^2}{\rho_{so}} - 2T^{\frac{2}{\alpha}}P_{STR}\int_{T^{\frac{-1}{\alpha}}}^{\infty}\frac{x}{1+x^\alpha}dx - 2\pi\lambda_p\left(\frac{T}{\rho_{so}}\right)^{\frac{2}{\alpha}} P_p^{\frac{2}{\alpha}}\int_0^{U_l}\frac{y}{1+y^\alpha}dy\right], \tag{4.4.11}$$

$$C_p^{(\mathrm{ivb})} = \exp\left[-T\frac{\sigma^2}{\rho_{so}} - 2T^{\frac{2}{\alpha}}P_{STR}\int_{T^{\frac{-1}{\alpha}}}^{\infty}\frac{x}{1+x^\alpha}dx - 2\pi\lambda_p\left(\frac{T}{\rho_{so}}\right)^{\frac{2}{\alpha}} P_p^{\frac{2}{\alpha}}\int_{L_l}^{\infty}\frac{y}{1+y^\alpha}dy\right]. \tag{4.4.12}$$

Proof: Lemma 4 combines the results of lemmas 2 and 3. For more details, see Appendix (**C.1 & C.2**).

***Closed-form expressions*:** If $\alpha = 4$, the integral expressions (4.4.7), (4.4.8), (4.4.9), (4.4.10), (4.4.11), and (4.4.12) can be reduced to the following closed-form expressions:

$$C_p^{(\mathrm{iia\ or\ iib})} = \exp\left[-T\frac{\sigma^2}{\rho_{so}} - \sqrt{T}P_{STR}\arctan\left(\sqrt{T}\right)\right], \tag{4.4.13}$$

$$C_p^{(\mathrm{iiia})} = \exp\left[-T\frac{\sigma^2}{\rho_{so}} - \pi\lambda_p\left(\sqrt{\frac{TP_p}{\rho_{so}}}\right)\arctan\left(\sqrt{\frac{r_{PER}^4\rho_{so}}{TP_p}}\right)\right], \tag{4.4.14}$$

$$C_p^{(\mathrm{iiib})} = \exp\left[-T\frac{\sigma^2}{\rho_{so}} - \pi\lambda_p\left(\sqrt{\frac{TP_p}{\rho_{so}}}\right)\left\{\frac{\pi}{2} - \arctan\left(\sqrt{\frac{r_{PER}^4\rho_{so}}{TP_p}}\right)\right\}\right], \tag{4.4.15}$$

$$C_p^{(\mathrm{iva})} = \exp\left[-T\frac{\sigma^2}{\rho_{so}} - \sqrt{T}P_{STR}\arctan\left(\sqrt{T}\right) - \pi\lambda_p\left(\sqrt{\frac{TP_p}{\rho_{so}}}\right)\cdot\arctan\left(\sqrt{\frac{r_{PER}^4\rho_{so}}{TP_p}}\right)\right], \tag{4.4.16}$$

$$C_p^{(\mathrm{ivb})} = \exp\left[-T\frac{\sigma^2}{\rho_{so}} - \sqrt{T}P_{STR}\arctan\left(\sqrt{T}\right) - \pi\lambda_p\left(\sqrt{\frac{TP_p}{\rho_{so}}}\right)\cdot\left\{\frac{\pi}{2} - \arctan\left(\sqrt{\frac{r_{PER}^4\rho_{so}}{TP_p}}\right)\right\}\right]. \tag{4.4.17}$$

Proof: See Appendix C (**C.3**).

4.4.2 Spectral Efficiency

In a CR network, higher spectral efficiency is required and it is necessary to provide a higher data rate to mobile phone users. The spectral efficiency is defined as the total number of information bits transmitted from the ST to a SR over a particular bandwidth in a CR network [84]. The spectral efficiency between the ST and a SR is related to the received SINR at the SR and is obtained by Shannon's formula, which can be expressed as $\mathbb{P}\left(X > x\right)$, where $X = \ln(1 + \mathrm{SINR})$ and x is the threshold value (x nats/sec/Hz). Due to the CR network, the SINR is given by (4.4.1) and (4.4.2), which we use in the following discussion.

Let us consider a single link between the ST and a SR in a CR network. For the received SINR at the SR, the probability that the Shannon capacity on the link is greater than a threshold (t) is called the spectral efficiency. Thus, the spectral efficiency can be represented by the following relation:

$$\begin{aligned} R^{(\mathrm{a})} &= \int_0^\infty \mathbb{P}\left[\ln\left(1 + \mathrm{SINR}_{(\mathrm{a})}\right) > t\right] dt \\ &= \int_0^\infty \mathbb{P}\left[\frac{\rho_{so}h_s^{(\mathrm{a})}}{\sigma^2 + I_{ss}^{(\mathrm{a})} + I_{sp}^{(\mathrm{a})}} > \mathrm{E}(t)\right] dt \\ &= \int_0^\infty \exp\left(-\frac{\sigma^2\mathrm{E}(t)}{\rho_{so}}\right)\mathcal{L}_{I_{ss}^{(\mathrm{a})}}\left(\frac{\mathrm{E}(t)}{\rho_{so}}\right)\mathcal{L}_{I_{sp}^{(\mathrm{a})}}\left(\frac{\mathrm{E}(t)}{\rho_{so}}\right) dt \\ &\overset{(i)}{=} \int_0^\infty \frac{1}{1+z}\exp\left(-z\frac{\sigma^2}{\rho_{so}}\right)\mathcal{L}_{I_{ss}^{(\mathrm{a})}}\left(\frac{z}{\rho_{so}}\right)\mathcal{L}_{I_{sp}^{(\mathrm{a})}}\left(\frac{z}{\rho_{so}}\right) dz, \end{aligned} \tag{4.4.18}$$

$$R^{(\mathrm{b})} \overset{(i)}{=} \int_0^\infty \frac{1}{1+z}\exp\left(-z\frac{\sigma^2}{\rho_{so}}\right)\mathcal{L}_{I_{ss}^{(\mathrm{b})}}\left(\frac{z}{\rho_{so}}\right)\mathcal{L}_{I_{sp}^{(\mathrm{b})}}\left(\frac{z}{\rho_{so}}\right) dz. \tag{4.4.19}$$

where $\mathrm{E}(t) = e^t - 1$ and (i) is obtained by replacing the variable $z = \mathrm{E}(t)$. In order to derive the spectral efficiency in a CR network, there are four assumptions obtained from

spectrum sensing. Mathematical expressions for the spectral efficiency are given by the following lemmas, in which we consider two cases: (a) and (b).

Lemma 5. *In the single-tier uplink modeling of a Poisson CR network considering assumption* (i)*, the spectral efficiency of transmission by the tagged ST can be expressed as*

$$R^{(\mathrm{ia})} = \int_0^\infty \frac{1}{1+z} \exp\left(-z\frac{\sigma^2}{\rho_{so}}\right) dz, \tag{4.4.20}$$

$$R^{(\mathrm{ib})} = \int_0^\infty \frac{1}{1+z} \exp\left(-z\frac{\sigma^2}{\rho_{so}}\right) dz. \tag{4.4.21}$$

Proof: We apply assumption (i) in (4.4.18) and (4.4.19).

Lemma 6. *In the single-tier uplink modeling of a Poisson CR network considering interfering STs, the spectral efficiency of transmission by the tagged ST can be expressed as*

$$R^{(\mathrm{iia})} = \int_0^\infty \frac{1}{1+z} \exp\left[-z\frac{\sigma^2}{\rho_{so}} - 2z^{\frac{2}{\alpha}} P_{STR} \int_{z^{\frac{-1}{\alpha}}}^\infty \frac{x}{1+x^\alpha} dx\right] dz, \tag{4.4.22}$$

$$R^{(\mathrm{iib})} = \int_0^\infty \frac{1}{1+z} \exp\left[-z\frac{\sigma^2}{\rho_{so}} - 2z^{\frac{2}{\alpha}} P_{STR} \int_{z^{\frac{-1}{\alpha}}}^\infty \frac{x}{1+x^\alpha} dx\right] dz, \tag{4.4.23}$$

where $P_{STR} = \dfrac{\gamma\left(2, \pi\lambda_s \left(\frac{P_{max}}{\rho_{so}}\right)^{\frac{2}{\alpha}}\right)}{1-\exp\left\{-\pi\lambda_s \left(\frac{P_{max}}{\rho_{so}}\right)^{\frac{2}{\alpha}}\right\}}$.

Proof: We apply assumption (ii) in (4.4.18) and (4.4.19). Here, we assume that $\mathcal{L}_{I_{ss}^{(\mathrm{a})}}(\frac{z}{\rho_{so}}) = \mathcal{L}_{I_{ss}^{(\mathrm{b})}}(\frac{z}{\rho_{so}})$, as already explained for lemma 2. Then, we replace $\frac{z}{\rho_{so}}$ with $\frac{T}{\rho_{so}}$. The calculation of the Laplace transform $\mathcal{L}_{I_{ss}}(\frac{z}{\rho_{so}})$ follows the same procedure as in Appendix C (**C.1**).

Lemma 7. *In the single-tier uplink modeling of a Poisson CR network considering an interfering PT, the spectral efficiency of transmission by the tagged ST can be expressed as*

$$R^{(\mathrm{iiia})} = \int_0^\infty \frac{1}{1+z} \exp\left[-z\frac{\sigma^2}{\rho_{so}} - 2\pi\lambda_p \left(\frac{z}{\rho_{so}}\right)^{\frac{2}{\alpha}} P_p^{\frac{2}{\alpha}} \int_0^{U_l} \frac{y}{1+y^\alpha} dy\right] dz, \tag{4.4.24}$$

$$R^{(\mathrm{iiib})} = \int_0^\infty \frac{1}{1+z} \exp\left[-z\frac{\sigma^2}{\rho_{so}} - 2\pi\lambda_p \left(\frac{z}{\rho_{so}}\right)^{\frac{2}{\alpha}} P_p^{\frac{2}{\alpha}} \int_{L_l}^\infty \frac{y}{1+y^\alpha} dy\right] dz, \tag{4.4.25}$$

where $U_l = L_l = \left(\frac{r_{PER}^\alpha \rho_{so}}{z P_p}\right)^{\frac{1}{\alpha}}$ and r_{PER} is the radius of the PER.

Proof: We apply assumption (iii) in (4.4.18) and (4.4.19). Then, we replace $\frac{z}{\rho_{so}}$ with $\frac{T}{\rho_{so}}$. The calculation of the Laplace transforms $\mathcal{L}_{I_{sp}^{(\mathrm{a})}}(\frac{z}{\rho_{so}})$ and $\mathcal{L}_{I_{sp}^{(\mathrm{b})}}(\frac{z}{\rho_{so}})$ follows the same procedure as in Appendix C (**C.2**).

Lemma 8. *In the single-tier uplink modeling of a Poisson CR network considering interfering STs and an interfering PT, the spectral efficiency of transmission by the tagged ST can be expressed as*

$$R^{(\text{iva})} = \int_0^{\infty} \frac{1}{1+z} \exp\left[-z\frac{\sigma^2}{\rho_{so}} - 2z^{\frac{2}{\alpha}} P_{STR} \int_{z^{\frac{-1}{\alpha}}}^{\infty} \frac{x}{1+x^{\alpha}} dx - 2\pi\lambda_p \left(\frac{z}{\rho_{so}}\right)^{\frac{2}{\alpha}} \cdot P_p^{\frac{2}{\alpha}} \int_0^{U_l} \frac{y}{1+y^{\alpha}} dy \right] dz, \tag{4.4.26}$$

$$R^{(\text{ivb})} = \int_0^{\infty} \frac{1}{1+z} \exp\left[-z\frac{\sigma^2}{\rho_{so}} - 2z^{\frac{2}{\alpha}} P_{STR} \int_{z^{\frac{-1}{\alpha}}}^{\infty} \frac{x}{1+x^{\alpha}} dx - 2\pi\lambda_p \left(\frac{z}{\rho_{so}}\right)^{\frac{2}{\alpha}} \cdot P_p^{\frac{2}{\alpha}} \int_{L_l}^{\infty} \frac{y}{1+y^{\alpha}} dy \right] dz. \tag{4.4.27}$$

Proof: Lemma 8 combines the results of lemmas 6 and 7. See Appendix (**C.1 & C.2**) for a detailed proof.

Now we derive the expressions of spectral efficiency in a CR network for $\alpha = 4$. The theoretical expressions of spectral efficiency for (4.4.22), (4.4.23), (4.4.24), (4.4.25), (4.4.26), and (4.4.27) can be written as

$$R^{(\text{iia or iib})} = \int_0^{\infty} \frac{1}{1+z} \exp\left[-z\frac{\sigma^2}{\rho_{so}} - \sqrt{z} P_{STR} \arctan\left(\sqrt{z}\right) \right] dz, \tag{4.4.28}$$

$$R^{(\text{iiia})} = \int_0^{\infty} \frac{1}{1+z} \exp\left[-z\frac{\sigma^2}{\rho_{so}} - \pi\lambda_p \left(\sqrt{\frac{zP_p}{\rho_{so}}}\right) \arctan\left(\sqrt{\frac{r_{PER}^4 \rho_{so}}{zP_p}}\right) \right] dz, \tag{4.4.29}$$

$$R^{(\text{iiib})} = \int_0^{\infty} \frac{1}{1+z} \exp\left[-z\frac{\sigma^2}{\rho_{so}} - \pi\lambda_p \left(\sqrt{\frac{zP_p}{\rho_{so}}}\right) \left\{ \frac{\pi}{2} - \arctan\left(\sqrt{\frac{r_{PER}^4 \rho_{co}}{zP_p}}\right) \right\} \right] dz, \tag{4.4.30}$$

$$R^{(\text{iva})} = \int_0^{\infty} \frac{1}{1+z} \exp\left[-z\frac{\sigma^2}{\rho_{so}} - \sqrt{z} P_{STR} \arctan\left(\sqrt{z}\right) - \pi\lambda_p \left(\sqrt{\frac{zP_p}{\rho_{so}}}\right) \cdot \arctan\left(\sqrt{\frac{r_{PER}^4 \rho_{so}}{zP_p}}\right) \right] dz, \tag{4.4.31}$$

$$R^{(\text{ivb})} = \int_0^{\infty} \frac{1}{1+z} \exp\left[-z\frac{\sigma^2}{\rho_{so}} - \sqrt{z} P_{STR} \arctan\left(\sqrt{z}\right) - \pi\lambda_p \left(\sqrt{\frac{zP_p}{\rho_{so}}}\right) \cdot \left\{ \frac{\pi}{2} - \arctan\left(\sqrt{\frac{r_{PER}^4 \rho_{so}}{zP_p}}\right) \right\} \right] dz. \tag{4.4.32}$$

Proof: See Appendix C (**9.3**).

4.5 Numerical Examples and Discussion

To demonstrate the performance of a CR network, we present some numerical examples and evaluate the theoretical expressions given in the previous section for the four assumptions of spectrum sensing and the locations of the SR of (a) inside the PER and (b) outside the PER. First, we evaluate the coverage probability with respect to a predefined threshold (T) and cutoff threshold (ρ_{so}). Then we assess the effect of the spectral efficiency. For the numerical examples, we assume a few same parameters as in [77]. The simulation parameters for the following figures are: $P_{max} = 1$ W, $P_p = 100$ W, $r_{PER} = 1200$ m, $\alpha = 4$, and $\sigma^2 = -70$ dBm.

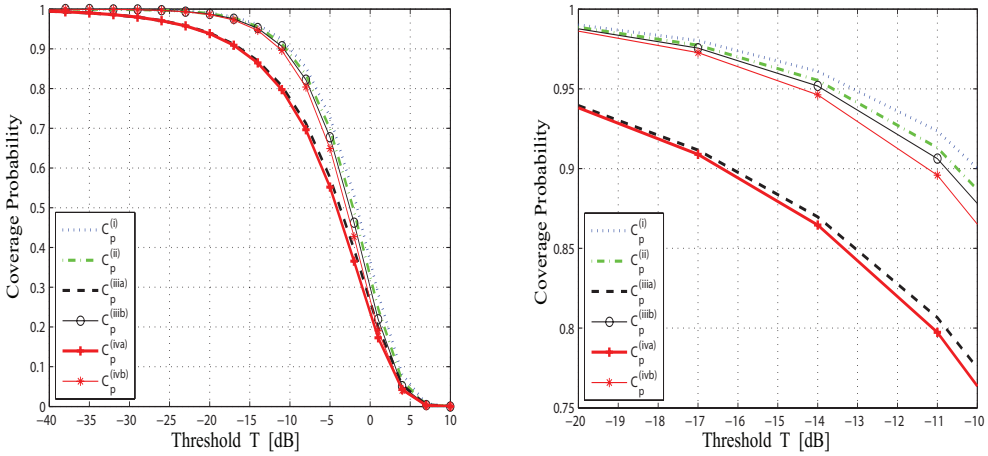

(a) Results of coverage probability for -40 dB $\leq T \leq 10$ dB.

(b) Results of coverage probability for -20 dB $\leq T \leq -10$ dB.

Figure 4.5: Comparison of analytical results of coverage probability for four assumptions with $\lambda_s = 1/\text{km}^2$, $\lambda_p = 1/9\text{km}^2$, and $\rho_{so} = -70$ dBm.

4.5.1 Examples of Coverage Probability

Analytical results for the CR network coverage probability are shown in Fig. 4.5, where the four assumptions are compared. It can be seen from Fig. 4.5(a) that assumptions (i) and (iv) have the best and worst coverage probability curves, respectively. This is because in assumption (i) there is no interference from the PT or the STs, whereas in assumption (iv) takes account of interference from the PT and STs. The coverage probability for the four assumptions is not clear in Fig. 4.5(a). For this reason, we plot Fig. 4.5(b) to compare the performances for the assumptions. In the case of assumptions (iii) and (iv), the coverage probability has better performance for case (b) when T increases because the SR is outside the PER. Moreover, the results show little difference in performance between assumptions (iii) and (iv) in cases (a) and (b).

The analytical results evaluated for assumption (iv) are shown in Figs. 4.6 to 4.9. We

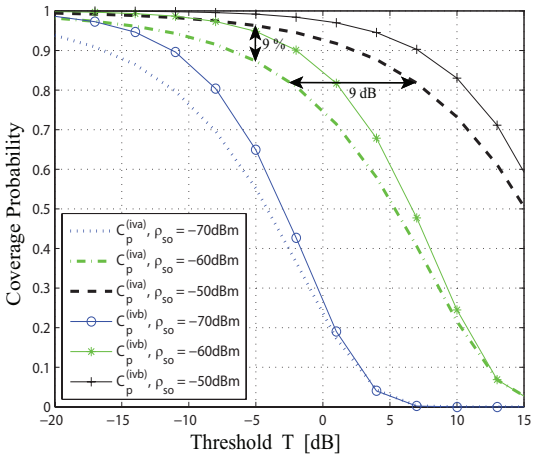

Figure 4.6: Impact of cutoff threshold ρ_{so} on coverage probability with $\lambda_s = 1/\text{km}^2$ and $\lambda_p = 1/9\text{km}^2$.

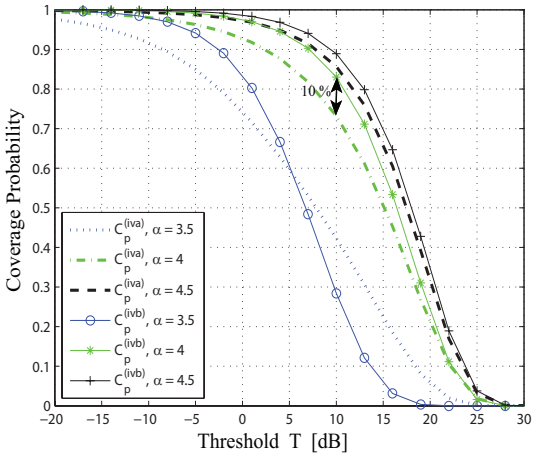

Figure 4.7: Impact of path-loss exponent α on coverage probability with $\lambda_s = 1/\text{km}^2$, $\lambda_p = 1/9\text{km}^2$, and $\rho_{so} = -50$ dBm.

demonstrate the improved of coverage probability with improvement of the cutoff threshold ρ_{so} in Fig. 4.6. For a predefined threshold of $T = -5$ dB, the coverage probability $C_p^{(\text{iva})}$ for $\rho_{so} = -60$ dBm is reduced to approximately 9% of that for $\rho_{so} = -50$ dBm. When $C_p^{(\text{iva})} = 0.81$, T for $\rho_{so} = -60$ dBm is reduced to 9 dB compared with $\rho_{so} = -50$ dBm. In addition, case (b) outperforms case (a) with the same value of ρ_{so}. However, above a certain predefined threshold T, case (a) performs only slightly better than case (b). For instance, case (a) performs slightly better when $T \geq 3.4$ dB for $\rho_{so} = -70$ dBm. This is because the integral form ($\int_0^{U_l} \frac{y}{1+y^\alpha} dy$) decreases with increasing T for case (a). On the other hand, the integral form ($\int_{L_l}^{\infty} \frac{y}{1+y^\alpha} dy$) increases with increasing T for case (b). Hence, the integral form affects the exponential function of the coverage probability. Thus, the predefined threshold T is an important factor of CR network design.

As shown in Fig. 4.7, the coverage probability increases significantly with increasing path-loss exponent α. Similar results were obtained for cases (a) and (b), as shown in Fig. 4.6. When T is low, the coverage probability in case (b) is higher than that in case (a). However, case (a) has better performance than case (b) for higher values of T and lower values of α. With the same values of $T = 10$ dB and $\alpha = 4$, the coverage probability for case (b) is approximately 10% higher than that for case (a).

A comparison of the performances of cases (a) and (b) is shown in Fig. 4.8 for various densities of the SR. As can be predicted from Figs. 4.6 and 4.7, case (b) still has better performance than case (a). It is also observed that the SR density impacts on coverage probability, the coverage probability decreases with increasing SR density. This is because that the variation of λ_s affects P_{STR}; P_{STR} is increased with increasing λ_s, consequently deceasing the coverage probability. For case (b), the improvement of the coverage probability is approximately 22.44% for the densities of $\lambda_s = 1$ and $\lambda_s = 10$ at $\rho_{so} = -51$ dBm.

Regarding the four assumptions, the coverage probability was similar for lower (i.e., approximately $\rho_{so} < -72$ dBm) and higher (i.e., approximately $\rho_{so} > -8$ dBm) cutoff thresholds.

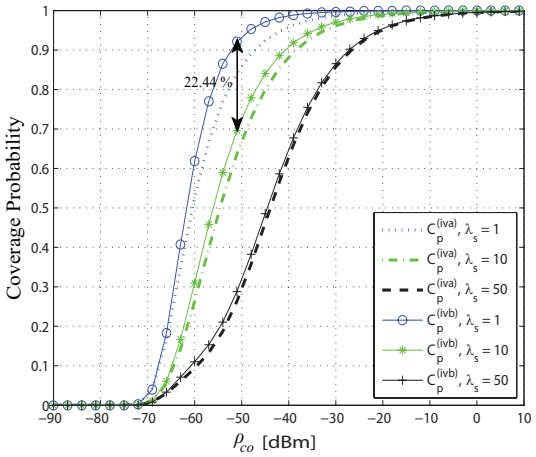

Figure 4.8: Impact of density λ_s on coverage probability with $T = 5$ dB.

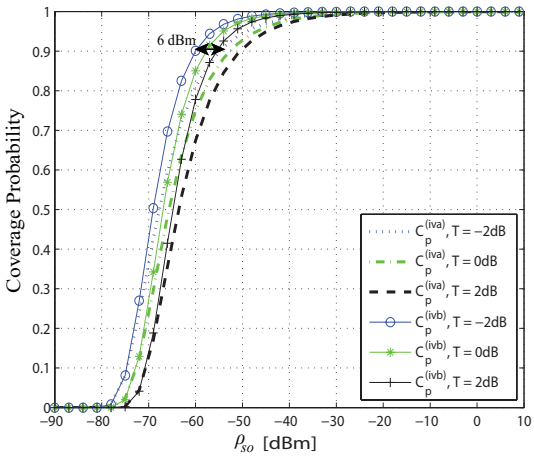

Figure 4.9: Impact of T on coverage probability with $\lambda_s = 1/\text{km}^2$ and $\lambda_p = 1/9\text{km}^2$.

In Fig. 4.9, we observe the effect of increasing the predefined threshold T on the coverage probability. It can be seen that for a particular value of ρ_{so}, increasing T decreases the coverage probability. Furthermore, case (b) has better performance than case (a) for the same value of T. When $T = -2$ dB, the cutoff threshold ρ_{so} can be reduced by approximately 6 dBm for case (b) to achieve a coverage probability of 0.9.

4.5.2 Examples of Spectral Efficiency

We now present the performance of the spectral efficiency considering the four assumptions in Fig. 4.10. Assumption (i) gives the best performance for the same reason as given before Fig. 4.5. Here, assumption (ii) obtains similar results (i.e., better performance than assumptions (iii) and (iv)) to those for the coverage probability. This is also because only the interference of STs is considered. Comparing cases (a) and (b) for assumptions (iii) and (iv), case (b) obtains the better performance. Fig. 4.10(a) does not allow a clear evaluation of the performance of the spectral efficiency; for this reason, Fig. 4.10(b) is provided.

The analytical results for assumption (iv) are presented in Fig. 4.11, which shows the spectral efficiency with respect to the cutoff threshold ρ_{so}. It can be observed that for the same SR density, case (b) has higher spectral efficiency than case (a). We observe that the spectral efficiency is 4.11 for case (a) compared with 4.49 for case (b) at $\rho_{so} = -46$ dBm. This is due to the fact that increasing the SR density significantly reduces the spectral efficiency. For a large λ_s, the spectral efficiency is determined by P_{STR}, which is proportional to λ_s and inversely related to ρ_{so}.

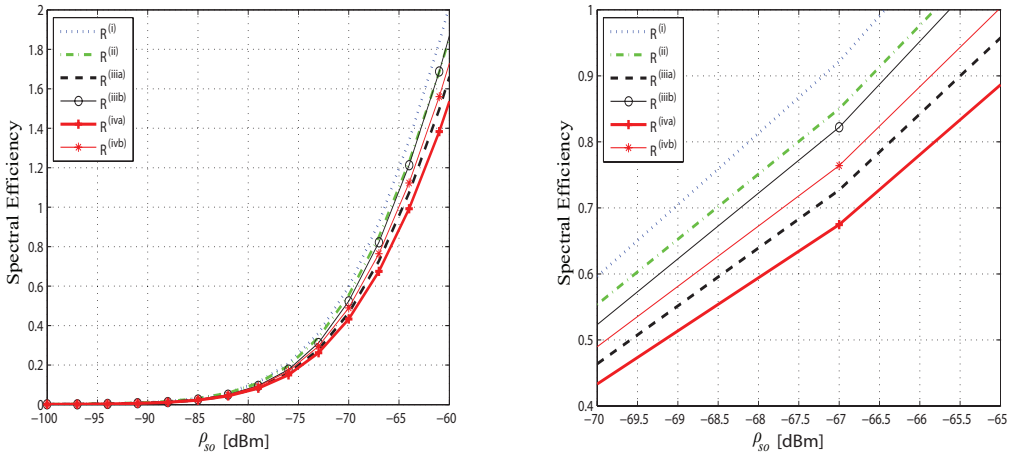

(a) Result of spectral efficiency for -100 dBm $\leq \rho_{so} \leq -60$ dBm.

(b) Result of spectral efficiency for -70 dBm $\leq \rho_{so} \leq -65$ dBm.

Figure 4.10: Comparison of analytical results of spectral efficiency for the four assumptions with $\lambda_s = 1/\text{km}^2$, $\lambda_p = 1/9\text{km}^2$.

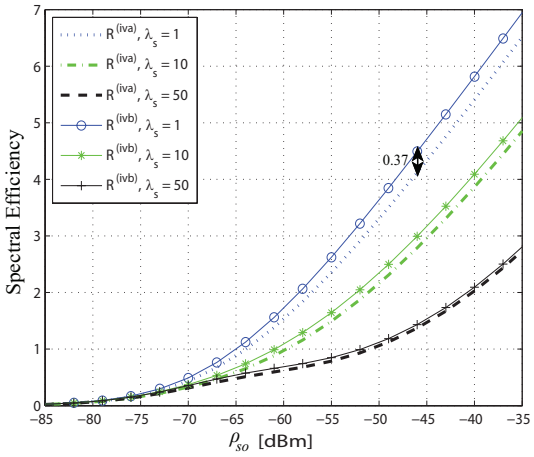

Figure 4.11: Impact of various densities λ_s on spectral efficiency.

Chapter 5

Energy Harvesting in CR Network

5.1 Literature Review

Energy harvesting from wireless networks has recently been the focus of substantial research on the provision/supply of power in battery-operated wireless devices. A practical scenario of simultaneous wireless information and power transfer is discussed in [92], which provides an overview of resource allocation and cooperative CR networks. RF energy harvesting in various types of wireless networks, for example, single-hop networks, multi-antenna networks, relay networks, and CR networks has been examined and surveyed comprehensively in [93]. A recent comprehensive survey of energy harvesting communications and networking provides a broad perspective of past, present, and future issues [94]. Y. Li *et al.* investigated the underlay cognitive relay network to derive outage probability under three power constraints, and also derived throughput in both delay-sensitive and delay-tolerant transmission modes [95]. In addition, Z. Wang *et al.* analyzed outage probability, rate-energy trade-off, and also three optimization techniques for improving spectrum and energy efficiency [96]. Y. Liu *et al.* in [97] presented a device-to-device communication design for energy harvesting in large-scale CR networks, and evaluated its power outage probability, secrecy outage probability, and secrecy throughput.

In [98], I. Krikidis investigated RF energy harvesting for cooperative and non-cooperative protocols when transmitter-receiver pairs are deployed following a Poisson point process (PPP). S. Lee *et al.* in [99] derived transmission probability, outage probability, and maximization of network throughput for a PPP in CR networks by considering a single-slope path-loss analytical model. In [100], A. H. Sakr and E. Hossain developed a multi-tier uplink cellular network using a PPP and investigated its transmission probability, coverage probability, and success probability. In [101], I. Flint *et al.* studied a wireless sensor network where sources are distributed as a Ginibre α-determinantal point process (DPP). They derived an expression for the expectation and variance of the energy harvesting rate and investigated the upper bound of power outage probability and transmission outage probability. In a recent study of Ginibre DPP, [102] analyzed the performance of self-sustainable communications with RF energy harvesting.

5.2 System Model

5.2.1 Network Topology

We consider here only the downlink of a CR network composed of primary network (PN) and secondary network (SN) and assume that all users are active. A PN consists of a primary transmitter (PT) and numerous primary receivers (PRs) and a SN consists of a secondary transmitter (ST) and numerous secondary receivers (SRs). The locations of PTs are distributed according to a homogeneous PPP $\Phi_{Pt} = \{a_1, a_2, ...\} \subset \mathbb{R}^2$ of density λ_{Pt} and also the PRs follow an independent PPP $\Phi_{Pr} = \{b_1, b_2, ...\} \subset \mathbb{R}^2$ of density λ_{Pr}. Each PT has a PER where STs are not allowed to utilize the licensed frequency band on account of interference [27, 56]. For simple analysis, it is assumed that all active STs (cognitive macro-BS) are outside the PER. The locations of STs are modeled according to a homogeneous PPP $\Phi_{St} = \{c_1, c_2, ...\} \subset \mathbb{R}^2$ of density λ_{St} and SRs follow an independent PPP $\Phi_{Sr} = \{d_1, d_2, ...\} \subset \mathbb{R}^2$ of density λ_{Sr}. A typical SR can be assumed to be located at the origin (0,0) without loss of generality.

5.2.2 Path-loss Model

In the environment of cellular networks, the standard path-loss model is considered for performance evaluation of cellular networks. However, standard path-loss model does not fit realistic scenarios [103]. According to the technique report of the 3rd Generation Partnership Project (known as 3GPP model or International Telecommunication Union Radiocommunication Sector (ITU-R) Urban Microcell (UMi) model), the two-slope path-loss model is more attractive for analysis of cellular networks [104]. The characteristic of two-slope path-loss follows line-of-sight (LoS) and non-line-of-sight (NLoS) propagation where LoS propagation may occur when the distance is less than the critical distance (i.e., $d_c \leq 18$m) [105].

In this analysis, all transmissions experience Rayleigh fading over each channel and the channel power gains are independent and identically distributed (i.i.d.) exponentially with unit mean. For simple notation, we denote as $l(d)$ rather than $l(\|d\|)$. In the path-loss model, it is assumed that the two-slope path-loss function, expressed as

$$l(d) = \begin{cases} \|d\|^{-\alpha_L}, & \|d\| \leq d_c \\ \kappa \|d\|^{-\alpha_N}, & \|d\| > d_c \end{cases} \tag{5.2.1}$$

where $\kappa = d_c^{\alpha_N - \alpha_L}$, α_L and α_N are the path-loss exponents for LOS and NLOS propagation, respectively, and d_c is the critical distance.

5.2.3 Timeslot and Sensing

Assume that ST opportunistically accesses the licensed spectrum. Then each frame of ST comprises a sensing slot of duration T_s and a transmission slot of duration T_p, as shown in Fig. 5.1. The function of frame can be detailed as follows:

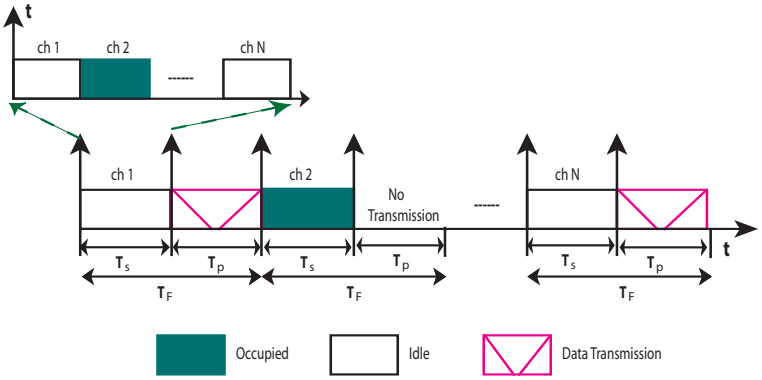

Figure 5.1: Illustration of timeslot structure of ST.

5.2.3.1 Sensing Period

During the time interval $[0, T_s]$, the ST accesses the licensed spectrum (i.e., spectrum of primary user) to detect idle and occupied channels. In the licensed spectrum, there are M idle channels and $N - M$ occupied channels among the N channels depicted in Fig. 5.1. Each ST randomly chooses one channel and then determines whether it is idle or not. As usual, PT transmits its own data for the corresponding PR, and at that moment, ST measures the signal-to-noise ratio (SNR) of PT ($\gamma_p(h, l(d))$). A detailed calculation of $\gamma_p(h, l(d))$ is provided in Appendix D.1. Subsequently, the received SNR at ST is compared with the SNR threshold (γ_t). If the received SNR is greater than the SNR threshold, the channel is classed as occupied and if opposite, the channel is classed as idle. Thus, we can represent the idle and occupied channels states by means of an indicator function, which can be defined as

$$\mathbb{I}_{\gamma_t}(\gamma_p(h, l(d))) = \begin{cases} 1, & \gamma_p(h, l(d)) \geq \gamma_t \\ 0, & \gamma_p(h, l(d)) < \gamma_t \end{cases} \tag{5.2.2}$$

By applying the indicator function, each ST knows which channels are idle, and ST utilizes the idle channels. Next, we discuss the *probability of successful selection of an idle channel*.

Probability of successful selection of an idle channel: In the sensing period, ST randomly selects a channel from N channels for data transmission where there are M idle channels and $N - M$ occupied channels. The *probability of successful selection of an idle channel* is stated as the probability that the channel is idle when ST selects it randomly from the N channels. The *probability of successful selection of an idle channel* is represented as

$$Q_s = \binom{M}{1} / \binom{N}{1} = \frac{M}{N}. \tag{5.2.3}$$

5.2.3.2 Transmission Period

During the time interval $[T_s, T_s + T_p]$, after considering the sensing results, ST decides whether or not to transmit on the channel. If a channel is sensed as idle, ST sends data to SR via that channel. If the channel is sensed as occupied, ST waits until the next frame.

5.2.4 Design of Receiver

One of the fundamental needs here is a new receiver architecture design for WEH. Several receiver designs have been discussed [106–108]. We introduce a dual mode (DM) power-splitting (PS) receiver that performs in both active and inactive mode. In active mode, it works as a PS with a PS ratio ρ, as depicted in Fig. 5.2(a). In inactive mode, PS only connects with the energy harvester (EH) node, that is $\rho = 0$, as depicted in Fig. 5.2(b).

5.2.4.1 Active Mode

ST is actively in communication with its associated SR. This is known as *on-mode*. In general, a SR receives a signal from a ST. In this circumstance, each SR is equipped with a PS device to synchronize the decoding of information and the harvesting of energy from the received signal power. In particular, the received signal power at the SR is divided such that a ρ portion of the signal power is used by the information decoder (ID) and the remaining $1 - \rho$ portion of the power is reserved for the EH.

5.2.4.2 Inactive Mode

ST is inactive on transmission. This is known as *off-mode*. In general, SR does not receive a signal from the ST. In this circumstance, each SR performs only energy harvesting. Hence, PS is connected to the EH.

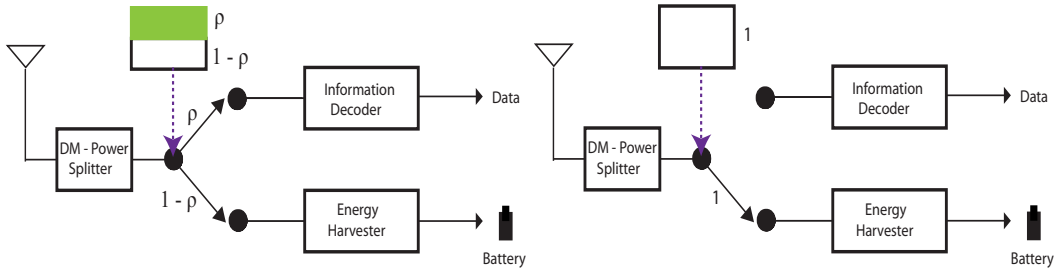

(a) Active mode (b) Inactive mode

Figure 5.2: Illustration of the SR architecture for active and inactive mode.

5.2.5 Signal Model

As has been mentioned above, in this section, we focus on the signal model for active and inactive modes.

5.2.5.1 Active Mode

For information decoding, received power at SR is given by

$$\mathbb{P}^{a}_{ID} = \rho \cdot \mathbb{E}\left[P_s h_{s_o} l(d_o) + I_{ss} + I_{sp}\right], \tag{5.2.4}$$

where $l(d_o) = d_c^{-\alpha_L} + \kappa(d_o - d_c)^{-\alpha_N}$. d_o is the distance between ST and its typical SR. In (4), it is assumed that typical SR is outside the critical distance. If typical SR is inside the critical distance, $l(d_o)$ is replaced with the $\|d_o\|^{-\alpha_L}$. P_s is the transmission power of ST. h_{s_o} is fading channel gain in associated ST-SR pair. I_{ss} and I_{sp} are interference power at the typical SR from STs and PTs, respectively. Hence, I_{ss} and I_{sp} can be expressed as

$$I_{ss} = \sum_{i \in \Phi_{St} \setminus \{o\}} P_{si} h_{si} l(d_{si}), \tag{5.2.5}$$

$$I_{sp} = \sum_{i \in \Phi_{Pt}} P_{pi} h_{pi} l(d_{pi}), \tag{5.2.6}$$

where o is the ST, which is in communication with its typical SR. h_{si} is the fading channel gain at the typical SR from interfering STs. d_{si} is the distance between typical SR and the interfering STs. h_{pi} is the fading channel gain at the typical SR from interfering PTs. d_{pi} is the distance between typical SR and the interfering PTs. P_p is the transmission power of PT.

Accordingly, the signal-to-interference-plus-noise ratio (SINR) at the ID of SR can be defined as

$$\mathrm{SINR}_o = \frac{\rho P_s h_{s_o} l(d_o)}{\rho(I_{ss} + I_{sp} + \sigma_s^2) + \sigma_c^2}, \tag{5.2.7}$$

in which σ_s^2 is the additive white Gaussian noise at SR and σ_c^2 is the circuit noise at the ID of SR.

For energy harvesting, received power at SR is given by

$$\mathbb{P}^{a}_{EH} = (1-\rho) \cdot \mathbb{E}\left[P_s h_{s_o} l(d_o) + I_{ss} + I_{sp}\right], \tag{5.2.8}$$

Using (5.2.8), average DC power harvested by the EH at SR is expressed as

$$\mathbb{P}^{a}_{DC} = \xi \cdot \mathbb{P}^{a}_{EH}, \tag{5.2.9}$$

where $\xi \in (0, 1]$ is the conversion efficiency from RF power to DC power.

5.2.5.2 Inactive Mode

SR receives the power from the interferers of PTs and STs. Hence, received power for energy harvesting at SR can be expressed as

$$\mathbb{P}^{i}_{EH} = \mathbb{E}\left[I'_{ss} + I_{sp}\right], \tag{5.2.10}$$

in which $I_{ss}^{'}$ is interference power at SR from STs. Hence, $I_{ss}^{'}$ is expressed as

$$I_{ss}^{'} = \sum_{i \in \Phi_{St}} P_{si} h_{si} l(d_{si}), \tag{5.2.11}$$

From (5.2.11), average DC power harvested by the EH at SR is expressed as

$$\mathbb{P}_{DC}^{i} = \xi \cdot \mathbb{P}_{EH}^{i}, \tag{5.2.12}$$

5.3 Performance Analysis

In this section, the performance metrics, outage probability and harvested DC power, are analyzed for SN. Also, an optimization algorithm is proposed for maximization of energy harvesting.

5.3.1 Outage Probability

Outage probability is an important factor in wireless network design. Therefore, researchers want to design their networks for low outage probability. The outage probability of SR is defined as the probability that the received SINR at a typical SR is higher than the predefined threshold θ_s. Thus, the outage probability of SR can be defined mathematically as

$$O_A = 1 - \Pr\left[\mathrm{SINR_o} > \theta_s\right], \tag{5.3.1}$$

Using (5.2.7) and (5.3.1), the outage probability of SR, where SR is located at the origin, can be expressed as

$$\begin{aligned} O_A &= 1 - \Pr\left[\frac{\rho P_s h_{s_o} l(d_o)}{\rho(I_{ss} + I_{sp} + \sigma_s^2) + \sigma_c^2} > \theta_s\right] \\ &= 1 - \Pr\left[h_{s_o} > \frac{\theta_s[\rho(I_{ss} + I_{sp} + \sigma_s^2) + \sigma_c^2]}{\rho P_s l(d_o)}\right] \\ &= 1 - \mathbb{E}_{I_{ss}, I_{sp}}\left[\exp\left(-\frac{\theta_s[\rho(I_{ss} + I_{sp} + \sigma_s^2) + \sigma_c^2]}{\rho P_s l(d_o)}\right)\right] \\ &= 1 - \exp\left(-\frac{\theta_s[\rho\sigma_s^2 + \sigma_c^2]}{\rho P_s l(d_o)}\right) \mathcal{L}_{I_{ss}}\left(\frac{\theta_s}{P_s l(d_o)}\right) \mathcal{L}_{I_{sp}}\left(\frac{\theta_s}{P_s l(d_o)}\right), \end{aligned} \tag{5.3.2}$$

where $\mathcal{L}_{I_{ss}}$ and $\mathcal{L}_{I_{sp}}$ are the Laplace transforms of the probability density functions of I_{ss} and I_{sp}. The Laplace transforms of $\mathcal{L}_{I_{ss}}$ and $\mathcal{L}_{I_{sp}}$ are conferred in the following lemmas:

Lemma 1. *The Laplace transform $\mathcal{L}_{I_{ss}}$ of the aggregate interference I_{ss} at the SR because of the interferers of STs is given by*

$$\mathcal{L}_{I_{ss}}(\theta_s(P_s l(d_o))^{-1}) = \exp\left(-\pi\lambda_s Q_s\left[\theta_s d_c^{2-\alpha_L}(l(d_o))^{-1} + 2\left(\frac{\kappa\theta_s}{l(d_o)}\right)^{\frac{2}{\alpha_N}} I(L_{ls}, \alpha_N)\right]\right),$$

in which λ_s is the density of STs except the intended ST. $I(L_{ls},\alpha_N)=\int_{L_{ls}}^{\infty}\frac{y}{1+y^{\alpha_N}}dy$ and $L_{ls}=\frac{d_c}{(\kappa\theta_s l(d_o)^{-1})^{2/\alpha_N}}$.

Proof: Please refer to Appendix D (**D.2**).

Lemma 2. *The Laplace transform $\mathcal{L}_{I_{sp}}$ of the aggregate interference I_{sp} at the SR because of the interferers of PTs is given by*

$$\mathcal{L}_{I_{sp}}(\theta_s(P_s l(d_o))^{-1})=\exp\left(-\pi\lambda_p Q_p\left[\theta_s P_p(P_s l(d_o))^{-1}d_c^{2-\alpha_L}+2\left(\frac{\kappa\theta_s P_p}{P_s l(d_o)}\right)^{\frac{2}{\alpha_N}}I(L_{lp},\alpha_N)\right]\right),$$

in which λ_p is the density of PTs. Q_p is the *probability of utilization of an idle channel*. $I(L_{lp},\alpha_N)=\int_{L_{lp}}^{\infty}\frac{y}{1+y^{\alpha_N}}dy$ and $L_{lp}=\frac{d_c}{(\kappa\theta_s P_p(P_s l(d_o))^{-1})^{2/\alpha_N}}$.

Proof: Please refer to Appendix D (**D.3**).

Substituting the value of lemmas 1 and 2 into (5.3.2), the outage probability can be found as

$$\begin{aligned}O_A=1-\exp\Bigg(&-\frac{\theta_s[\rho\sigma_s^2+\sigma_c^2]}{\rho P_s l(d_o^c)}-\pi\lambda_s Q_s\left[\theta_s d_c^{2-\alpha_L}l(d_o)^{-1}+2\left(\frac{\kappa\theta_s}{l(d_o)}\right)^{\frac{2}{\alpha_N}}I(L_{ls},\alpha_N)\right]\\&-\pi\lambda_p Q_p\left[\theta_s P_p(P_s l(d_o))^{-1}d_c^{2-\alpha_L}+2(\kappa\theta_s P_p(P_s l(d_o))^{-1})^{\frac{2}{\alpha_N}}I(L_{lp},\alpha_N)\right]\Bigg).\end{aligned}\tag{5.3.3}$$

Special Case 1: As defined in (5.3.3), the outage probability O_A cannot be derived closed-form; however, a closed-form expression is found if and only if $\alpha_L=2$ and $\alpha_N=4$. Substituting the values of α_L and α_N, we get

$$\begin{aligned}O_A^1=1-\exp\Bigg(&-\frac{\theta_s[\rho\sigma_s^2+\sigma_c^2]}{\rho P_s l(d_o^c)}-\pi\lambda_s Q_s\left[\theta_s l(d_o^c)^{-1}+\sqrt{\kappa\theta_s l(d_o^c)^{-1}}\tan^{-1}\left(\frac{\kappa\theta_s}{d_c^2 l(d_o^c)}\right)\right]\\&-\pi\lambda_p Q_p\left[\theta_s P_p(P_s l(d_o^c))^{-1}+\sqrt{\kappa\theta_s P_p(P_s l(d_o^c))^{-1}}\tan^{-1}\left(\frac{\kappa\theta_s P_p}{d_c^2 P_s l(d_o^c)}\right)\right]\Bigg),\end{aligned}\tag{5.3.4}$$

where $l(d_o^c)=d_c^{-2}+\kappa(d_o-d_c)^{-4}$.

Remark 1: *As outage probability is a monotonic decreasing function of P_s, the derived result in* (5.3.4) *shows that outage probability decreases with increasing P_s. Also, outage probability increases linearly with increasing λ_s.*

Special Case 2: Consider the noise-limited system where there is no interference. The outage probability for the noise-limited system can be approximated as

$$O_A^2=1-\exp\left(-\theta_s[\rho\sigma_s^2+\sigma_c^2](\rho P_s l(d_o^c))^{-1}\right).\tag{5.3.5}$$

Remark 2: *The derived result in* (5.3.5) *shows that outage probability is a monotonic decreasing function of P_s.*

Special Case 3: Consider the interference-limited system where there is no Gaussian noise or circuit noise. The outage probability for the interference-limited system can be approximated as

$$O_A^3 = 1 - \exp\left(-\pi\lambda_s Q_s\left[\theta_s l(d_o^c)^{-1} + \sqrt{\kappa\theta_s l(d_o^c)^{-1}}\tan^{-1}\left(\frac{\kappa\theta_s}{d_c^2 l(d_o^c)}\right)\right]\right.$$
$$\left.-\pi\lambda_p Q_p\left[\theta_s P_p(P_s l(d_o^c))^{-1} + \sqrt{\kappa\theta_s P_p(P_s l(d_o^c))^{-1}}\tan^{-1}\left(\frac{\kappa\theta_s P_p}{d_c^2 P_s l(d_o^c)}\right)\right]\right). \tag{5.3.6}$$

Remark 3: *The derived result in* (5.3.6) *reveals that outage probability is a monotonic decreasing function of* P_s. *On the other hand, outage probability is a linear increasing function of* λ_s.

5.3.2 Harvested Power

5.3.2.1 Active Mode

According to (5.2.9), the average DC power harvested from the STs (except the intended ST) and PTs can be written as

$$\mathbb{P}_{DC}^a = \xi\cdot(1-\rho)\cdot\left[P_s\left\{\Gamma(1+2/\alpha_L)d_c^{-\alpha_L} + \kappa\Gamma(1+2/\alpha_N)(d_o-d_c)^{-\alpha_N}\right\} + \mathbb{E}[I_{ss}] + \mathbb{E}[I_{sp}]\right]. \tag{5.3.7a}$$

$$\mathbb{E}(I_{ss}) = \pi\lambda_s P_s Q_s\left[\Gamma(1+2/\alpha_L)d_c^{2-\alpha_L} + 2\kappa\Gamma(1+2/\alpha_N)d_c^{2-\alpha_N}/(\alpha_N-2)\right]. \tag{5.3.7b}$$

$$\mathbb{E}(I_{sp}) = \pi\lambda_p P_p Q_p\left[\Gamma(1+2/\alpha_L)d_c^{2-\alpha_L} + 2\kappa\Gamma(1+2/\alpha_N)d_c^{2-\alpha_N}/(\alpha_N-2)\right]. \tag{5.3.7c}$$

Proof: Please refer to Appendix D (**D.4**).

Special Case 4: For consideration of $\alpha_L = 2$ and $\alpha_N = 4$, we obtain the simplified expression of average DC power for active mode as

$$\mathbb{P}_{DC}^{a4} = \xi\cdot(1-\rho)\cdot\left[P_s\left\{d_c^{-2} + 0.5\kappa\sqrt{\pi}(d_o-d_c)^{-4}\right\} + \mathbb{E}[I_{ss}^4] + \mathbb{E}[I_{sp}^4]\right]. \tag{5.3.8a}$$

$$\mathbb{E}(I_{ss}^4) = \pi\lambda_s P_s Q_s\left[1 + 0.5\kappa\sqrt{\pi}d_c^{-2}\right]. \tag{5.3.8b}$$

$$\mathbb{E}(I_{sp}^4) = \pi\lambda_p P_p Q_p\left[1 + 0.5\kappa\sqrt{\pi}d_c^{-2}\right]. \tag{5.3.8c}$$

5.3.2.2 Inactive Mode

According to (5.2.12), the average DC power harvested from the STs and PTs can be written as

$$\mathbb{P}_{DC}^i = \xi\cdot\left[\mathbb{E}[I_{ss}^{'}] + \mathbb{E}[I_{sp}]\right]. \tag{5.3.9a}$$

$$\mathbb{E}(I_{ss}^{'}) = \pi\lambda_s^{'} P_s Q_s\left[\Gamma(1+2/\alpha_L)d_c^{2-\alpha_L} + 2\kappa\Gamma(1+2/\alpha_N)d_c^{2-\alpha_N}/(\alpha_N-2)\right]. \tag{5.3.9b}$$

$$\mathbb{E}(I_{sp}) = \pi\lambda_p P_p Q_p\left[\Gamma(1+2/\alpha_L)d_c^{2-\alpha_L} + 2\kappa\Gamma(1+2/\alpha_N)d_c^{2-\alpha_N}/(\alpha_N-2)\right]. \tag{5.3.9c}$$

Proof: The proof is straightforward for average DC power in inactive mode. In (21b), the density $\lambda_s^{'} = \lambda_s + 1$. Following similar steps in active mode and simply replacing the density $\lambda_s^{'}$ with λ_s, we determine average DC power in active mode.

Special Case 5: For consideration of $\alpha_L = 2$ and $\alpha_N = 4$, we obtain the simplified expression for average DC power in inactive mode as

$$\mathbb{P}_{DC}^{i5} = \xi \cdot \left[\mathbb{E}[I_{ss}^5] + \mathbb{E}[I_{sp}^5]\right]. \tag{5.3.10a}$$

$$\mathbb{E}(I_{ss}^5) = \pi \lambda_s^{'} P_s Q_s \left[1 + 0.5\kappa\sqrt{\pi} d_c^{-2}\right]. \tag{5.3.10b}$$

$$\mathbb{E}(I_{sp}^5) = \pi \lambda_p P_p Q_p \left[1 + 0.5\kappa\sqrt{\pi} d_c^{-2}\right]. \tag{5.3.10c}$$

5.3.3 Maximization of Harvested Power - Active Mode

In this section, we investigate the maximization of harvested power with outage probability constraint in CR network active mode. The maximization of harvested power is still difficult to solve because of the outage probability in (5.3.2); therefore, $\alpha_L = 2$ and $\alpha_N = 4$ are considered for solving the optimization problem. In the design, the harvested energy ($\mathbb{P}_{DC}^{a4}$) is maximized over P_s and λ_s under a particular outage probability of ϵ_c. The $\mathbb{P}_{DC}^{a4}$ maximization can be formulated as

$$\max_{P_s, \lambda_s} \quad \mathbb{P}_{DC}^{a4}(P_s, \lambda_s) \tag{5.3.11a}$$

$$\text{s.t.} \quad \text{C1} : O_A^1(P_s, \lambda_s) \leq \epsilon_c \tag{5.3.11b}$$

$$\text{C2} : 0 \leq \rho \leq 1 \tag{5.3.11c}$$

$$\text{C3} : P_s \geq 0, \lambda_s \geq 0. \tag{5.3.11d}$$

In (5.3.11), constraint C1 ensures that the outage probability O_A^1 does not exceed the particular value of ϵ_c. C2 verifies the PS ratio between 0 and 1. C3 confirms the non-negative value of P_s and λ_s. Specifically, considering constraint C2, it is clear that the objective function in (5.3.11a) decreases with increased ρ. Thus, the maximum harvested power can be obtained via the following expression

$$\max_{P_s, \lambda_s} \quad \mathbb{P}_{DC}^{a4}(P_s, \lambda_s) \Leftrightarrow \min_{\rho} \left(\max_{P_s, \lambda_s} \quad \mathbb{P}_{DC}^{a4}(P_s, \lambda_s) \right). \tag{5.3.12}$$

In accordance with the above discussion, we avoid constraint C2. Furthermore, the Hessian of the objective function is less than zero; therefore, the objective function must have a saddle point. Thus, the optimum solution of P_s has a maximum point and the optimum solution of λ_s has a minimum point. From this point of view, the objective function is stated as, $\min_{\lambda_s} \left(\max_{P_s} \quad \mathbb{P}_{DC}^{a4}(P_s, \lambda_s) \right)$. Following a similar discussion as in [109, chapter 10], the maximization problem can be formulated as

$$\max_{P_s, \lambda_s} \quad \mathbb{P}_{DC}^{a4}(P_s, \lambda_s) \tag{5.3.13a}$$

$$\text{s.t.} \quad \text{C1} : O_A^1(P_s, \lambda_s) \leq \epsilon_c. \tag{5.3.13b}$$

The above optimization solution is presented as a theorem, below.

Theorem. *The maximum harvested power* $\mathbb{P}_{DC}^{a4}(P_s, \lambda_s)$ *in* (5.3.11a) *can be expressed as*

$$\mathbb{P}_{DC}^{a4}(P_s, \lambda_s) = \xi \cdot (1-\rho) \cdot \left[P_s^* \cdot (v_1 + \pi v_2 \lambda_s^* Q_s) + \pi v_2 P_p \lambda_p Q_p\right], \tag{5.3.14}$$

in which $v_1 = d_c^{-2} + 0.5\kappa\sqrt{\pi}(d_o - d_c)^{-4}$ and $v_2 = 1 + 0.5\kappa\sqrt{\pi}d_c^{-2}$.

The optimum solution of P_s^* *and* λ_s^* *are presented as*

$$\tan^{-1}\left(\frac{\kappa\theta_s P_p}{d_c^2 P_s^* l(d_o^c)}\right) - \frac{2\kappa\theta_s P_p}{d_c^2 P_s^* l(d_o^c)}\left(1 + \left(\frac{\kappa\theta_s P_p}{d_c^2 P_s^* l(d_o^c)}\right)^2\right)^{-1} = k_o\sqrt{\frac{d_c^2 P_s^* l(d_o^c)}{\kappa\theta_s P_p}}, \tag{5.3.15a}$$

$$\lambda_s^* = \left|\min(\lambda_s, 0)\right|, \tag{5.3.15b}$$

in which

$$\lambda_s = \frac{\epsilon_{cc} - \theta_s[\rho\sigma_s^2 + \sigma_c^2](\rho P_s^* l(d_o^c))^{-1} - \pi\lambda_p Q_p\left(\theta_s P_p (P_s^* l(d_o^c))^{-1} + \nu_0\right)}{\pi Q_s\left(\theta_s l(d_o^c)^{-1} + \sqrt{\kappa\theta_s l(d_o^c)^{-1}}\tan^{-1}\left(\frac{\kappa\theta_s}{d_c^2 l(d_o^c)}\right)\right)}. \tag{5.3.16a}$$

$$k_o = \frac{2}{\pi\lambda_p Q_p d_c}\left[\frac{d_c^{-2} + 0.5\kappa\sqrt{\pi}(d_o - d_c)^{-4}}{1 + 0.5\kappa\sqrt{\pi}d_c^{-2}}\left\{\theta_s l(d_o^c)^{-1} + \nu_1\right\} + \epsilon_{cc}\right]. \tag{5.3.16b}$$

$$\epsilon_{cc} = -\ln(1 - \epsilon_c). \tag{5.3.16c}$$

$$\nu_0 = \sqrt{\kappa\theta_s P_p (P_s^* l(d_o^c))^{-1}}\tan^{-1}\left(\frac{\kappa\theta_s P_p}{d_c^2 P_s^* l(d_o^c)}\right). \tag{5.3.16d}$$

$$\nu_1 = \sqrt{\kappa\theta_s l(d_o^c)^{-1}}\tan^{-1}\left(\frac{\kappa\theta_s}{d_c^2 l(d_o^c)}\right). \tag{5.3.16e}$$

Proof: Please refer to Appendix D (**D.5**).

It is noted that (5.3.15a) is optimally solved as a nonlinear equation, which is difficult to deal with. Its numerical solution can be found using the bisection method [109, chapter 5]. Here we use matlab function FZERO to find the optimal solution. In general, one optimum solution is found in (5.3.15a). If the resulting solutions in (5.3.15a) are more than one, we choose the maximum solution.

As mentioned earlier, we find one non-negative optimum solution and one negative. Subsequently, we propose the following algorithm to obtain maximum energy harvesting where optimum solutions have different signs. The steps of the algorithm are as follows:

5.4 Numerical Results and Discussion

In this section, outage probability, harvested power and optimization, described in section 5.3, are numerically examined. We employ the following parameters for evaluation of this network: total number of channels $N = 20$, idle channels $M = 8$, critical distance $d_c = 14$ m, distance $d_o = 100$ m, SINR threshold $\theta_s = 2$ dBm, circuit noise $\sigma_c^2 = 1$, Gaussian noise $\sigma_s^2 = 1$, LoS exponent $\alpha_L = 2.09$ as given in [110], NLoS exponent $\alpha_N = 3.75$ as given in [110], PS ratio $\rho = 0.5$, and conversion efficiency $\xi = 0.5$. Some parameters were changed, as indicated in the figure.

Algorithm: To achieve optimum P_s, λ_s and maximum $\mathbb{P}_{DC}^{a4}(P_s, \lambda_s)$

1. Initialize the parameters θ_s, P_p, λ_p, σ_s, σ_c, $\alpha_L = 2$, $\alpha_N = 4$ and ϵ_c;
2. For each ρ, find k_o and also solve in (5.3.15a);
3. Find optimum P_s^* using FZERO function;
4. Obtain optimum $\lambda_s^* = |\min(\lambda_s, 0)|$ and plug it into (5.3.16a);
5. Obtain maximum $\mathbb{P}_{DC}^{a4}(P_s, \lambda_s)$ in (5.3.11a) by substituting P_s^* and λ_s^*;
6. Goto step (2).

5.4.1 Outage Probability

In Fig. 5.3, it presents the impact of transmission power of P_s and PS of ρ on outage probability. It is clear from Fig. 5.3 that outage probability is a decreasing function with P_s and ρ. Outage probability decreases significantly with P_s when ρ is greater than 0.2. Moreover, when the value of ρ is above 0.5, the outage performance improves more rapidly. For instance, the outage probability decreased from 12.24% to 3.25% (i.e., distinction of 8.99%) when ρ changed from 0.6 to 0.8 at $P_s = 48$ dBm. However, the outage probability decreased from 3.25% to 3.15% (i.e., distinction of 0.10%) when P_s varied from 48 dBm to 50 dBm at $\rho = 0.8$. This indicates that, in practice, the impact of ρ on outage performance is greater than the impact of P_s. When ρ becomes larger, it means that the signal power of ID is sufficient. On the other hand, if ρ is set smaller, it means that the signal power of ID is relatively low. Thus, ρ should be carefully chosen for the quality-of-service of cellular user (SR) in active mode.

Figure 5.4 shows the effect of the densities of PTs and STs (λ_p and λ_s) on the outage probability. As we assume a fixed transmission power, the densities λ_p and λ_s affect the outage probability. We observe that the larger the density, the greater the effect on outage performance. This is because when the density is high, numerous PTs and STs exit and they create interference among themselves.

5.4.2 Harvested Power

Figure 5.5 shows the harvested DC power in active mode for different transmission powers of P_s and P_p. We observed that each SR can harvest large DC power when transmission power of STs and PTs is high, although each transmitter (i.e., ST and PT) has a transmission power restriction. Evidently, P_p is dominant when DC power harvesting is in active mode.

The harvested DC power in inactive mode is shown in Fig. 5.6. Inactive mode demonstrates performance characteristics similar to those of active mode. A comparison of active and inactive modes follows. For $P_p = 30$ dBm and 35 dBm, we observe better DC power

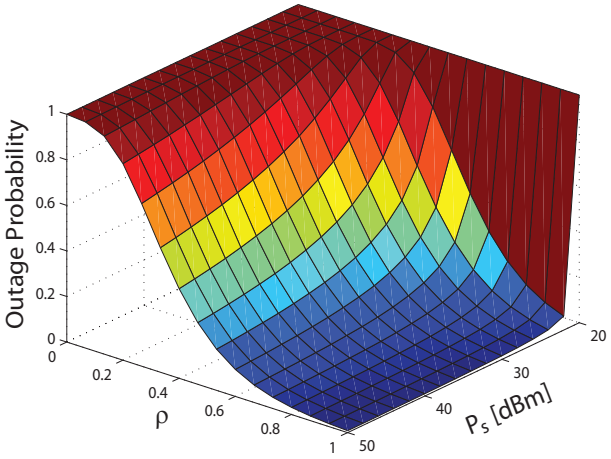

Figure 5.3: Outage performance vs. various transmission powers of P_s and PS of ρ. Parameter values are $P_p = 60$ dBm, $\lambda_s = 50/km^2$, and $\lambda_p = 15/km^2$.

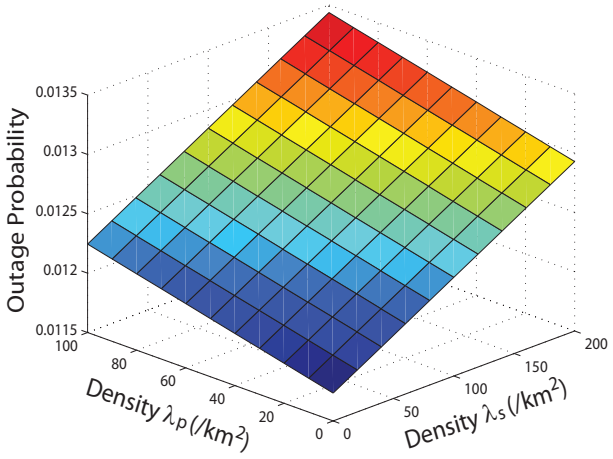

Figure 5.4: Outage performance vs. various densities of λ_s and λ_p. Parameter values are $P_s = 50$ dBm and $P_p = 60$ dBm.

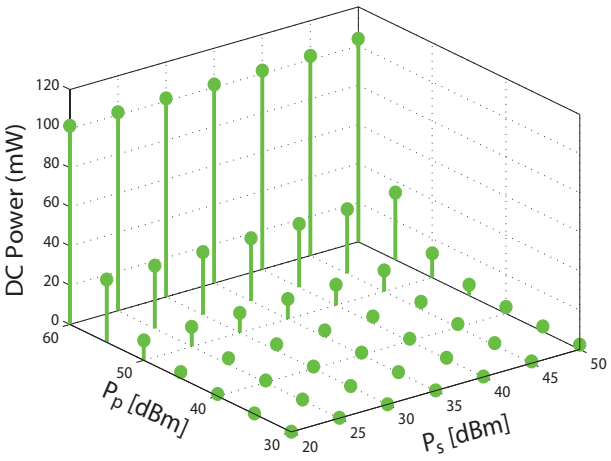

Figure 5.5: DC power vs. various transmission powers of P_s and P_p in active mode. Parameter values are $\lambda_s = 50/km^2$ and $\lambda_p = 15/km^2$.

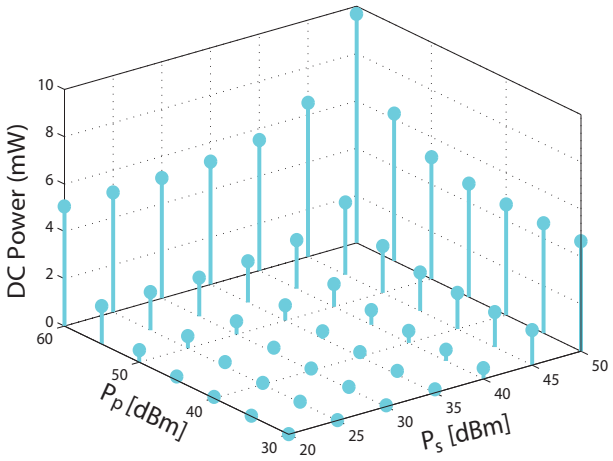

Figure 5.6: DC power vs. various transmission powers of P_s and P_p in inactive mode. Parameter values are $\lambda_s^{'} = 51/km^2$ and $\lambda_p = 15/km^2$.

harvesting in active mode than in inactive mode for the values $P_s = 20$ dBm ~ 40 dBm, respectively. For example, the improvement of DC power in inactive mode is nearly 15.2% for values $P_s = 35$ dBm and $P_p = 30$ dBm compared to active mode. When P_p increased, the resultant DC power for active mode increased rapidly. We find a similar result for $P_p = 45$ dBm ~ 60 dBm where harvested DC power is better in active mode than in inactive mode for all the values of P_s. For instance, DC power in active mode is enhanced 18.5 times than inactive mode for $P_s = 35$ dBm and $P_p = 60$ dBm. However, inactive mode

outperforms active mode when P_s is set to 45 dBm and 50 dBm and P_p is set to 30 dBm and 35 dBm.

Figures 5.7 and 5.8 show the effect of densities λ_s and λ_p for DC power in active and inactive modes, respectively. In Fig. 5.7, as expected, the DC power increased due to the increase in densities λ_s and λ_p. This is because radiant power from the PTs and STs increased continuously when the densities increased. As a result, interference power increased. For this reason, CR harvested more DC power from the CR network. As can be seen in Fig. 5.8, harvested DC power in inactive mode showed the lower performance, followed by active mode performance for similar parameters. Inactive mode harvested approximately 12.4 times less DC power than active mode at $\lambda_s = 30/km^2$ and $\lambda_p = 15/km^2$. In addition, we compared the harvested DC power in inactive mode with 3G mobile phone in idle mode as reported in [111]. This confirms that higher densities of λ_s and λ_p resulted in significant improvement for DC power in inactive mode. For example, the harvested DC power in inactive mode was approximately 13.12% higher than idle mode in a 3G phone (comparing at 23.4 mW) at $\lambda_s^{'} = 150/km^2$ and $\lambda_p = 15.2/km^2$.

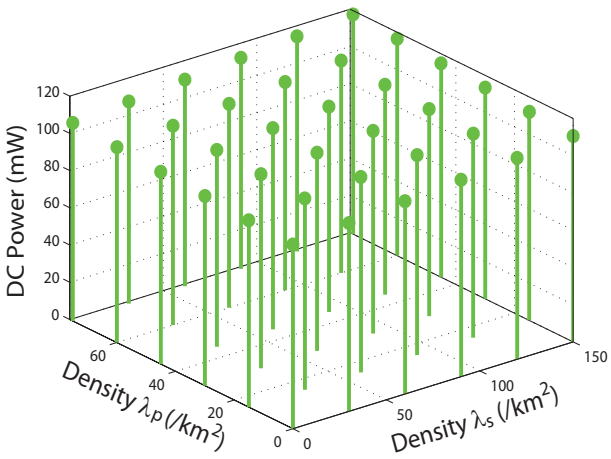

Figure 5.7: DC power vs. various densities of λ_s and λ_p in active mode. Parameter values are $P_s = 50$ dBm and $P_p = 60$ dBm.

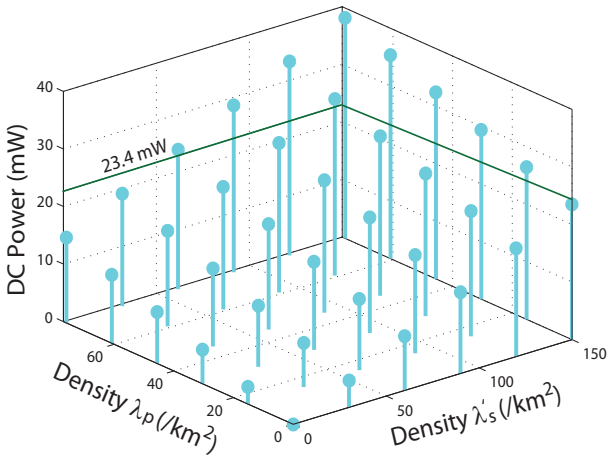

Figure 5.8: DC power vs. various densities of $\lambda_s^{'}$ and λ_p in inactive mode. Parameter values are $P_s = 50$ dBm and $P_p = 60$ dBm.

The comparison of active and inactive mode with conversion efficiency ξ is shown in Fig. 5.9. DC power is an increasing function with ξ in both active and inactive modes. In addition, we observe that harvested DC power in active mode can be increased by nearly 142% for $\xi = 0.5$ compared to that in inactive mode. As discussed in section 5.2.5, SR harvests radiated power from PTs and STs in inactive mode, when SR is not performing information decoding; therefore, all received interference power is converted to DC power.

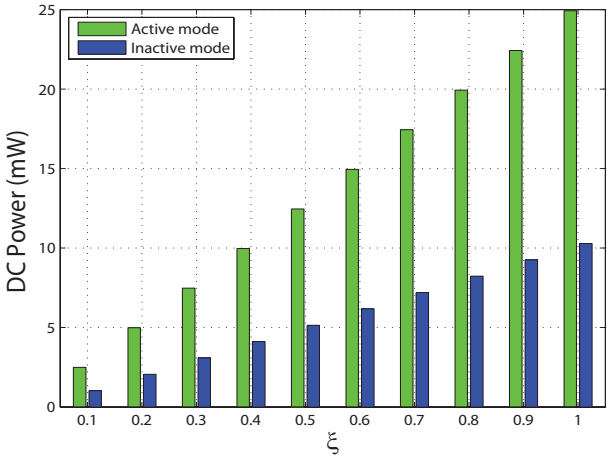

Figure 5.9: Comparison of DC power in active and inactive modes for different values of ξ. Parameter values are $P_s = 40$ dBm, $P_p = 60$ dBm, $\lambda_s = 50/km^2$, $\lambda_p = 15/km^2$ and $\lambda_s^{'} = 51/km^2$.

5.4.3 Maximization - Active Mode

Numerical results are presented in this section for the maximization of harvested energy in active mode, as discussed in section in 5.3.3. As the results are evaluated for closed-form expressions, the LoS exponent $\alpha_L = 2$ and NLoS exponent $\alpha_N = 4$ are assumed. We demonstrate the superior performance of DC power based on the optimization technique given in theorem.

Figure 5.10 shows DC power with respect to ρ. It can be seen that DC power decreased with increasing ρ. This indicates low ρ, which means that the PS is more connected to the EH node and less connected to the ID node, and collects more DC power. We can observe from the plot that DC power decreased by approximately 40.28% for an increase of $\rho = 0.5$ to $\rho = 0.6$. The opposite trends are observed in Fig. 5.11, where DC power increases as ξ increases. This suggests that more DC power is harvested when conversion efficiency is high. Using the optimization technique, more DC power can be harvested if density of ST (λ_s) is an optimal value. The optimum value λ_s^* with reference to ρ is shown in Fig. 5.12.

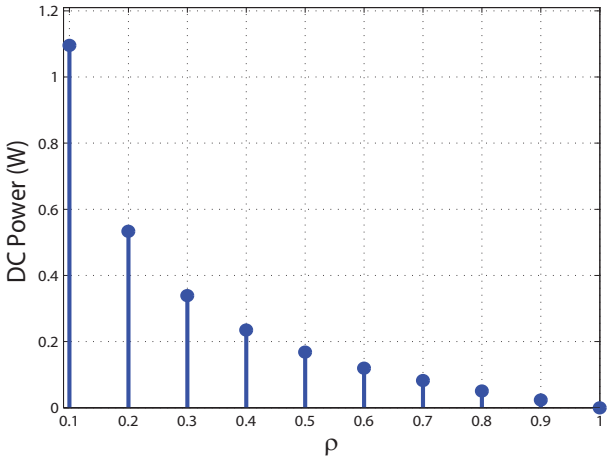

Figure 5.10: DC power vs. ρ in active mode. Parameter values are $P_p = 60$ dBm, $\lambda_p = 15/km^2$, $\xi = 0.5$ and $\epsilon_c = 10^{-4}$.

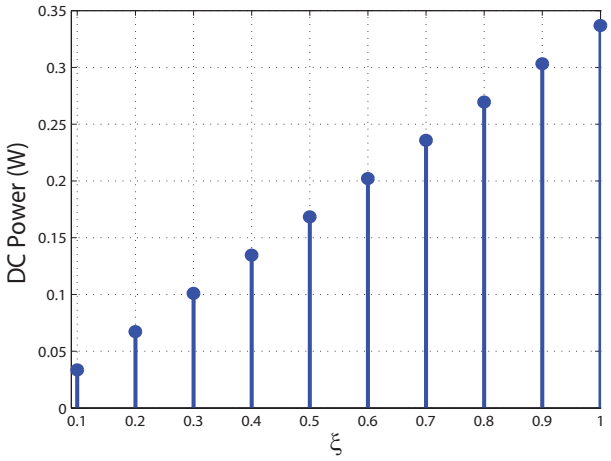

Figure 5.11: DC power vs. ξ in active mode. Parameter values are $P_p = 60$ dBm, $\lambda_p = 15/km^2$, $\rho = 0.5$ and $\epsilon_c = 10^{-4}$.

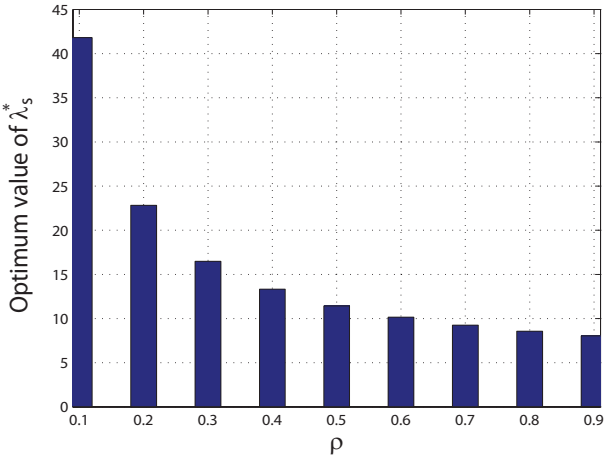

Figure 5.12: Optimum value of λ_s^* for different values of ρ. Parameter values are $P_p = 60$ dBm, $\lambda_p = 15/km^2$, $\epsilon_c = 10^{-4}$ and optimum value of $P_s^* = 13.88$ dBm.

Chapter 6

Conclusion and Future Work

6.1 Conclusion

A detailed analytical analysis is carried out to evaluate the random CR network. In this thesis, first we derived an analytical downlink model of random CR network. Analytical expressions of interference, outage probability and energy efficiency were derived for the developed model. The model presented here will be extended to work on the transmit antenna selection technique. Then we performed a theoretical analysis of random CR network in Rayleigh-lognormal fading to develop an expression for coverage probability and transmission rate of that network. Finally we developed an analytical uplink model of CR network with truncated channel inversion power control, and derived mathematical expressions for the coverage probability and spectral efficiency.

The salient features of our work are summarized chapter by chapter below:

Chapter 2

The salient features of the energy-efficient random CR networks based on the numerical results as follows:

(i) Outage probability is reduced for increasing number of transmitters, though at the same time energy efficiency is maximized for low threshold.

(ii) The SINR threshold impacts on energy efficiency performance, and there exists an optimal threshold that maximizes energy efficiency.

(iii) It was found that there is a point of maximum energy efficiency for a particular value of threshold, referred to here as optimal threshold, for various densities λ_s and λ_p. Energy efficiency was low for high values of λ_s and λ_p.

Chapter 3

The salient features of the random CR networks in Rayleigh-lognormal fading based on the numerical results as follows:

(i) Coverage probability and transmission rate are better under high transmission power.

(ii) Coverage probability and transmission rate are better for low density PTs and STs.

(iii) When the Shannon capacity gap increases, transmission rate decreases.

Chapter 4

The salient features of the uplink model of CR network with truncated channel inversion power control based on the numerical results are as follows:

(i) Coverage probability and spectral efficiency are better when the SR is located outside the PER.

(ii) Coverage probability and spectral efficiency depend on the path-loss exponent and SR density.

(iii) Coverage probability increases with increasing cutoff threshold.

Chapter 5

Several key observations can be made based on the numerical results of energy harvesting of CR network model:

(i) Outage probability decreases with increasing transmission power and increases with increasing densities of PTs and STs.

(ii) As expected, harvested DC power increases when transmission power (P_s and P_p) and densities (λ_s and λ_p) are increased.

(iii) The PS ratio and conversion efficiency has an effect on DC power. When PS ratio is low, harvested DC power is large. However, harvested DC power is large when energy conversion efficiency is high.

6.2 Future Work

Recently, random CR network has gained widespread popularity in academia and industry due to the current practical BS locations scenario. In the studies presented in this thesis, we designed an analytical model of uplink and downlink CR network. The results and observations discussed here point to numerous issues regarding random CR network that need to be investigated; some of them are listed below as topics for future research.

- In this thesis, we investigated a single-tier uplink and downlink model of CR network scenario. One straightforward research extension is to investigate multi-tier uplink and downlink scenario.
- Another interesting extension of the present findings is to develop an optimization technique for maximizing coverage probability, spectral efficiency and energy efficiency and also minimizing outage probability.
- In future, we expect to design two-way cooperative MIMO-OFDM communication with single and multi-relaying technique and also incorporating beam-forming.

- Investigation of device-to-device communication, massive MIMO and higher frequency bands, such as millimeter wave will be an interesting future direction.
- A detailed investigation of percolation theory is another promising direction for future research.

Appendix A

A.1 Proof of lemma 1

The sum of interference from all PTs outside the PER (except the tagged PT denoted by p_0 which is inside the PER) can be expressed as

$$I_{pp} = \sum_{i \in \Phi_{pt} \setminus \{p_0\}} P_p g_{pi} R_{pi}^{-\alpha}, \tag{A.1.1}$$

where R_{pi} is the distance between the ith interfering PT and tagged PR taken by the homogeneous PPP. The interference channel gains g_{pi} are considered to be independent and identical distribution for all channels.

The Laplace transform of the pdf of I_{pp} can be written as

$$\begin{aligned}
\mathcal{L}_{I_{pp}}(s_p) &= \mathbb{E}_{I_{pp}}\left[\exp(-s_p I_{pp})\right] \\
&= \mathbb{E}_{\Phi_{pt}, g_p}\left[\exp(-s_p \sum_{i \in \Phi_{pt} \setminus \{p_0\}} P_p g_{pi} R_{pi}^{-\alpha})\right] \\
&\overset{(i)}{=} \mathbb{E}_{\Phi_{pt}}\left[\prod_{i \in \Phi_{pt} \setminus \{p_0\}} \mathbb{E}_{g_p}\left[\exp(-s_p P_p g_p R_{pi}^{-\alpha})\right]\right],
\end{aligned} \tag{A.1.2}$$

where $s_p = \mu_p \theta_p r_p^{\alpha} P_p^{-1}$. Equality (i) follows the independence of channel fading. Then, the probability generating functional[1] (PGFL) [70] of the PPP, applied in eq. (A.1.2), can be calculated as

$$\mathcal{L}_{I_{pp}}(s_p) = \exp\left\{-\mathbb{E}_{g_p}\left[\int_{r_p}^{\infty} (1 - \exp(-s_p P_p g_p R_p^{-\alpha})) \lambda'_{pp}(R_p) dR_p\right]\right\}. \tag{A.1.3}$$

From eq. (A.1.3), it can be seen that when the nearest interfering PT is at least at distance r_p from the tagged PR, the integration limit is from r_p to infinite. Then, we calculate the density of all PTs outside the region $b(0, r_p)$. In other words, interference is

[1]The function of $f(x)$ is defined as $\mathbb{E}\left[\prod_{x \in \Phi} f(x)\right] = \exp(-\int_{\mathbb{R}} (1 - f(x)) \lambda dx)$.

perceived from all active PTs located in the area $\mathbb{R}^d \setminus b(0, r_p)$, where $b(a, b)$ is a sphere of radius b centered at point a. Φ_{pt} and $\Phi_{pt}^{'}$ constitute independent thinning ($\Phi_{pt}^{'} \subset \Phi_{pt}$), where Φ_{pt} is thinned of the homogeneous PPP over the plane for all PTs and $\Phi_{pt}^{'}$ is the thinned homogeneous PPP over the entire plane for all PTs outside the region $b(0, r_p)$. So, λ_p is the density of all PTs, and $\lambda_p^{'}$ is the density of all PTs except the region $b(0, r_p)$. Considering the mapping theorem [32, 37], the density of the homogeneous PPP can be derived as

$$\lambda_{pp}^{'}(R_p) = \lambda_p^{'} b_d d R_p^{d-1}, \tag{A.1.4}$$

where b_d is the d-dimensional volume of a unit sphere over $\mathbb{R}^d$, represented as, $b_d = \frac{\pi^{d/2}}{\Gamma(1+d/2)}$. When $d = 2$, $b_2 = \pi$.

Now, substituting the density of $\lambda_{pp}^{'}$ into eq. (A.1.4), we obtain

$$\mathcal{L}_{I_{pp}}(s_p) = \exp\left\{-\mathbb{E}_{g_p}\left[\int_{r_p}^{\infty}(1 - \exp(-s_p P_p g_p R_p^{-\alpha}))\lambda_p^{'} b_d d R_p^{d-1} d R_p\right]\right\}. \tag{A.1.5}$$

Corollary A. *Let P is the transmission power, g is the interfering channel gain, $\lambda(c)$ is the density of corresponding interfering users and X is the distance from the interfering transmitter to the tagged receiver. So the Laplace transform of the interference integration from x to ∞ is given by*

$$\begin{aligned}\mathcal{L}_I(s) &= \exp\left\{-\mathbb{E}_g\left[\int_x^{\infty}(1 - \exp(-sPgX^{-\alpha}))\lambda(c) d X^{d-1} d X\right]\right\} \\ &= \exp\left\{x^d \lambda(c) - \frac{d}{\alpha}\lambda(c)(sP)^{d/\alpha}\left[g^{d/\alpha} U(\theta, \alpha)\right]\right\},\end{aligned}$$

where $U(\theta, \alpha) = \Gamma(-d/\alpha, sPgx^{-\alpha}) - \Gamma(-d/\alpha)$.

Proof: The detailed proof is given in Theorem 1 [70].

According to corollary A, the eq. (A.1.5) can be written as

$$\mathcal{L}_{I_{pp}}(s_p) = \exp\left\{\lambda_p^{'} b_d r_p^d - (\frac{d}{\alpha})\lambda_p^{'} b_d (\mu_p \theta_p r_p^{\alpha})^{\frac{d}{\alpha}}\left[(g_p)^{\frac{d}{\alpha}} V(\theta_p, \alpha)\right]\right\} \tag{A.1.6}$$

where $V(\theta_p, \alpha) = \Gamma(-d/\alpha, \mu_p \theta_p g_p) - \Gamma(-d/\alpha)$.

A.2 Proof of lemma 2

The STs are not allowed to transmit inside the PER because of interference between the PUs. Then the sum of interference from all the active STs outside the PER can be calculated as

$$I_{ps} = \sum_{i \in \Phi_{st}} P_s g_{si} R_{si}^{-\alpha}, \tag{A.2.1}$$

where R_{si} is the distance between the ith interfering ST and tagged PR. The interference channel gains g_{si} are considered to be independent and identical distribution for all channels.

Applying the Laplace transform in the above equation, we obtain

$$\begin{aligned}\mathcal{L}_{I_{ps}}(s_p) &= \mathbb{E}_{I_{ps}}\left[\exp(-s_p I_{ps})\right] \\ &= \mathbb{E}_{\Phi_{st},g_s}\left[\exp(-s_p \sum_{i\in\Phi_{st}} P_s g_{si} R_{si}^{-\alpha})\right] \\ &\overset{(i)}{=} \mathbb{E}_{\Phi_{st}}\left[\prod_{i\in\Phi_{st}} \mathbb{E}_{g_s}\left[\exp(-s_p P_s g_s R_{si}^{-\alpha})\right]\right] \\ &\overset{(ii)}{=} \exp\left\{-\mathbb{E}_{g_s}\left[\int_{r_{PER}}^{\infty}(1-\exp(-s_p P_s g_s R_s^{-\alpha}))\lambda_{ps}^{'}(R_s)dR_s\right]\right\}, \end{aligned} \tag{A.2.2}$$

where $s_p = \mu_p \theta_p r_p^{\alpha} P_p^{-1}$. $\lambda_{ps}^{'}(R_s)$ is the density of all active STs outside the PER and also follow the condition of $p_{ic,im}$ and $p_{st,im}$. That density can be described as $\lambda_{ps}^{'}(R_s) = \lambda_s b_d p_{ic,im} p_{st,im} dR_s^{d-1}$. In the expression for this density, $p_{ic,im}$ and $p_{st,im}$ are the *probability of unoccupied channel selection* and the *probability of successful transmission* for imperfect detection. It should be noted that the equality (i) is obtained by the independence of channel fading and the equality (ii) is obtained by PGFL of homogeneous PPP.

Application of the similar corollary A in eq. (A.2.2), we obtain the desired result given by lemma 2.

A.3 Proof of lemma 3

Now we calculate the interference at the location of the tagged SR from other STs without tagged ST. Thus the sum of interference is

$$I_{ss} = \sum_{i\in\Phi_{st}\setminus\{s_0\}} P_s G_{si} L_{si}^{-\alpha}, \tag{A.3.1}$$

where L_{si} is the distance between the ith interfering ST and the tagged SR. The interference channel gains G_{si} are considered to be independent and identical distribution for all channels.

Working from the interference expression, the Laplace transform can be derived as

$$\begin{aligned}\mathcal{L}_{I_{ss}}(s_s) &= \mathbb{E}_{I_{ss}}\left[\exp(-s_s I_{ss})\right] \\ &= \mathbb{E}_{\Phi_{st},G_s}\left[\exp(-s_s \sum_{i\in\Phi_{st}\setminus\{s_0\}} P_s G_{si} L_{si}^{-\alpha})\right] \\ &= \mathbb{E}_{\Phi_{st}}\left[\prod_{i\in\Phi_{st}\setminus\{s_0\}} \mathbb{E}_{G_s}\left[\exp(-s_s P_s G_s L_{si}^{-\alpha})\right]\right]\end{aligned}$$

$$\stackrel{(i)}{=} \exp\left\{-\mathbb{E}_{G_s}\left[\int_{r_s}^{\infty}(1-\exp(-s_s P_s G_s L_s^{-\alpha}))\lambda_{ss}^{'}(L_s)dL_s\right]\right\}$$
$$\stackrel{(ii)}{=} \exp\left\{\lambda_s^{'} b_d p_{im} r_s^d - (\frac{d}{\alpha})\lambda_s^{'} b_d p_{im}(\mu_s\theta_s r_s^{\alpha})^{\frac{d}{\alpha}}(G_s)^{\frac{d}{\alpha}}X(\theta_s,\alpha)\right\}, \tag{A.3.2}$$

where $s_s = \mu_s\theta_s r_s^{\alpha} P_s^{-1}$ and $X(\theta_s,\alpha) = \Gamma(-d/\alpha, \mu_s\theta_s G_s) - \Gamma(-d/\alpha)$. The equality (i) follows the PGFL of PPP for the STs, while (ii) follows similar corollary A. $\lambda_{ss}^{'}(L_s)$, the density of all active STs outside the region $b(0,r_s)$ and also satisfy the condition of $p_{ic,im}$ and $p_{st,im}$, is equal to $\lambda_s^{'} b_d p_{im} dL_s^{d-1}$ and $p_{im} = p_{ic,im}p_{st,im}$. In this density expression, $p_{ic,im}$ and $p_{st,im}$ are the *probability of unoccupied channel selection* and the *probability of successful transmission* for the imperfect detection, these have already explained in chapter 2.

A.4 Proof of lemma 4

We derive an expression for the sum of interference of SR from all PTs, given by

$$I_{sp} = \sum_{i\in\Phi_{pt}} P_p G_{pi} L_{pi}^{-\alpha}, \tag{A.4.1}$$

where L_{pi} is the distance between the ith interfering PT and the tagged SR. The interference channel gains G_{pi} are considered to be independent and identical distribution for all channels.

The Laplace transform of interference received by a SR can be written as

$$\begin{aligned}
\mathcal{L}_{I_{sp}}(s_s) &= \mathbb{E}_{I_{sp}}\left[\exp(-s_s I_{sp})\right] \\
&= \mathbb{E}_{\Phi_{pt},G_p}\left[\exp(-s_s\sum_{i\in\Phi_{pt}} P_p G_{pi} L_{pi}^{-\alpha})\right] \\
&= \mathbb{E}_{\Phi_{pt}}\left[\prod_{i\in\Phi_{pt}} \mathbb{E}_{G_p}\left[\exp(-s_s P_p G_p L_{pi}^{-\alpha})\right]\right] \\
&\stackrel{(i)}{=} \exp\left\{-\mathbb{E}_{G_p}\left[\int_0^{\infty}(1-\exp(-s_s P_p G_p L_p^{-\alpha}))\lambda_{sp}^{'}(L_p)dL_p\right]\right\} \\
&\stackrel{(ii)}{=} \exp\left\{-\lambda_p b_d p_{ic,pt}(\mu_s\theta_s r_s^{\alpha} P_s^{-1} P_p G_p)^{\frac{d}{\alpha}}\Gamma(1-d/\alpha)\right\},
\end{aligned} \tag{A.4.2}$$

where $s_s = \mu_s\theta_s r_s^{\alpha} P_s^{-1}$ and $\lambda_{sp}^{'}(L_p) = \lambda_p b_d p_{ic,pt} dL_p^{d-1}$. During spectrum sensing, the SUs determine the unoccupied channels of the PUs. After track out the unoccupied channel, the PUs start to transmit signal in their own unoccupied channel. For this reason, active PT creates interference with the SR. Thus the probability of selection of a channel from a union of unoccupied channel is $p_{ic,pt}$, which can be defined as $C(M,1)/C(N,1)$. $C(x,y)$ is the y combinations of channels among a set of x channels. M is unoccupied PUs channels and N is total no. of PUs channels. The equality (i) obtains from the PGFL of the homogeneous PPP and (ii) obtains from the corollary B.

Corollary B. *Let P be transmission power, g be interfering channel gain, $\lambda(c)$ be the density of corresponding interfering users and x be the distance from the interfering transmitter to the tagged receiver. Then the integral of the Laplace transform of interference, from 0 to ∞ is given by*

$$\begin{aligned}\mathcal{L}_I(s) &= \exp\left\{-\mathbb{E}_g\left[\int_0^\infty (1-\exp(-sPgx^{-\alpha}))\lambda(c)dx^{d-1}dx\right]\right\} \\ &= \exp\left\{-\lambda(c)(sPg)^{d/\alpha}\Gamma(1-d/\alpha)\right\}.\end{aligned}$$

Proof: The detailed proof is given in [23, pp. 103].

A.5 Proof of eq. (2.4.28)

The outage probability for the N_t active transmit antenna can be expressed as

$$\begin{aligned}\epsilon_s^{(d)} &= \left[1-\frac{\lambda_s}{a+\lambda_p p_{ic,pt}(\mu_s\theta_s P_s^{-1}P_p)^{\frac{2}{\alpha}}(G_p)^{\frac{2}{\alpha}}b}\right]^{N_t} \\ \Rightarrow \frac{\lambda_s}{a+\lambda_p p_{ic,pt}(\mu_s\theta_s P_s^{-1}P_pG_p)^{\frac{2}{\alpha}}b} &= 1-(\epsilon_s^{(d)})^{\frac{1}{N_t}} \\ \Rightarrow a+\lambda_p p_{ic,pt}(\mu_s\theta_s P_s^{-1}P_pG_p)^{\frac{2}{\alpha}}b &= \frac{\lambda_s}{1-(\epsilon_s^{(d)})^{\frac{1}{N_t}}} \\ \Rightarrow (\mu_s\theta_s P_s^{-1}P_p)^{\frac{2}{\alpha}} &= \frac{1}{\lambda_p p_{ic,pt}(G_p)^{\frac{2}{\alpha}}b}\left(\frac{\lambda_s}{1-(\epsilon_s^{(d)})^{\frac{1}{N_t}}}-a\right) \\ \Rightarrow P_s^{-1} &= \frac{1}{\mu_s\theta_s P_p}\left[\frac{1}{\lambda_p p_{ic,pt}(G_p)^{\frac{2}{\alpha}}b}\left(\frac{\lambda_s}{1-(\epsilon_s^{(d)})^{\frac{1}{N_t}}}-a\right)\right]^{\frac{\alpha}{2}} \\ P_s^* &= \mu_s\theta_s P_p\left[\frac{1}{\lambda_p p_{ic,pt}(G_p)^{\frac{2}{\alpha}}b}\left(\frac{\lambda_s}{1-(\epsilon_s^{(d)})^{\frac{1}{N_t}}}-a\right)\right]^{-\frac{\alpha}{2}}, \qquad \text{(A.5.1)}\end{aligned}$$

where $a=\lambda_s-\lambda_s^{'}p_{im}+(\frac{2}{\alpha})\lambda_s^{'}p_{im}(\mu_s\theta_s)^{\frac{2}{\alpha}}(G_s)^{\frac{2}{\alpha}}X(\theta_s,\alpha)$ and $b=\Gamma(1-2/\alpha)$.

A.6 Proof of eq. (2.4.29)

The energy efficiency of the N_t active transmit antenna, calculated using eq. (2.4.22), can be expressed as

$$\eta_{EE}^{N_t}=\frac{\lambda_s\log_2(1+\theta_s)}{\left\{a+\lambda_p p_{ic,im}(\mu_s\theta_s\frac{P_p}{P_s^*(N_t)})^{\frac{2}{\alpha}}(G_p)^{\frac{2}{\alpha}}\Gamma(1-2/\alpha)\right\}P_z}, \qquad \text{(A.6.1)}$$

where $a = \lambda_s - \lambda_s^{'} p_{im} + (\frac{2}{\alpha})\lambda_s^{'} p_{im}(\mu_s\theta_s)^{\frac{2}{\alpha}}(G_s)^{\frac{2}{\alpha}} X(\theta_s, \alpha)$ and $P_z = N_{TRX}P_oT_t + p_{ic,im}p_{st,im}\Delta_s P_s^*(N_t)T_p + P_{sp}T_s + P_s^*(N_t)T_p$.

Now putting the value of $P_s^*(N_t)$ (i.e. eq. (2.4.28)) in eq. (A.6.1), after some calculations, we arrive at

$$\eta_{EE}^{N_t} = \frac{\lambda_s \log_2(1+\theta_s)}{\left(\frac{\lambda_s}{1-\left[\epsilon_s^{(d)}\right]^{\frac{1}{N_t}}}\right) P_z}, \tag{A.6.2}$$

Appendix B

B.1 Proof of $\mathcal{L}_{I_{ss}}(f(n))$

The interference signals at target SR come from all active STs, which can be expressed as (3.2.9). By using (3.2.9), the Laplace transform of interference can be represented as

$$\begin{aligned}
\mathcal{L}_{I_{ss}}(f(n)) &= \mathbb{E}\left[\exp\left(-f(n)\sum_{i\in\Phi_{St}\setminus y} P_{si}G_{ssi}\left\|R_{ssi}\right\|^{-\alpha}\right)\right] \\
&\overset{(i)}{=} \mathbb{E}_{\Phi_{St}}\left[\prod_{i\in\Phi_{St}\setminus y}\mathbb{E}_{P_s,G_{ss}}\left\{-f(n)P_sG_{ss}\left\|R_{ssi}\right\|^{-\alpha}\right\}\right] \\
&\overset{(ii)}{=} \exp\left[-2\pi\lambda_{St}\mathbb{E}_{P_s,G_{ss}}\left\{\int_{r_s}^{\infty}\left[1-\exp\left(-f(n)P_sG_{ss}\left\|R_{ss}\right\|^{-\alpha}\right)\right]R_{ss}dR_{ss}\right\}\right] \\
&= \exp\left[-2\pi\lambda_{St}\left(\sum_{n_1=1}^{N_{p_1}}\frac{w_{n_1}}{\sqrt{\pi}}\int_{r_s}^{\infty}\left\{1-\frac{1}{1+\gamma(a_{n_1})f(n)\frac{P_s}{R_{ss}^{\alpha}}}\right\}R_{ss}dR_{ss}\right)\right] \quad \text{(B.1.1)}
\end{aligned}$$

where $f(n)=\frac{T_s\|r_s\|^{\alpha}}{P_s\gamma(a_n)}$. Equality (i) follows the independence of transmission power and channel fading for all active ST. Equality (ii) follows the probability generating functional of PPP [72]. Then, considering $\left(\frac{R_{ss}}{r_s}\right)^2=t$ in (B.1.1), the integral can be written as

$$\begin{aligned}
&= \int_{r_s}^{\infty}\left\{1-\frac{1}{1+\gamma(a_{n_1})f(n)P_sR_{ss}^{-\alpha}}\right\}R_{ss}dR_{ss} \\
&= \int_{r_s}^{\infty}\left\{1-\frac{1}{1+\gamma(a_{n_1})\frac{T_sr_s^{\alpha}}{P_s\gamma(a_n)}P_sR_{ss}^{-\alpha}}\right\}R_{ss}dR_{ss} \\
&= \int_{r_s}^{\infty}\left\{1-\frac{1}{1+C_{ss}\frac{r_s^{\alpha}}{R_{ss}^{\alpha}}}\right\}R_{ss}dR_{ss} = \int_{r_s}^{\infty}\left\{1-\frac{1}{1+C_{ss}\left(\frac{R_{ss}}{r_s}\right)^{-\alpha}}\right\}R_{ss}dR_{ss}
\end{aligned}$$

$$
\begin{aligned}
&= \int_1^{\infty} \left\{ 1 - \frac{1}{1 + C_{ss}\,(t)^{-\alpha/2}} \right\} \frac{r_s^2}{2} dt \\
&= \frac{r_s^2}{2} \int_1^{\infty} \left\{ 1 - \frac{1}{1 + C_{ss}\,(t)^{-\alpha/2}} \right\} dt = \frac{r_s^2}{2} \int_1^{\infty} \left\{ \frac{C_{ss}\,(t)^{-\alpha/2}}{1 + C_{ss}\,(t)^{-\alpha/2}} \right\} dt \\
&= \frac{r_s^2}{2} \left[\int_0^{\infty} \left\{ \frac{C_{ss}}{(t)^{\alpha/2} + C_{ss}} \right\} dt - \int_0^{1} \left\{ \frac{C_{ss}}{(t)^{\alpha/2} + C_{ss}} \right\} dt \right] \qquad \text{(B.1.2)}
\end{aligned}
$$

where $C_{ss} = \frac{T_s \gamma(a_{n_1})}{\gamma(a_n)}$. The first-term of (B.1.2) can be written as

$$
I_1 = \int_0^{\infty} \left\{ \frac{C_{ss}}{(t)^{\alpha/2} + C_{ss}} \right\} dt = \frac{2\pi C_{ss}^{\frac{2}{\alpha}}}{\alpha \sin\left(\frac{2\pi}{\alpha}\right)} \qquad \text{(B.1.3)}
$$

where $\alpha > 0$ and $C_{ss} \neq 0$. The second-term of (B.1.2) can be written as

$$
\begin{aligned}
I_2 &= \int_0^{1} \left\{ \frac{C_{ss}}{(t)^{\alpha/2} + C_{ss}} \right\} dt \\
&= {}_2F_1\left([1, 2/\alpha]; 1 + 2/\alpha; -1/C_{ss}\right) \qquad \text{(B.1.4)}
\end{aligned}
$$

where ${}_2F_1\left([a, b]; c; t\right)$ is a hypergeometric function. For $\alpha = 4$, (B.1.4) reduces to $\sqrt{C_{ss}} \tan^{-1}\left(1/\sqrt{C_{ss}}\right)$.

Plugging (B.1.3), (B.1.4) and (B.1.2) into (B.1.1), we obtain the Laplace transform of interference from the active STs.

B.2 Proof of $\mathcal{L}_{I_{sp}}(f(n))$

The interference signals at target SR come from all active PTs, which is expressed as (3.2.10). By using (3.2.10), the Laplace transform of interference can be written as

$$
\begin{aligned}
\mathcal{L}_{I_{sp}}(f(n)) &= \mathbb{E}\left[\exp\left(-f(n) \sum_{i \in \Phi_{Pt}} P_{pi} G_{spi} \left\| R_{spi} \right\|^{-\alpha} \right) \right] \\
&\overset{(i)}{=} \mathbb{E}_{\Phi_{Pt}} \left[\prod_{i \in \Phi_{Pt}} \mathbb{E}_{P_p, G_{sp}} \left\{ -f(n) P_p G_{sp} \left\| R_{spi} \right\|^{-\alpha} \right\} \right] \\
&\overset{(ii)}{=} \exp\left[-2\pi \lambda_{Pt} \mathbb{E}_{P_p, G_{sp}} \left\{ \int_0^{\infty} \left[1 - \exp\left(-f(n) P_p G_{sp} \left\| R_{sp} \right\|^{-\alpha} \right) \right] R_{sp} dR_{sp} \right\} \right] \\
&= \exp\left[-2\pi \lambda_{Pt} \left(\sum_{n_2=1}^{N_{p_2}} \frac{w_{n_1}}{\sqrt{\pi}} \int_0^{\infty} \left\{ 1 - \frac{1}{1 + \gamma(a_{n_2}) f(n) \frac{P_p}{R_{sp}^{\alpha}}} \right\} R_{sp} dR_{sp} \right) \right] \qquad \text{(B.2.1)}
\end{aligned}
$$

where $f(n) = \frac{T_s \|r_s\|^{\alpha}}{P_s \gamma(a_n)}$. Equality (i) and (ii) follow a rule similar to (B.1.1). Then, changing the variable $\left(\frac{R_{sp}}{r_s}\right)^2 = t$ in (B.2.1), the integral can be written as

$$
\begin{aligned}
&= \int_0^{\infty} \left\{ 1 - \frac{1}{1 + \gamma(a_{n_2}) f(n) P_p R_{sp}^{-\alpha}} \right\} R_{sp} dR_{sp} \\
&= \int_0^{\infty} \left\{ 1 - \frac{1}{1 + \gamma(a_{n_2}) \frac{T_s r_s^{\alpha}}{P_s \gamma(a_n)} P_p R_{sp}^{-\alpha}} \right\} R_{sp} dR_{sp} \\
&= \int_0^{\infty} \left\{ 1 - \frac{1}{1 + C_{sp} \frac{r_s^{\alpha}}{R_{sp}^{\alpha}}} \right\} R_{sp} dR_{sp} = \int_0^{\infty} \left\{ 1 - \frac{1}{1 + C_{sp} \left(\frac{R_{sp}}{r_s}\right)^{-\alpha}} \right\} R_{sp} dR_{sp} \\
&= \int_0^{\infty} \left\{ 1 - \frac{1}{1 + C_{sp} (t)^{-\alpha/2}} \right\} \frac{r_s^2}{2} dt = \frac{r_s^2}{2} \int_0^{\infty} \left\{ 1 - \frac{1}{1 + C_{sp} (t)^{-\alpha/2}} \right\} dt \\
&= \frac{r_s^2}{2} \int_0^{\infty} \left\{ \frac{C_{sp} (t)^{-\alpha/2}}{1 + C_{sp} (t)^{-\alpha/2}} \right\} dt = \frac{r_s^2}{2} \left[\int_0^{\infty} \left\{ \frac{C_{sp}}{(t)^{\alpha/2} + C_{sp}} \right\} dt \right] \\
&= \frac{r_s^2}{2} \cdot \frac{2\pi C_{sp}^{\frac{2}{\alpha}}}{\alpha \sin\left(\frac{2\pi}{\alpha}\right)}
\end{aligned}
\tag{B.2.2}
$$

where $C_{sp} = \frac{T_s P_p \gamma(a_{n_2})}{P_s \gamma(a_n)}$. Substituting (B.2.2) into (B.2.1), we obtain the Laplace transform of interference from the active PTs.

Appendix C

C.1 Proof of $\mathcal{L}_{I_{ss}}(s_s)$

The sum of the interferences received at the tagged SR can be written as

$$I_{ss} = \sum_{i \in \Phi_{ST} \setminus \{o\}} \mathbb{I}\left(P_{si} \|r_i\|^{-\alpha} < \rho_{so}\right) P_{si} h_i \|r_i\|^{-\alpha}, \tag{C.1.1}$$

where o represents the tagged ST, $\Phi_{ST} \setminus \{o\}$ is an independent PPP with the density λ_s describing the interfering STs, P_{si} is the transmission power in accordance with truncated channel inversion power control, h_i is the channel power gain, and r_i is the distance between the interfering STs and the tagged SR. $\mathbb{I}(\cdot)$ is the indicator function, which equals 1 if the statement $(\cdot)$ is true and 0 otherwise, and $\|\cdot\|$ denotes the Euclidean norm. A detailed derivation of Theorem 1 is provided in [77] so the full calculation is omitted here.

The Laplace transform (LT) of the sum of the interferences from the interfering STs received at the tagged SR can be obtained as

$$\begin{aligned}\mathcal{L}_{I_{ss}}(s_s) &= \mathbb{E}\left[\exp\left(-s_s I_{ss}\right)\right] \\ &= \exp\left[-2\pi\lambda_s (s_s)^{\frac{2}{\alpha}} \mathbb{E}_{P_s}\left[P_s^{\frac{2}{\alpha}}\right] \int_{(s_s \rho_{so})^{\frac{-1}{\alpha}}}^{\infty} \frac{x}{1+x^{\alpha}} dx\right],\end{aligned} \tag{C.1.2}$$

where $\mathbb{E}_t[\cdot]$ is the expected value with respect to the random variable t and P_s is the transmission power of a ST in the uplink, which is given by (4.3.1). Substituting (4.3.1) into (C.1.2), we obtain lemma 2.

C.2 Proof of $\mathcal{L}_{I_{sp}}(s_s)$

The calculation of the interference of a PT depends on the location of the SR, as shown in Fig. 4.3. There are two cases: (a) the SR is located inside the PER and (b) the SR is located outside the PER. For each of the two cases, we determine the LT of the sum of the interferences I_{sp}.

Case (a): The summation of the interferences received at the tagged SR can be written as

$$I_{sp} = \sum_{i \in \Phi_{PT}} P_{pi} h_{pi} \left\| r_{pi} \right\|^{-\alpha}. \tag{C.2.1}$$

In this case, the SR is inside the PER of the PT; thus, only the nearest PT creates interference in the SR, as already explained in Fig. 4.3. For this reason, the integration is from 0 to r_{PER}. In the rest of the calculation, we exclude the Euclidean norm to simplify notation. The LT of the interference from the interfering PT received at the tagged SR can be expressed as

$$\begin{aligned}
\mathcal{L}_{I_{sp}^{(\mathrm{a})}}(s_s) &= \mathbb{E}\left[\exp\left(-s_s I_{sp}\right)\right] \\
&\overset{(i)}{=} \exp\left[-2\pi\lambda_p \int_0^{r_{PER}} \mathbb{E}_{P_p,h_p}\left[1-\exp\left(-s_s P_p h_p r_p^{-\alpha}\right)\right] r_p dr_p\right] \\
&\overset{(ii)}{=} \exp\left[-2\pi\lambda_p \int_0^{r_{PER}} \mathbb{E}_{P_p}\left[1-\frac{1}{1+s_s P_p r_p^{-\alpha}}\right] r_p dr_p\right] \\
&\overset{(iii)}{=} \exp\left[-2\pi\lambda_p (s_s)^{\frac{2}{\alpha}} \mathbb{E}_{P_p}\left[P_p^{\frac{2}{\alpha}}\right] \int_0^{\left(\frac{r_{PER}^{\alpha}}{s_s P_p}\right)^{\frac{1}{\alpha}}} \frac{y}{1+y^{\alpha}} dy\right].
\end{aligned} \tag{C.2.2}$$

Equality (i) is obtained from the probability generating functional of the PPP [72]. Equality (ii) is obtained from the Laplace transform of h_p. Equality (iii) is obtained by replacing variables $y = \left(\frac{r_p^{\alpha}}{s_s P_p}\right)^{\frac{1}{\alpha}}$.

Case (b): In this case, the SR is outside the PER. Hence, the same interference as in case (a) occurs in the SR; however, the integration of the distance is from r_{PER} to ∞. For these limits, the LT of the interference from the interfering PT received at the tagged SR can be obtained as

$$\begin{aligned}
\mathcal{L}_{I_{sp}^{(\mathrm{b})}}(s_s) &= \mathbb{E}\left[\exp\left(-s_s I_{sp}\right)\right] \\
&\overset{(i)}{=} \exp\left[-2\pi\lambda_p \int_{r_{PER}}^{\infty} \mathbb{E}_{P_p,h_p}\left[1-\exp\left(-s_s P_p h_p r_p^{-\alpha}\right)\right] r_p dr_p\right].
\end{aligned} \tag{C.2.3}$$

Then, equality (i) follows from the same procedure as in case (a). After the calculation of (C.2.2) and (C.2.3), we substitute the values into (4.4.3) and (4.4.4). Finally we obtain lemma 3 (i.e., (4.4.9) and (4.4.10)).

C.3 Formula

For the derivation of the closed-form expressions for the coverage probability (4.4.13)-(4.4.17), we use the following integration formula [85]:

$$\int \frac{x}{1+x^4} dx = \frac{1}{2}\left[\arctan x^2\right]. \tag{C.3.1}$$

A similar integration formula is used to derive the expressions for spectral efficiency (4.4.28)-(4.4.32).

Appendix D

D.1 Proof of $\gamma_p(h, l(d))$

Corollary 1: The probability of detection (P_d) by an energy detector employed at a SR can be expressed by the relation

$$P_d = Q\left[\frac{Q^{-1}(P_{fa}) - \sqrt{\tau f_s}\gamma_p(h, l(d))}{1 + \gamma_p(h, l(d))}\right],$$

where $Q(y) = \frac{1}{\sqrt{2\pi}}\int_y^\infty \exp(-x^2/2)dx$ is a complementary Gaussian distribution, P_{fa} is the probability of a false alarm, τ is the sensing time, f_s is the sampling frequency, $\gamma_p(h, l(d))$ is the received SNR of the PT, h is channel fading, and $l(d)$ is path-loss function.

Proof: The corollary is derived from Eqs. (7) and (8) in [112].

Following the corollary, we obtain

$$\gamma_p(h, l(d)) = \frac{Q^{-1}(P_{fa}) - Q^{-1}(P_d)}{Q^{-1}(P_d) + \sqrt{\tau f_s}}. \tag{D.1.1}$$

D.2 Proof of lemma 1

The interference I_{ss} signals at target SR appear from all active STs, defined as (5.2.5). Applying (5.2.5), the Laplace transform of interference I_{ss} can be written as

$$\begin{aligned}
\mathcal{L}_{I_{ss}}(s) &= \mathbb{E}_{I_{ss}}\left[\exp\left(-sI_{ss}\right)\right] \\
&= \mathbb{E}_{I_{ss}}\left[\exp\left(-s\sum_{i\in\Phi_{St}\setminus\{o\}} P_{si}h_{si}l(d_{si})\right)\right] \\
&= \mathbb{E}_{\Phi_{St}}\left[\prod_{i\in\Phi_{St}\setminus\{o\}} \mathbb{E}_{h_s}\left[\exp\left(-sP_sh_sl(d_{si})\right)\right]\right]
\end{aligned}$$

$$
\begin{aligned}
&\overset{(i)}{=} \mathbb{E}_{\Phi_{St}}\left[\prod_{i\in\Phi_{St}\setminus\{o\},\ d_s\le d_c} \mathbb{E}_{h_s}\left[\exp\left(-sP_sh_sd_s^{-\alpha_L}\right)\right]\right] \\
&\qquad \cdot \mathbb{E}_{\Phi_{St}}\left[\prod_{i\in\Phi_{St}\setminus\{o\},\ d_s> d_c} \mathbb{E}_{h_s}\left[\exp\left(-s\kappa P_sh_sd_s^{-\alpha_N}\right)\right]\right] \\
&\overset{(ii)}{=} \exp\left(-sQ_sP_sd_c^{-\alpha_L}\int_{b(0,d_c)}\lambda_s dx\right) \\
&\qquad \cdot \exp\left(-2\pi\lambda_sQ_s\int_{d_c}^{\infty}\mathbb{E}_{h_s}\left[1-\exp\left(-s\kappa P_sh_sx^{-\alpha_N}\right)\right]xdx\right) \\
&\overset{(iii)}{=} \exp\left(-s\pi\lambda_sQ_sP_sd_c^{2-\alpha_L}\right)\cdot\exp\left(-2\pi\lambda_sQ_s\int_{d_c}^{\infty}\left[1-\frac{1}{1+s\kappa P_sx^{-\alpha_N}}\right]xdx\right) \\
&= \exp\left(-s\pi\lambda_sQ_sP_sd_c^{2-\alpha_L}\right)\cdot\exp\left(-2\pi\lambda_sQ_s(s\kappa P_s)^{\frac{2}{\alpha_N}}\int_{\frac{d_c}{(\kappa sP_s)^{2/\alpha_N}}}^{\infty}\frac{y}{1+y^{\alpha_N}}dy\right), \qquad \text{(D.2.1)}
\end{aligned}
$$

where step (i) is obtained from the two-slope path-loss function, the first part of step (ii) is defined as the average number of points falling within a disk of radius d_c, obtained from section 2.4.2 in [23], the second part of step (ii) is obtained by the probability generating functional of PPP [72], and the second part of step (iii) is obtained by taking $y = x/(s\kappa P_s)^{(1/\alpha_N)}$.

Our proof is crowned by substituting the value $s = \frac{\theta_s}{P_s l(d_o)}$ into (D.2.1).

D.3 Proof of lemma 2

The interference I_{sp} signals at target SR appear from all active PTs, which is defined as (5.2.6). By using (5.2.6), the Laplace transform of interference I_{sp} can be written as

$$
\begin{aligned}
\mathcal{L}_{I_{sp}}(s) &= \mathbb{E}_{I_{sp}}\left[\exp\left(-sI_{sp}\right)\right] \\
&= \mathbb{E}_{\Phi_{Pt}}\left[\prod_{i\in\Phi_{Pt}} \mathbb{E}_{h_p}\left[\exp\left(-sP_ph_pl(d_{pi})\right)\right]\right] \\
&\overset{(i)}{=} \mathbb{E}_{\Phi_{Pt}}\left[\prod_{i\in\Phi_{Pt},\ d_p\le d_c} \mathbb{E}_{h_p}\left[\exp\left(-sP_ph_pd_p^{-\alpha_L}\right)\right]\right] \\
&\qquad \cdot \mathbb{E}_{\Phi_{Pt}}\left[\prod_{i\in\Phi_{St},\ d_p> d_c} \mathbb{E}_{h_p}\left[\exp\left(-s\kappa P_ph_pd_p^{-\alpha_N}\right)\right]\right]
\end{aligned}
$$

$$\overset{(ii)}{=} \exp\left(-sQ_pP_pd_c^{-\alpha_L}\int_{b(0,d_c)}\lambda_p dx\right)$$
$$\cdot \exp\left(-2\pi\lambda_pQ_p\int_{d_c}^{\infty}\mathbb{E}_{h_p}\left[1-\exp\left(-s\kappa P_ph_px^{-\alpha_N}\right)\right]xdx\right)$$
$$\overset{(iii)}{=} \exp\left(-s\pi\lambda_pQ_pP_pd_c^{2-\alpha_L}\right)\cdot\exp\left(-2\pi\lambda_pQ_p\int_{d_c}^{\infty}\left[1-\frac{1}{1+s\kappa P_px^{-\alpha_N}}\right]xdx\right)$$
$$= \exp\left(-s\pi\lambda_pQ_pP_pd_c^{2-\alpha_L}\right)\cdot\exp\left(-2\pi\lambda_pQ_p(s\kappa P_p)^{\frac{2}{\alpha_N}}\int_{\frac{d_c}{(\kappa sP_p)^{2/\alpha_N}}}^{\infty}\frac{y}{1+y^{\alpha_N}}dy\right), \quad \text{(D.3.1)}$$

where the steps (i), (ii), and (iii) are obtained by the same procedure. Q_p is the *probability of utilization of an idle channel*. The interferences come from the PTs in the CR network who utilize their own idle channel. After selection of idle channel by STs, each ST assigns an idle channel to its associated cellular users (SR). However, PT transmits its own data using an idle channel at any time when ST is utilizing it as an idle channel under dynamic spectrum access policy. At that time, ST must be shifted to other idle channels for cellular communication with its associated SR. Thus, the *probability of utilization of an idle channel* is the probability that a channel is utilized by the PT owing to data transmission from among the M idle channels, which can be expressed as $Q_p = 1/\binom{M}{1} = \frac{1}{M}$.

Our proof is crowned by substituting the value $s = \frac{\theta_s}{P_s l(d_o)}$ into (D.3.1).

D.4 Proof of lemma 3

The expectation of interference I_{ss} is obtained by using Campbell's theorem [23, Theorem 4.1]. The expectation of interference I_{ss} can be represented as for the two-slope path-loss function

$$\mathbb{E}(I_{ss}) = \mathbb{E}_{h_s}\left[\sum_{i\in\Phi_{St}\setminus\{o\},\ d_s\le d_c}P_sh_sd_s^{-\alpha_L}\right] + \mathbb{E}_{h_s}\left[\sum_{i\in\Phi_{St}\setminus\{o\},\ d_s> d_c}\kappa P_sh_sd_s^{-\alpha_N}\right]$$
$$\overset{(i)}{=} P_sQ_s\Gamma(1+2/\alpha_L)d_c^{-\alpha_L}\int_{b(0,d_c)}\lambda_s dx + 2\pi\kappa P_sQ_s\Gamma(1+2/\alpha_N)\int_{d_c}^{\infty}\lambda_s x^{-\alpha_N}xdx$$
$$= \pi\lambda_sP_sQ_s\Gamma(1+2/\alpha_L)d_c^{2-\alpha_L} + 2\pi\kappa\lambda_sP_sQ_s\Gamma(1+2/\alpha_N)d_c^{2-\alpha_N}/(\alpha_N-2), \quad \text{(D.4.1)}$$

where in step (i), we use the $\mathbb{E}[h_p] = \Gamma(1+2/\alpha_L)$ for LoS propagation and $\mathbb{E}[h_p] = \Gamma(1+2/\alpha_N)$ for NLoS propagation because the channel model is design for Rayleigh fading [23, Section 5.1.7].

Using Campbell's theorem, the expectation of interference I_{sp} can be represented similar

to the two-slope path-loss function

$$\begin{aligned}\mathbb{E}(I_{sp}) &= \mathbb{E}_{h_p}\left[\sum_{i\in\Phi_{Pt},\ d_p\le d_c} P_p h_p d_p^{-\alpha_L}\right] + \mathbb{E}_{h_p}\left[\sum_{i\in\Phi_{Pt},\ d_p> d_c} \kappa P_p h_p d_p^{-\alpha_N}\right] \\ &\overset{(i)}{=} P_p Q_p \Gamma(1+2/\alpha_L) d_c^{-\alpha_L} \int_{b(0,d_c)} \lambda_p dx + 2\pi\kappa P_p Q_p \Gamma(1+2/\alpha_N) \int_{d_c}^{\infty} \lambda_p x^{-\alpha_N} x dx \\ &= \pi\lambda_p P_p Q_p \Gamma(1+2/\alpha_L) d_c^{2-\alpha_L} + 2\pi\kappa\lambda_p P_p Q_p \Gamma(1+2/\alpha_N) d_c^{2-\alpha_N}/(\alpha_N-2), \quad \text{(D.4.2)}\end{aligned}$$

where in step (i), the same assumption is made as in (D.4.1).

D.5 Proof of Optimization

The objective function is

$$f(P_s,\lambda_s) = \xi\cdot(1-\rho)\cdot\left[v_1 P_s + \pi v_2\lambda_s P_s Q_s + \pi v_2\lambda_p P_p Q_p\right], \quad \text{(D.5.1)}$$

where $v_1 = d_c^{-2} + 0.5\kappa\sqrt{\pi}(d_o-d_c)^{-4}$ and $v_2 = 1 + 0.5\kappa\sqrt{\pi}d_c^{-2}$.

The constraint is

$$v_3(P_s)^{-1} + \pi v_4\lambda_s Q_s + \pi\lambda_p Q_p\left[v_5(P_s)^{-1} + v_6\sqrt{P_s^{-1}}\tan^{-1}\left(\frac{\kappa\theta_s P_p}{d_c^2 P_s l(d_o^c)}\right)\right] \le \epsilon_{cc}, \quad \text{(D.5.2)}$$

where $v_3 = \theta_s[\rho\sigma_s^2+\sigma_c^2](\rho l(d_o^c))^{-1}$, $v_4 = \theta_s l(d_o^c)^{-1} + \sqrt{\kappa\theta_s l(d_o^c)^{-1}}\tan^{-1}\left(\frac{\kappa\theta_s}{d_c^2 l(d_o^c)}\right)$, $v_5 = \theta_s P_p l(d_o^c)^{-1}$, $v_6 = \sqrt{\kappa\theta_s P_p l(d_o^c)^{-1}}$, and $\epsilon_{cc} = -\ln(1-\epsilon_c)$.

The first-order derivatives of $f(P_s,\lambda_s)$ with respect to P_s and λ_s are given by

$$\frac{\partial f(P_s,\lambda_s)}{\partial P_s} = \xi\cdot(1-\rho)\cdot\left[v_1 + \pi\lambda_s Q_s v_2\right]. \quad \text{(D.5.3)}$$

$$\frac{\partial f(P_s,\lambda_s)}{\partial \lambda_s} = \xi\cdot(1-\rho)\cdot\left[\pi P_s Q_s v_2\right]. \quad \text{(D.5.4)}$$

The partial derivatives of $f(P_s,\lambda_s)$ with respect to P_s and λ_s are given by

$$\frac{\partial^2 f(P_s,\lambda_s)}{\partial P_s\partial\lambda_s} = \xi\cdot(1-\rho)\cdot\left[\pi Q_s v_2\right]. \quad \text{(D.5.5)}$$

$$\frac{\partial^2 f(P_s,\lambda_s)}{\partial \lambda_s\partial P_s} = \xi\cdot(1-\rho)\cdot\left[\pi Q_s v_2\right]. \quad \text{(D.5.6)}$$

The Hessian of $f(P_s,\lambda_s)$ is

$$\mathbf{H} = \begin{bmatrix} \frac{\partial^2 f(P_s,\lambda_s)}{\partial P_s^2} & \frac{\partial^2 f(P_s,\lambda_s)}{\partial P_s\partial\lambda_s} \\ \frac{\partial^2 f(P_s,\lambda_s)}{\partial\lambda_s\partial P_s} & \frac{\partial^2 f(P_s,\lambda_s)}{\partial\lambda_s^2}\end{bmatrix}. \quad \text{(D.5.7)}$$

From (D.5.7), it can be easily observed that the determinant is less than zero. Therefore, the stationary point is an indefinite saddle point. Using (D.5.1) and (D.5.2), the Lagrangian can be expressed as

$$\mathcal{L}(P_s,\lambda_s,\mu)=\xi\cdot(1-\rho)\cdot\left[v_1P_s+v_2\pi\lambda_sP_sQ_s+\pi v_2\lambda_pP_pQ_p\right]-\mu\left[v_3(P_s)^{-1}+\pi v_4\lambda_sQ_s \right. \\ \left. +\pi\lambda_pQ_p\left(v_5(P_s)^{-1}+v_6\sqrt{P_s^{-1}}\tan^{-1}\left(\frac{\kappa\theta_sP_p}{d_c^2P_sl(d_o^c)}\right)\right)-\epsilon_{cc}\right]. \tag{D.5.8}$$

By taking the first-order derivatives of $\mathcal{L}(P_s,\lambda_s,\mu)$ with respect to P_s, λ_s, and μ, respectively, we obtain

$$\frac{\partial\mathcal{L}(P_s,\lambda_s,\mu)}{\partial P_s}=\xi\cdot(1-\rho)\cdot\left[v_1+\pi v_2\lambda_sQ_s\right]-\mu\left[-\frac{v_3}{P_s^2}+\pi\lambda_pQ_p\left(-\frac{v_5}{P_s^2} \right.\right. \\ \left.\left. -\frac{v_6\kappa\theta_sP_p}{d_c^2l(d_o^c)P_s^{5/2}\left(1+\frac{\kappa^2\theta_s^2P_p^2}{d_c^4l(d_o^c)^2P_s^2}\right)}-\frac{v_6\tan^{-1}\left(\frac{\kappa\theta_sP_p}{d_c^2P_sl(d_o^c)}\right)}{2P_s^{3/2}}\right)\right]=0. \tag{D.5.9}$$

$$\frac{\partial\mathcal{L}(P_s,\lambda_s,\mu)}{\partial\lambda_s}=\xi\cdot(1-\rho)\cdot\left[\pi v_2P_sQ_s\right]-\mu\left[\pi v_4Q_s\right]=0. \tag{D.5.10}$$

$$\frac{\partial\mathcal{L}(P_s,\lambda_s,\mu)}{\partial\mu}=-v_3(P_s)^{-1}-\pi v_4\lambda_sQ_s-\pi\lambda_pQ_p\left(v_5(P_s)^{-1}+v_6\sqrt{P_s^{-1}}\tan^{-1}\left(\frac{\kappa\theta_sP_p}{d_c^2P_sl(d_o^c)}\right)\right) \\ +\epsilon_{cc}=0. \tag{D.5.11}$$

From (D.5.10), we obtain

$$\mu=\frac{\xi\cdot(1-\rho)\cdot v_2P_s}{v_4}. \tag{D.5.12}$$

From (D.5.11), we obtain

$$\lambda_s=\frac{\epsilon_{cc}-v_3(P_s)^{-1}-\pi\lambda_pQ_p\left(v_5(P_s)^{-1}+v_6\sqrt{P_s^{-1}}\tan^{-1}\left(\frac{\kappa\theta_sP_p}{d_c^2P_sl(d_o^c)}\right)\right)}{\pi v_4Q_s}. \tag{D.5.13}$$

Substituting (D.5.12) and (D.5.13) into (D.5.9), we can characterize the relationship

between P and k as

$$v_1 + v_2 \left\{ \frac{\epsilon_{cc} - v_3(P_s)^{-1} - \pi\lambda_p Q_p \left(v_5(P_s)^{-1} + v_6\sqrt{P_s^{-1}} \tan^{-1}\left(\frac{\kappa\theta_s P_p}{d_c^2 P_s l(d_o^c)}\right)\right)}{v_4} \right\}$$

$$- \frac{v_2 P_s}{v_4}\left[-\frac{v_3}{P_s^2} + \pi\lambda_p Q_p \left(-\frac{v_5}{P_s^2} - \frac{v_6\kappa\theta_s P_p}{d_c^2 l(d_o^c) P_s^{5/2}\left(1+\frac{\kappa^2\theta_s^2 P_p^2}{d_c^4 l(d_o^c)^2 P_s^2}\right)} - \frac{v_6 \tan^{-1}\left(\frac{\kappa\theta_s P_p}{d_c^2 P_s l(d_o^c)}\right)}{2P_s^{3/2}}\right)\right] = 0$$

$$\Rightarrow v_1 + \frac{v_2}{v_4}\left\{ \epsilon_{cc} - v_3(P_s)^{-1} - \pi\lambda_p Q_p \left(v_5(P_s)^{-1} + v_6\sqrt{P_s^{-1}} \tan^{-1}\left(\frac{\kappa\theta_s P_p}{d_c^2 P_s l(d_o^c)}\right)\right)\right\}$$

$$- \frac{v_2}{v_4}\left[-\frac{v_3}{P_s} + \pi\lambda_p Q_p \left(-\frac{v_5}{P_s} - \frac{v_6\kappa\theta_s P_p}{d_c^2 l(d_o^c) P_s^{3/2}\left(1+\frac{\kappa^2\theta_s^2 P_p^2}{d_c^4 l(d_o^c)^2 P_s^2}\right)} - \frac{v_6 \tan^{-1}\left(\frac{\kappa\theta_s P_p}{d_c^2 P_s l(d_o^c)}\right)}{2P_s^{1/2}}\right)\right] = 0$$

$$\Rightarrow v_1 + \frac{v_2}{v_4}\left\{ \epsilon_{cc} - \pi\lambda_p Q_p \left(\frac{v_6 \tan^{-1}\left(\frac{\kappa\theta_s P_p}{d_c^2 P_s l(d_o^c)}\right)}{2P_s^{1/2}}\right)\right\} + \frac{v_2}{v_4}$$

$$\left[\pi\lambda_p Q_p \left(\frac{v_6\kappa\theta_s P_p}{d_c^2 l(d_o^c) P_s^{3/2}\left(1+\frac{\kappa^2\theta_s^2 P_p^2}{d_c^4 l(d_o^c)^2 P_s^2}\right)}\right)\right] = 0$$

$$\Rightarrow \frac{v_4}{v_2\pi\lambda_p Q_p}\left[v_1 + \frac{v_2\epsilon_{cc}}{v_4}\right] = \left(\frac{v_6 \tan^{-1}\left(\frac{\kappa\theta_s P_p}{d_c^2 P_s l(d_o^c)}\right)}{2P_s^{1/2}}\right) - \left(\frac{v_6\kappa\theta_s P_p}{d_c^2 l(d_o^c) P_s^{3/2}\left(1+\frac{\kappa^2\theta_s^2 P_p^2}{d_c^4 l(d_o^c)^2 P_s^2}\right)}\right)$$

$$\Rightarrow \frac{v_4}{v_2\pi\lambda_p Q_p}\left[v_1 + \frac{v_2\epsilon_{cc}}{v_4}\right] = \left(\frac{v_6 \tan^{-1}(P)}{2P_s^{1/2}}\right) - \left(\frac{v_6 P}{P_s^{1/2}(1+P^2)}\right)$$

$$\Rightarrow \frac{\tan^{-1}(P)}{2\sqrt{P_s}} - \frac{P}{\sqrt{P_s}(1+P^2)} = \frac{1}{v_6\pi\lambda_p Q_p}\left[\frac{v_1 v_4}{v_2} + \epsilon_{cc}\right]$$

$$\Rightarrow \frac{\tan^{-1}(P)}{2\sqrt{P_s}} - \frac{P}{\sqrt{P_s}(1+P^2)} = \frac{1}{v_6\pi\lambda_p Q_p}\left[\frac{v_1 v_4}{v_2} + \epsilon_{cc}\right]$$

$$\Rightarrow \frac{\tan^{-1}(P)}{2} - \frac{P}{(1+P^2)} = \frac{\sqrt{P_s}}{v_6\pi\lambda_p Q_p}\left[\frac{v_1 v_4}{v_2} + \epsilon_{cc}\right]$$

$$\Rightarrow \frac{\tan^{-1}(P)}{2} - \frac{P}{(1+P^2)} = \frac{1}{\sqrt{P}} \cdot \frac{\sqrt{\kappa\theta_s P_p}}{v_6\pi\lambda_p Q_p d_c\sqrt{l(d_o^c)}}\left[\frac{v_1 v_4}{v_2} + \epsilon_{cc}\right]$$

$$\Rightarrow \frac{\tan^{-1}(P)}{2} - \frac{P}{(1+P^2)} = k_1\frac{1}{\sqrt{P}}, \tag{D.5.14}$$

where $P = \frac{\kappa\theta_s P_p}{d_c^2 P_s l(d_o^c)}$ and $k_1 = \frac{1}{\pi\lambda_p Q_p d_c}\left[\frac{v_1 v_4}{v_2} + \epsilon_{cc}\right]$.

Theorem is crowned after some manipulations in (D.5.14).

Bibliography

[1] [Online]. Available: http://www.emarketer.com/Article/Smartphone-Users-Worldwide-Will-Total-175-Billion-2014/1010536, collected: 05 May, 2016.

[2] [Online]. Available: http://www.emarketer.com/Article/Mobile-Phone-Users-Japan-Upgrade-Smartphones-Finally/1012880, collected: 05 May, 2016.

[3] [Online]. "Ericsson Mobility Report: on the pulse of the networked society" , Available: http://www.ericsson.com/mobility-report, collected: 05 May, 2016.

[4] [Online]. "Mobile's Green Manifesto 2012" GSM Association. Available: http://www.gsma.com/publicpolicy/wp-content/uploads/2012/06/Green-Manifesto-2012.pdf, collected: 05 May, 2016.

[5] [Online]. "Sustainable energy use in mobile communications" ERICSSON White Paper, Tech. Rep., 2007., collected: 05 May, 2016.

[6] Federal Communications Commission, "Spectrum policy task force report," FCC 02-155, Nov. 2002.

[7] J. Mitola, "Cognitive radio an integrated agent architecture for software defined radio," Ph.D. dissertation, KTH, Sweden, Dec. 2000.

[8] S. Haykin, "Cognitive radio: Brain-empowered wireless communications," *IEEE J. Sel. Areas Commun.*, vol. 23, pp.201-220, Feb. 2005.

[9] E. Hossain, D. Niyato and Z. Han, *Dynamic Spectrum Access and Management in Cognitive Radio Networks*, Cambridge University Press, 2009.

[10] I. F. Akyildiz, W.-Y. Lee, M. C. Vuran, and S. Mohanty, "A Survey on spectrum management in cognitive radio networks," *IEEE Commun. Mag.*, vol. 46, no. 4, pp. 40-48, 2008.

[11] M. T. Masonta, M. Mzyece, and N. Ntlatlapa, "Spectrum decision in cognitive radio networks: A survey," *IEEE Commun. Surveys Tuts.*, vol. 15, no. 3, pp. 1088-1107, Third quarter 2013.

[12] I. F. Akyildiz, W.-Y. Lee, M. C. Vuran, and S. Mohanty, "Next generation/Dynamic spectrum access/Cognitive radio wireless networks: A survey, " *Computer Networks (Elsevier) J.*, vol. 50, no. 4, pp. 2127-2159, September 2006.

[13] E. Biglieri, A. Goldsmith, L. J. Greenstein, N. B. Mandayam, and H. V. Poor, *Principles of Cognitive Radio*, Cambridge, U.K., Cambridge Univ. Press, 2013.

[14] A. G. Marques, L. M. L. -Ramos, G. B. Giannakis, and J. Ramos, "Resource allocation for interweave and underlay CRs under probability-of-interference constraints," *IEEE J. Sel. Areas Commun.*, vol. 30, no. 10, pp. 1922-1933, Nov. 2012.

[15] S. Ohmori, "Report on Japan Study in Cognitive Radio and Networks," 2011.

[16] ———, "NICT news," vol. 7, no. 394, July 2013.

[17] H. Murakami and H. Harada, "Cognitive Radio based Spectrum Sharing in the Television Broadcast Bands," *Smart Wireless Laboratory*, NICT, 2013.

[18] [Online]. Available: http://www.nict.go.jp/en/press/2014/01/23-1.html, collected: 05 May, 2016.

[19] [Online]. Available: http://www2.nict.go.jp/wireless/smartlab/project/astra_sensing.html, collected: 05 May, 2016.

[20] [Online]. Available: http://www2.nict.go.jp/wireless/smartlab/project/pbb.html, collected: 05 May, 2016.

[21] A. D. Wyner, "Shannon-theoretic approach to a gaussian cellular multiple-access channel," *IEEE Trans. Inf. Theory*, vol. 40, no. 6, pp. 1713-1727, 1994.

[22] A. Guo and M. Haenggi, "Spatial stochastic models and metrics for the structure of base stations in cellular networks," *IEEE Trans. Wireless Commun.*, vol. 12, no. 11, pp. 5800-5812, Nov. 2013.

[23] M. Haenggi, *Stochastic Geometry for Wireless Networks*, Cambridge University Press, 2012.

[24] [Online]. Available: http://stakeholders.ofcom.org.uk/sitefinder/about-sitefinder, accessed: Mar. 2015.

[25] A. M. Ibrahim, T. ElBatt, A. El-Keyi, "Coverage probability analysis for wireless networks using repulsive point processes," Sept. 2013.

[26] M. Vu, N. Devroye, and V. Tarokh, "On the primary exclusive region of cognitive networks," *IEEE Trans. Wireless Commun.*, vol. 8, no. 7, pp. 3380-3385, July 2009.

[27] S. R. Sabuj and M. Hamamura, "Energy efficiency analysis of cognitive radio network using stochastic geometry," in *Proc. IEEE CSCN*, pp. 153-159, Oct. 2015.

[28] S. R. Sabuj and M. Hamamura, "Outage and energy-efficiency analysis of cognitive radio networks: A stochastic approach to transmit antenna selection," *Pervasive and Mobile Computing*, Elsevier, 2017.

[29] X. Hong, J. Wang, C. -X. Wang, and J. Shi, "Cognitive radio in 5G: A perspective on energy-spectral efficiency trade-off," *IEEE Commun. Mag.*, vol. 52, no. 7, pp. 46-53, July 2014.

[30] H. ElSawy, E. Hossain, and M. Haenggi, "Stochastic geometry for modeling, analysis, and design of multi-tier and cognitive cellular wireless networks: A survey," *IEEE Commun. Surveys Tuts.*, vol. 15, no. 3, pp. 996-1019, Third quarter 2013.

[31] C. -H. Lee and M. Haenggi, "Interference and outage in poisson cognitive networks," *IEEE Trans. Wireless Commun.*, vol. 11, no. 4, pp. 1392-1401, April 2012.

[32] S. A. R. Zaidi, D. C. McLernon, and M. Ghogho, "Outage probability analysis of cognitive radio networks under self-coexistence constraint," *Proc. Annu. Conf. on Information Sciences and Systems*, pp. 1-6, 2010.

[33] T. V. Nguyen and F. Baccelli, "A Stochastic geometry model for cognitive radio networks," *The Computer Journal*, vol. 55 no. 5, pp. 534-552, 2012.

[34] M. G. Khoshkholgh, K. Navaie, and H. Yanikomeroglu, "Outage performance of the primary service in spectrum sharing networks," *IEEE Trans. Mob. Comput.*, vol. 12, no. 10, pp. 1955-1971, Oct. 2013.

[35] A. Ghasemi and E. S. Sousa, "Interference aggregation in spectrum-sensing cognitive wireless Networks," *IEEE J. Sel. Topics Signal Process.*, vol. 2, no. 1, pp. 41-56, Feb. 2008.

[36] C. H. M. de Lima, M. Bennis, and M. Latva-aho, "Coordination mechanisms for self-organizing femtocells in two-tier coexistence scenarios," *IEEE Trans. Wireless Commun.*, vol. 11, no. 6, pp. 2212-2223, June 2012.

[37] F. H. Panahi and T. Ohtsuki, "Stochastic geometry modeling and analysis of cognitive heterogeneous cellular networks," *EURASIP Journal on Wireless Communications*, pp. 1-19, 2015.

[38] H. ElSawy and E. Hossain, "Two-tier hetnets with cognitive femtocells: downlink performance modeling and analysis in a multichannel environment," *IEEE Trans. Mob. Comput.*, vol. 13, no. 3, pp. 649-663, Mar. 2014.

[39] A. H. Sakr and E. Hossain, "Cognitive and energy harvesting-based D2D communication in cellular networks: stochastic geometry modeling and analysis," *IEEE Trans. Commun.*, vol. 63, no. 5, pp. 1867-1880, May 2015.

[40] Y. S. Soh, T. Q. S. Quek, M. Kountouris, and H. Shin, "Energy efficient heterogeneous cellular networks," *IEEE J. Sel. Areas Commun.*, vol. 31, no. 5, pp. 840-850, May 2013.

[41] N. Deng, S. Zhang, W. Zhou, and J. Zhu, "A Stochastic geometry approach to energy efficiency in relay-assisted cellular networks," in *Proc. IEEE Globecom*, pp. 3484-3489, Dec. 2012.

[42] J. Peng, H. Tang, P. Hong, and K. Xue, "Stochastic geometry analysis of energy efficiency in heterogeneous network with sleep control," *IEEE Wireless Commun. letters*, vol. 2, no. 6, pp. 615-618, Dec. 2013.

[43] A. He, Y. Chen, and T. Zhang, "Stochastic geometry analysis of energy efficiency in hetnets with combined CoMP and BS sleeping," in *Proc. IEEE PIMRC*, Sept. 2014.

[44] A. G. Marques, L. M. L. -Ramos, G. B. Giannakis, and J. Ramos, "Resource allocation for interweave and underlay CRs under probability-of-interference constraints," *IEEE J. Sel. Areas Commun.*, vol. 30, no. 10, pp. 1922-1933, Nov. 2012.

[45] Y.-C. Liang, Y. Zeng, E. C. Y. Peh, and A. T. Hoang, "Sensing-throughput tradeoff for cognitive radio networks," *IEEE Trans. Wireless Commun.*, vol. 7, no. 4, pp. 1326-1337, April 2008.

[46] [Online]. Available: IEEE 802.22 working group on wireless regional area networks, http://www.ieee802.org/22/, accessed: Mar. 2017.

[47] K. -L. Du and M. N. S. Swamy, *Wireless Communication Systems: From RF Subsystems to 4G Enabling Technologies*, Cambridge, U.K, Cambridge University Press, 2010.

[48] [Online]. Available: IEEE Std. 802.22-2011, IEEE Standard for wireless regional area networks, http://standards.ieee.org/getieee802/download/802.22-2011.pdf, accessed: Mar. 2017.

[49] X. Li, H. Liu, S. Roy, J. Zhang, P. Zhang, and C. Ghosh, "Throughput analysis for a multi-user, multi-channel ALOHA cognitive radio system," *IEEE Trans. Wireless Commun.*, vol. 11, no. 11, pp. 3900-3909, Nov. 2012.

[50] C. Li, J. Zhang, and K. B. Letaief, "Throughput and energy efficiency analysis of small cell networks with multi-antenna base stations," *IEEE Trans. Wireless Commun.*, vol. 13, no. 5, pp. 2505-2517, May 2014.

[51] G. Auer, V. Giannini, C. Desset, I. Godor, P. Skillermark, M. Olsson, M. A. Imran, D. Sabella, M. J. Gonzalez, O. Blume, and A. Fehske, "How much energy is needed to run a wireless network?," *IEEE Commun. Mag.*, vol. 18, no. 5, pp. 40-49, Oct. 2011.

[52] M. T. Kakitani, G. Brante, R. D. Souza, and M. A. Imran, "Energy efficiency of transmit diversity systems under a realistic power consumption model," *IEEE Commun. Lett.*, vol. 17, no. 1, pp. 119-122, Jan. 2013.

[53] L. Li, X. Zhou, H. Xu, G. Y. Li, D. Wang, and A. Soong, "Energy-efficient transmission in cognitive radio networks," in *Proc. IEEE CCNC*, pp. 1-5, 2010.

[54] [Online]. Available: http://en.wikipedia.org/wiki/Television_station, accessed: Mar. 2015.

[55] C. Y. Chen, A. Sezgin, J. M. Ciof, and A. Paulraj, "Antenna selection in space-time block coded systems: performance analysis and low-complexity algorithm," *IEEE Trans. Signal Process.*, vol. 56, no. 7, pp. 3303-3314, July 2008.

[56] S. R. Sabuj and M. Hamamura, "Random cognitive radio network performance in Rayleigh-lognormal environment," in *Proc. IEEE CCNC*, 2017, pp. 999-1004.

[57] S. Weber and J. G. Andrews, "A stochastic geometry approach to wideband ad hoc networks with channel variations," in *Proc. Int. Symp. on Modeling and Optimization in Mobile, Ad Hoc and Wireless Networks*, 2006.

[58] M. D. Renzo, "A stochastic geometry approach to the rate of downlink cellular networks over correlated lognormal shadowing," in *IEEE VTC*, 2013.

[59] X. Yang and A. O. Fapojuwo, "Performance analysis of poisson cellular networks with lognormal shadowed Rayleigh fading," in *Proc. IEEE ICC*, pp. 1042-1047, 2014.

[60] J. Chen, L.-C. Wang, and C.-H. Liu, "Coverage probability of small cell networks with composite fading and shadowing," in *Proc. PIMRC*, pp. 1965-1969, 2014.

[61] X. Zhang and M. Haenggi, "A stochastic geometry analysis of inter-cell interference coordination and intra-cell diversity," *IEEE Trans. Wireless Commun.*, vol. 13, no. 12, pp. 6655-6669, 2014.

[62] A. Mahmud and K. A. Hamdi, "A unified framework for the analysis of fractional frequency reuse techniques," *IEEE Trans. Commun.*, vol. 62, no. 10, pp. 3692-3705, 2014.

[63] S. C. Lam, R. Heidary, and K. Sandrasegaran, "A closed-form expression for coverage probability of random cellular network in composite Rayleigh-lognormal fading channels," in *Proc. ITNAC*, pp. 162-166, 2015.

[64] P. Herath, C. Tellambura, and W. A. Krzymien, "Stochastic geometry modeling of cellular uplink power control under composite Rayleigh-lognormal fading," in *IEEE VTC*, 2015.

[65] M. Z. Win, P. C. Pinto, and L. A. Shepp, "A mathematical theory of network interference and its applications," *Proceedings of the IEEE*, vol. 97, no. 2, pp. 205-230, 2009.

[66] Y. Wen, S. Loyka, and A. Yongacoglu, "Asymptotic analysis of interference in cognitive radio networks," *IEEE J. Sel. Areas Commun.*, vol. 30, no. 10, pp. 2040-2052, Nov. 2012.

[67] L. T. Dung and B. An, "Connectivity analysis of cognitive radio ad-hoc networks with shadow fading," *KSII Transactions on Internet and Information Systems*, vol. 9, no. 9, pp. 3335-3356, Sept. 2015.

[68] M. Patzold, *Mobile Radio Channels*, John Wiley & Sons, Ltd, 2012.

[69] M. Abramowitz and I. A. Stegun, *Handbook of Mathematical Functions: with Formulas, Graphs, and Mathematical Tables*, Dover Publications, New York, 1965.

[70] J. Andrews, F. Baccelli, and R. K. Ganti, "A tractable approach to coverage and rate in cellular networks," *IEEE Trans. Commun.*, vol. 59, no. 11, pp. 3122-3134, Nov. 2011.

[71] [Online]. Available://en.wikipedia.org/wiki/Euclidean_distance, accessed: Mar. 2016.

[72] M. Haenggi and R. K. Ganti, "Interference in large wireless networks," in *Foundations and Trends in Networking*, vol. 3, no. 2, pp. 127-248, The Netherlands: NOW Publishers, 2008.

[73] T. D. Novlan, H. S. Dhillon, and J. G. Andrews, "Analytical modeling of uplink cellular networks," *IEEE Trans. Wireless Commun.*, vol. 12, no. 6, pp. 2669-2679, June 2013.

[74] F. J. M.-Vega, F. J. L.-Martinez, G. Gomez, and M. C. A.-Torres, "Multi-user coverage probability of uplink cellular systems: a stochastic geometry approach," in *Proc. IEEE GLOBECOM*, pp. 3989-3994, 2014.

[75] G. Yuchen, N. Kai, and L. Jiaru, "Stochastic geometric analysis of the uplink throughput in cognitive radio cellular networks," *China Communications*, pp. 44-53, Aug. 2013.

[76] X. Hong, C. -X. Wang, and J. Thompson, "Uplink cell capacity of cognitive radio networks with peak interference power constraints," in *Proc. Int. Conf. on Communications, Circuits and Systems*, pp. 372-377, 2008.

[77] H. ElSawy and E. Hossain, "On stochastic geometry modeling of cellular uplink transmission with truncated channel inversion power control," *IEEE Trans. Wireless Commun.*, vol. 13, no. 8, Aug. 2014.

[78] T. Kobayashi and N. Miyoshi, "Uplink cellular network models with Ginibre deployed base stations," in *Proc. 26th Int. Teletrafc Congress*, pp. 1-7, Sept. 2014.

[79] A. H. Sakr and E. Hossain, "Analysis of K-tier uplink cellular networks with ambient RF energy harvesting," *IEEE J. Sel. Areas Commun.*, 2015.

[80] P. Herath, C. Tellambura, and W. A. Krzymien, "Stochastic geometry modeling of cellular uplink power control under composite rayleigh-lognormal fading," in *Proc. IEEE VTC*, 2015.

[81] M. Wildemeersch, T. Q. S. Quek, M. Kountouris, and C. H. Slump, "Successive interference cancellation in uplink cellular networks," in *Proc. IEEE 14th Workshop on SPAWC*, pp. 315-319. 2013.

[82] A. Goldsmith, *Wireless Communications*, Cambridge, U.K, Cambridge University Press, 2005.

[83] S. Kumar, *Wireless Communications Fundamental and Advanced Concepts: Design Planning and Applications*, River Publishers, 2015.

[84] S. Mukherjee, *Analytical Modeling of Heterogeneous Cellular Networks : Geometry, Coverage, and Capacity*, Cambridge University Press, 2014.

[85] I. S. Gradshteyn and I. M. Ryzhik, *Table of Integrals, Series, and Products*, Boston: academic press, inc., 1980.

[86] N. Shinohara, *Wireless Power Transfer via Radiowaves*, Wiley, 2014.

[87] X. Lu, P. Wang, D. Niyato, and E. Hossain, "Dynamic spectrum access in cognitive radio networks with RF energy harvesting," *IEEE Wireless Commun.*, vol. 21, no. 3, pp. 102-110, June 2014.

[88] [Online]. Available: http://www.powercastco.com/power-calculator/

[89] H. Tabassum, E. Hossain, A. Ogundipe, and D. I. Kim, "Wireless-powered cellular networks: key challenges and solution techniques," *IEEE Commun. Mag.*, vol. 53, no. 6, pp. 63-71, June 2015.

[90] H. Ju and R. Zhang, "Throughput maximization for wireless powered communication networks," *IEEE Trans. Wireless Commun.*, vol. 13, no. 1, pp. 418-428, Jan. 2014.

[91] S. Lee and R. Zhang, "Cognitive wireless powered network: spectrum sharing models and throughput maximization," *IEEE Trans. on Cognitive Commun. and Networking*, vol. 1, no. 3, pp. 335-346, 2015.

[92] I. Krikidis, S. Timotheou, S. Nikolaou, G. Zheng, D. W. K. Ng, and R. Schober, "Simultaneous wireless information and power transfer in modern communication systems," *IEEE Commun. Mag.*, vol. 52, no. 11, pp.104-110, 2014.

[93] X. Lu, P. Wang, D. Niyato, D. I. Kim, and Z. Han, "Wireless networks with RF energy harvesting: a contemporary survey," *IEEE Commun. Surveys Tuts.*, vol. 17, no. 2, pp.757-789, second quarter 2015.

[94] M.-L. Ku, W. Li, Y. Chen, and K. J. R. Liu, "Advances in energy harvesting communications: past, present, and future challenges," *IEEE Commun. Surveys Tuts.*, vol. 18, no. 2, pp. 1384-1412, second quarter 2016.

[95] Y. Liu, S. A. Mousavifar, Y. D., C. Leung, and M. Elkashlan, "Wireless energy harvesting in a cognitive relay network," *IEEE Trans. Wireless Commun.*, vol. 15, no. 4, pp. 2498-2508, April 2016.

[96] Z. Wang, Z. Chen, B. Xia, L. Luo, and J. Zhou, "Cognitive relay networks with energy harvesting and information transfer: design, analysis, and optimization," *IEEE Trans. Wireless Commun.*, vol. 15, no. 4, pp. 2562-2576, April 2016.

[97] Y. Liu, L. Wang, S. A. R. Zaidi, M. Elkashlan, and T. Q. Duong, "Secure D2D communication in large-scale cognitive cellular networks: a wireless power transfer model," *IEEE Trans. Commun.*, vol. 64, no. 1, pp. 329-342, January 2016.

[98] I. Krikidis, "Simultaneous information and energy transfer in large-scale networks with/without relaying," *IEEE Trans. Commun.*, vol. 62, no. 3, pp. 900-912, March 2014.

[99] S. Lee, R. Zhang, and K. Huang, "Opportunistic wireless energy harvesting in cognitive radio networks," *IEEE Trans. Wireless Commun.*, vol. 12, no. 9, pp. 4788-4799, September 2013.

[100] H. Sakr, and E. Hossain, "Analysis of K-tier uplink cellular networks with ambient RF energy harvesting," *IEEE J. Sel. Areas Commun.*, vol. 33, no. 10, pp. 2226-2238, October 2015.

[101] I. Flint, X. Lu, N. Privault, D. Niyato, and P. Wang, "Performance analysis of ambient RF energy harvesting with repulsive point process modeling," *IEEE Trans. Wireless Commun.*, vol. 14, no. 10, pp. 5402-5416, October 2015.

[102] X. Lu, I. Flint, D. Niyato, N. Privault, and P. Wang, "Self-sustainable communications with RF energy harvesting: Ginibre point process modeling and analysis," *IEEE J. Sel. Areas Commun.*, vol. 34, no. 5, pp. 1518-1535, May 2016.

[103] X. Zhang and J. G. Andrews, "Downlink cellular network analysis with multi-slope path loss models," *IEEE Trans. Commun.*, vol. 63, no. 5, pp. 1881-1894, Mar 2015.

[104] 3GPP, "Technical specification group radio access network; evolved universal terrestrial radio access (E-UTRA); further advancements for E-UTRA physical layer aspects (Release 9). TR 36.814," 2010.

[105] J. Arnau, I. Atzeni, and M. Kountouris, "Impact of LOS/NLOS propagation and path loss in ultra-dense cellular networks," in *Proc. IEEE ICC*, pp. 1-6, 2016.

[106] X. Zhou, R. Zhang, and C. K. Ho, "Wireless information and power transfer: architecture design and rate-energy tradeoff," *IEEE Trans. Commun.*, vol. 61, no. 11, pp. 4754-4767, Nov. 2013.

[107] L. Liu, R. Zhang, and K.-C. Chua, "Wireless information and power transfer: a dynamic power splitting approach," *IEEE Trans. Commun.*, vol. 61, no. 9, pp. 3990-4001, Sept. 2013.

[108] A. A. Nasir, X. Zhou, S. Durrani, and R. A. Kennedy "Relaying protocols for wireless energy harvesting and information processing," *IEEE Trans. Wireless Commun.*, vol. 12, no. 7, pp. 3622-3636, July 2013.

[109] R. E. Miller, *Optimization - foundations and applications*, John Wiley and Sons, Inc, 1999.

[110] C. Galiotto, N. K. Pratas, N. Marchetti, and L. Doyle, "A stochastic geometry framework for LOS/NLOS propagation in dense small cell networks," in *Proc. IEEE ICC*, pp. 2851-2856, 2015.

[111] G. P. Perrucci, F. H. P. Fitzek, and J. Widmer, "Survey on energy consumption entities on the smartphone platform," in *Proc. IEEE VTC*, pp. 1-6, 2011.

[112] W. Chung, S. Park, S. Lim, and D. Hong, "Spectrum sensing optimization for energy-harvesting cognitive radio systems," *IEEE Trans. Wireless Commun.*, vol. 13, no. 5, pp. 2601-2613, May 2014.